ORNL/SUB/99-XSZ175V-1

OAK RIDGE NATIONAL LABORATORY

LOCKHEED MARTIN

Neutronics Benchmarks for the Utilization of Mixed-Oxide Fuel: Joint U.S./Russian Progress Report for Fiscal Year 1997

Volume 4, Part 4—ESADA Plutonium Program Critical Experiments: Single-Region Core Configurations

Fissile Materials Disposition Program

MANAGED AND OPERATED BY
LOCKHEED MARTIN ENERGY RESEARCH CORPORATION
FOR THE UNITED STATES
DEPARTMENT OF ENERGY

ORNL-27 (3-96)

This report was prepared as an account of work sponsored by an agency of the United States Government. Neither the United States Government nor any agency thereof, nor any of their employees, makes any warranty, express or implied, or assumes any legal liability or responsibility for the accuracy, completeness, or usefulness or any information, apparatus, product, or process disclosed, or represents that its use would not infringe privately owned rights. Reference herein to any specific commercial product, process, or service by trade name, trademark, manufacturer, or otherwise, does not necessarily constitute or imply its endorsement, recommendation, or favoring by the United States Government or any agency thereof. The views and opinions of authors expressed herein do not necessarily state or reflect those of the United States Government or any agency thereof.

ORNL/SUB/99-XSZ175V-1

NEUTRONICS BENCHMARKS FOR THE UTILIZATION OF MIXED-OXIDE FUEL: JOINT U.S./RUSSIAN PROGRESS REPORT FOR FISCAL YEAR 1997

Volume 4, Part 4—ESADA Plutonium Program Critical Experiments: Single-Region Core Configurations

Hatice Akkurt
Naeem M. Abdurrahman

Date Published: May 1999

Report prepared by
LOCKHEED MARTIN ENERGY RESEARCH CORP.
P.O. Box 2008
Oak Ridge, Tennessee 37831-6363
Under
Subcontract Number 85B99398V

Funded by
Office of Fissile Materials Disposition
United States Department of Energy

Prepared for

Computational Physics and Engineering Division
Oak Ridge National Laboratory
Oak Ridge, Tennessee 37831
managed by
LOCKHEED MARTIN ENERGY RESEARCH CORP.
for the
U.S. DEPARTMENT OF ENERGY
under contract DE-96OR22464

FINAL REPORT

NEUTRONICS BENCHMARKS FOR THE UTILIZATION OF MIXED-OXIDE FUEL: JOINT U.S./RUSSIAN PROGRESS REPORT FOR FISCAL YEAR 1997

Volume 4, Part 4—ESADA Plutonium Program Critical Experiments: Single-Region Core Configurations

Hatice Akkurt and Naeem M. Abdurrahman

College of Engineering
Department of Mechanical Engineering
University of Texas
Austin, TX 78712

CONTENTS

1 DETAILED DESCRIPTION 1
1.1 Overview of Experiment 1
1.2 Description of Experimental Configuration 1
1.2.1 Lattice Grids 1
1.2.2 Types of Measurements 2
1.3 Single-Region Critical Experiments with 8% ^{240}Pu MOX Fuel 2
1.4 Single-Region Critical Experiments with 24 wt% ^{240}Pu MOX Fuel 31
1.5 Single-Region Critical Experiments with UO_2 Fuel 35
1.6 Description of Fuel Rods 38
1.7 Description of Test Configurations 39
1.8 Description of Materials 40
1.9 Supplemental Experimental Measurements 43
2 EVALUATION OF THE EXPERIMENTAL DATA 43
2.1 Sensitivity Calculations for Core Configurations with MOX Fuel 44
2.1.1 Fuel Rod Characterization 44
2.1.2 Structural Material 47
2.1.3 Moderator 48
2.1.4 Others 49
2.1.5 Total Uncertainties 50
2.2 Sensitivity Calculations for Core Configurations with UO_2 Fuel 50
2.2.1 Fuel Rod Characterization 50
2.2.2 Structural Material 52
2.2.3 Moderator 53
2.2.4 Others 53
2.2.5 Total Uncertainties 54
3 BENCHMARK SPECIFICATIONS 54
3.1 Description of Model 54
3.2 Dimensions 54
3.3 Material Data 54
3.4 Temperature Data 58
4 RESULTS OF CALCULATIONS 58
REFERENCES 60
Appendix A. ATOMIC NUMBER DENSITY CALCULATIONS 62
Appendix B. PuO_2 PARTICLE EFFECT 64

LIST OF TABLES

Table 1. Reported data for single-region experiments with 8% ^{240}Pu 7
Table 2. Reported data for single-region experiments with 24% ^{240}Pu 31
Table 3. Reported data for single-region experiments with 2.72 wt% UO_2 36
Table 4. MOX and UO_2 fuel rod specifications 39
Table 5. Isotopic composition of the metal plutonium in the MOX fuel rods 40
Table 6. Percentages of the elements in the MOX fuel rods 40
Table 7. Zircaloy-2 composition used for MOX fuel 40
Table 8. Chemical analysis of UO_2 fuel 41
Table 9. Chemical analysis of Zircaloy-4 clad used for UO_2 fuel 42
Table 10. Isotopic distribution of Al-6061 42
Table 11. Isotopic composition of Ag-In-Cd control rod 43
Table 12. Isotopic composition of stainless steel 43
Table 13. Sensitivity of k_{eff} to uncertainties in fuel rod characterization for core configurations with 8% ^{240}Pu MOX fuel 45
Table 14. Sensitivity of k_{eff} to uncertainties in fuel rod characterization for core configurations with 24% ^{240}Pu MOX fuel 46
Table 15. Sensitivity of k_{eff} to uncertainties in aluminum type and holes in the supporting plate for core configurations with 8% ^{240}Pu MOX fuel 48
Table 16. Sensitivity of k_{eff} to uncertainties in aluminum type and holes in aluminum supporting plate for core configurations with 24% ^{240}Pu MOX fuel 48
Table 17. Sensitivity of k_{eff} to uncertainty in the reference plane for CWH measurements for core configurations with 8% ^{240}Pu MOX fuel 49
Table 18. Sensitivity of k_{eff} to uncertainty in the reference plane for CWH measurements for core configurations with 24% ^{240}Pu MOX fuel 49
Table 19. Sensitivity of k_{eff} to ^{241}Am content and PuO_2 particle effect for core configurations with 8% ^{240}Pu MOX fuel 50
Table 20. Sensitivity of k_{eff} to ^{241}Am content and PuO_2 particle effect for core configurations with 24% ^{240}Pu MOX fuel 50
Table 21. Total uncertainty in k_{eff} due to uncertainties in experimental data for core configurations with 8% ^{240}Pu MOX fuel 51
Table 22. Total uncertainty in k_{eff} due to uncertainties in experimental data for core configurations with 24% ^{240}Pu MOX fuel 51
Table 23. Sensitivity of k_{eff} to uncertainties in fuel rod characterization for core configurations with UO_2 fuel 52

Table 24. Sensitivity of k_{eff} to aluminum type for core configurations with UO_2 fuel 52
Table 25. Sensitivity of k_{eff} to uncertainty in the reference plane for CWH measurements for core configurations with UO_2 fuel 53
Table 26. Sensitivity of k_{eff} to uncertainties in fuel rod characterization for core configurations with UO_2 fuel 53
Table 27. Total uncertainty in k_{eff} due to uncertainties in experimental data for core configurations with UO_2 fuel 54
Table 28. Atomic densities for the 8% and 24% ^{240}Pu MOX fuels 55
Table 29. Atomic densities for the UO_2 powder at the top of the MOX fuels 55
Table 30. Atomic densities for the Zircaloy-2 clad used for MOX fuel 55
Table 31. Atomic densities for the UO_2 fuel 56
Table 32. Atomic densities for the Zircaloy-4 clad 56
Table 33. Atomic densities for the Al-6061 56
Table 34. Atomic densities for water 56
Table 35. Atomic densities for borated water for the specified boron concentrations 57
Table 36. Atomic densities for air 57
Table 37. Atomic densities for the control rod 57
Table 38. Atomic densities for the stainless steel 58
Table 39. Atomic densities for the cobalt rod 58
Table 40. MCNP benchmark calculation results for 8% ^{240}Pu MOX fuel 59
Table 41. MCNP benchmark calculation results for 24% ^{240}Pu 60
Table 42. MCNP benchmark calculation results for 2.72% UO_2 fuel 60
Table A.1. The calculated values of the C_B and the densities for the specified boron concentrations 63
Table B.1. Change in k_{eff} for 25-μm grain size for 8% and 24% ^{240}Pu fuel 64

LIST OF FIGURES

Fig. 1. Installation of MOX fuel in a uniform lattice 4
Fig. 2. A typical single-region core configuration in a standard lattice pitch 5
Fig. 3. Core configuration with a $\sqrt{2}$ lattice pitch 5
Fig. 4. Single-region core configuration with a nine-rod uniform local void pattern 6
Fig. 5. Single-region configuration with a nine-rod slot pattern 6
Fig. 6. Cylindrical core configuration with 8% ^{240}Pu in a 1.7526-cm lattice 8
Fig. 7. A 24x23 rectangular core configuration with 8% ^{240}Pu in a 1.7526-cm lattice 9
Fig. 8. Cylindrical core configuration with 8% ^{240}Pu in a 1.9050-cm lattice 10
Fig. 9. Cylindrical core configuration with 8% ^{240}Pu in a 2.4785-cm lattice 11
Fig. 10. A 13x13 square core configuration with 8% ^{240}Pu in a 2.4785-cm lattice 12
Fig. 11. Cylindrical core configuration with 8% ^{240}Pu in a 2.6942-cm lattice 13
Fig. 12. Cylindrical core configuration with 8% ^{240}Pu in a 3.5052-cm lattice 14
Fig. 13. Cylindrical borated core configuration with 8% ^{240}Pu in a 1.7526-cm lattice 15
Fig. 14. Cylindrical borated core configuration with 8% ^{240}Pu in a 2.4785-cm lattice 16
Fig. 15. Cylindrical borated core configuration with 8% ^{240}Pu in a 1.7526-cm lattice 17
Fig. 16. Cylindrical borated core configuration with 8% ^{240}Pu in a 2.4785-cm lattice 18
Fig. 17. A 23x25 rectangular core configuration with a center test position in a 1.7526-cm lattice 19
Fig. 18. A 23x25 rectangular core configuration with a five-rod slot pattern in a 1.7526-cm lattice 20
Fig. 19. A 27x27 rectangular core configuration with a nine uniformly distributed rod 21
Fig. 20. A 27x27 rectangular core configuration with a nine loose cluster rod pattern 22
Fig. 21. A 27x27 rectangular core configuration with a nine tight cluster rod pattern 23
Fig. 22. A 27x27 rectangular core configuration with a nine-rod slot pattern in a 1.7526-cm lattice 24
Fig. 23. A 27x27 rectangular core configuration with a center test position in a 1.7526-cm lattice 25
Fig. 24. A 27x27 rectangular core configuration with a five-rod slot pattern in a 1.7526-cm lattice 26
Fig. 25. A 21x21 rectangular core configuration with a nine uniformly distributed rod 27
Fig. 26. A 21x21 rectangular core configuration with a center test position in a 1.9050-cm lattice 28
Fig. 27. A 21x21 rectangular core configuration with a 4×4 central void pattern in a 29
Fig. 28. A 21x21 rectangular core configuration with a 10×10 central void pattern in a 30
Fig. 29. Cylindrical core configuration with 24% ^{240}Pu in a 2.4785-cm lattice 32
Fig. 30. Cylindrical core configuration with 24% ^{240}Pu in a 2.6942-cm lattice 33
Fig. 31. Cylindrical core configuration with 24% ^{240}Pu in a 2.6942-cm lattice with a 34
Fig. 32. Installation of UO_2 fuel in a uniform lattice 35
Fig. 33. Cylindrical core diagram for UO_2 fuel in a 1.7526-cm lattice 36
Fig. 34. Cylindrical core configuration for enriched UO_2 fuel in a 2.4785-cm lattice 37

Fig. 35. MOX fuel rod 38
Fig. 36. Uranium fuel rod 39
Fig. B.1. Change in the k_{eff} value for 25-μm particle effect with increasing lattice pitch for 8% and 24% ^{240}Pu fuel 65
Fig. B.2. Change of corrected k_{eff} values along with the uncorrected values of k_{eff} for grain size effect with increasing lattice pitch for 8% ^{240}Pu fuel 66

FOREWORD

The purpose of this study is to simulate and assess the findings from selected ESADA experiments. It is presented in the format prescribed by the Nuclear Energy Agency Nuclear Science Committee for material to be included in the *International Handbook of Evaluated Criticality Safety Benchmark Experiments*.

ESADA PLUTONIUM PROGRAM CRITICAL EXPERIMENTS: SINGLE-REGION CORE CONFIGURATIONS*

1 DETAILED DESCRIPTION

1.1 Overview of Experiment

In 1967, a series of critical experiments was conducted at the Westinghouse Reactor Evaluation Center (WREC) using mixed-oxide (MOX) PuO_2-UO_2 and/or UO_2 fuels in various lattices and configurations.[1] These experiments were performed under the joint sponsorship of the Empire State Atomic Development Associates (ESADA) Plutonium Program and Westinghouse.[2] Both single-region and multiregion core configurations were constructed during the experimental program. The purpose of these experiments was to develop experimental data useful in validating analytical methods used in the design of plutonium-bearing replacement fuel for water reactors.

Three different types of fuel were used during the experimental program: two types of MOX fuels and a low-enriched UO_2 fuel. MOX fuels were distinguished by their ^{240}Pu content: 8 wt% ^{240}Pu and 24 wt% ^{240}Pu. Both MOX fuels contained 2.0 wt% PuO_2 in natural UO_2. The UO_2 fuel with 2.72% enrichment was used for comparison with the plutonium data and for use in multiregion experiments.

1.2 Description of Experimental Configuration

A total of 88 different critical core configurations were constructed for the experimental program. These core configurations were constructed by changing the lattice pitch, fuel configuration, and fuel isotopic composition. Fifty-three of these experiments were performed for single-region core configurations. All experiments were performed in a ~112-cm-diam pool. Criticality was achieved by adjusting the height of the light-water moderator in the pool. Buckling, reactivity worth, and power distribution measurements were performed during the experimental program.

Both single-and multiregion core configurations were used in the ESADA experiments. The single-region cores were constructed primarily by varying the lattice pitch, core layout, and fuel isotopic composition. The installations of MOX and UO_2 fuels at the WREC facility for the construction of the single-core configurations are given in Fig. 1 and Sect. 1.5 (Fig. 32). The multiregion core configurations were constructed in three ways: concentric region core configurations; salt and pepper core configurations; and a third configuration that can be generally described as two rectangular slabs loaded with UO_2, sandwiching a center region loaded with MOX fuel.

1.2.1 Lattice Grids

Two standard lattice plates were available for the experimental program. One plate had a lattice pitch of 1.7526 cm (0.69 in.) and the other of 1.9050 cm (0.75 in.). To change lattice pitches further, fuel rods were loaded on the diagonal, thus increasing the lattice pitch by a factor of $\sqrt{2}$. In this way, the standard lattice pitches become 2.4785 cm (0.9758 in.) and 2.6942 cm (1.0607 in.), respectively. It was also possible to double the standard pitch by leaving an empty hole between two rods. By this loading pattern, the standard 1.7526 cm (0.69 in.) lattice pitch became 3.5052 cm (1.38 in.).

---

*Configurations with MOX fuel containing 8 wt% ^{240}Pu with no boron in water are designated 006.
Configurations with MOX fuel containing 8 wt% ^{240}Pu with boron in water are designated 007.
Configurations with MOX fuel containing 24 wt% ^{240}Pu with boron in water are designated 008.
Configurations with MOX fuel containing 24 wt% ^{240}Pu with uranium pins are designated 009.
Identification Numbers: MIX-COMP-THERM-006 through 009.

Keywords: critical experiments, mixed-oxide, MOX, plutonium, plutonium dioxide, PuO_2, water reactor, natural uranium, enriched uranium, UO_2, ESADA, Westinghouse, WREC.

One of the reasons for performing critical experiments using many different lattice pitches with the same fuel rods is to provide data that cover a wide range of moderator-to-fuel volume ratios. In this way, since the only changing variable is the moderator-to-fuel ratio, the evaluation of theoretical models for systematic error can be performed.[3]

1.2.2 Types of Measurements

Measurements done in the ESADA experimental program are summarized as follows:

1. Buckling and reflector saving measurements were made in a number of lattices using three types of fuel. By varying the loading pattern, five critical buckling measurements were made in clean cores for different lattice pitches of 1.7526 cm, 1.9050 cm, 2.4785 cm, 2.6942 cm, and 3.5052 cm with the 8% ^{240}Pu fuel, thus extending the range of experimental information over a wide range of moderator-to-fuel ratios. Additional measurements with the 8% ^{240}Pu fuel were made at two different boron concentrations for two different lattices. Fuel rods of 24% ^{240}Pu were used in a single-region clean core with two different lattice pitches of 2.4785 cm and 2.6942 cm. Measurements were also made in two clean lattices of 1.7526 cm and 2.4785 cm using the 2.72% enriched UO_2.

2. The reactivity worths of different materials were measured in various test configurations. Several test positions were formed by removing fuel rods, and these holes were either filled with control rods or left as empty water holes. The reactivity effect of having a water gap in the center of the core, caused by removing one, five, or nine fuel rods, was determined. Also, the reactivity effect of either one or nine silver-indium-cadmium rods in place of fuel rods was measured for various geometrical arrays of slots and clusters. The reactivity effects of an empty zirconium tube and a cobalt rod were measured. Moreover, the reactivity effect of voids was measured by inserting aluminum tubes between the fuel rods in the central zone. Reactivity worths were obtained by measuring the critical water heights of the reference and perturbed cores and integrating the differential water worth curve between the measured water heights. The reactivity worth measurements were arranged in a different set of experiments distinguished by the number of core regions, fuel type, and lattice pitch. Single-region experiments were carried out for clean and borated core configurations with two different lattice pitches of 1.7526 cm and 1.9050 cm with 8% ^{240}Pu fuel. Reactivity worth measurement experiments were also done with the 24% ^{240}Pu fuel in a 2.6942-cm lattice pitch.

3. Power distribution measurements were made for various core configurations. Measurements were made by relating the fission product gamma activity of irradiated fuel rods to the temperature rise of the fuel clad surface, which is proportional to the rod power. The power distribution measurements for single-region experiments were performed for the 8% ^{240}Pu fuel in 1.7526-cm and 1.9050-cm lattices. Also, one power distribution measurement was performed for the 24% ^{240}Pu fuel core configuration in a 2.6942-cm lattice.

1.3 Single-Region Critical Experiments with 8% ^{240}Pu MOX Fuel

The single-region core configurations were constructed for various pitches and layouts. Buckling, reactivity worth, and power distribution measurements were performed.

Buckling measurements were carried out for 11 different core configurations, and seven of these measurements were performed for clean cores. Clean core buckling measurements were performed for five different lattice pitches. The other buckling measurements were made at two different boron concentrations with different lattice pitches. Buckling measurements were performed for cylindrical, rectangular, and square cores.

Reactivity worth measurements were performed for two different lattice pitches, 1.7526 and 1.9050 cm. Several configurations were constructed by changing the loading pattern. Measurements were performed for rectangular core configurations for both clean and borated cores. Reactivity worths were obtained by measuring the critical water heights (CWHs) of the reference and perturbed cores and

integrating the differential water worth curve between the measured water heights. Perturbed core configurations were formed by removing fuel rods from several locations. The reactivity effects from the water gap, silver-indium-cadmium control rods, an empty zirconium tube, and a cobalt rod were measured. Reactivity effects of having the same material for different geometries were also measured. For this purpose, fuel rods were removed in various arrays. Fuel rods were removed either in a uniform manner or from the center as a slot or as a tight or loose cluster. Also, the reactivity effect of voids was measured, and for this purpose aluminum tubes were inserted into the center of the lattice for various geometrical arrays.

Power distribution measurements were also made for various core configurations. The power distribution measurements were performed in 1.7526-cm and 1.9050-cm lattices. Measurements were made for both clean and borated cores. Power distribution measurements were carried out for core configurations having test configurations either as a center water hole or as five-rod slot patterns. These core configurations were identical to the core configurations constructed for reactivity measurements. However, for some of the cases, a small difference between CWHs was observed.

Installation of MOX fuel rods in a uniform lattice at the WREC facility is shown in Fig. 1. Fuel rods were supported by three layers of aluminum plates. The thickness of the bottom and midcore plates was 0.635 cm, and the thickness of the top plate was 1.27 cm. Fuel rods rested on a 5.24-cm-thick aluminum plate.

A typical single-region core configuration is shown in Fig. 2, and the core configuration with $\sqrt{2}$ lattice pitch is given in Fig. 3. Void regions were also present for some of the configurations; typical configurations for these cases are presented in Figs. 4 and 5.

Reported data for single-region core configurations with 8% ^{240}Pu fuel are given in Table 1. The related core configurations are shown in Figs. 6 to 28. For the schematic representation of the core configurations, the midplane of the midcore aluminum plate is taken as the reference plane. In these figures, the legend label “hole” refers to the fuel rod holes in the aluminum plate. In the absence of fuel or other rods (control rods), these holes were filled with water. Information on core diagram numbers and measurement types are also included in Table 1.

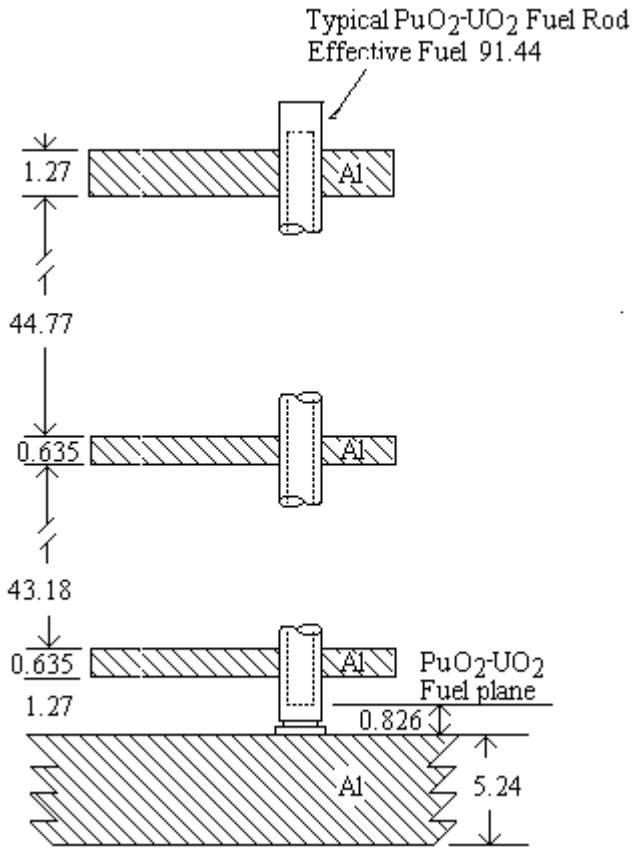

Fig. 1. Installation of MOX fuel in a uniform lattice.

(Not drawn to scale; units in centimeters except where specified otherwise.)

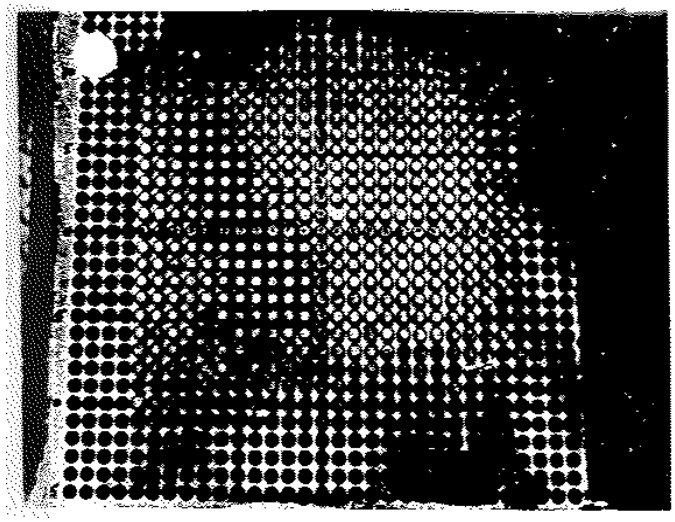

Fig. 2. A typical single-region core configuration in a standard lattice pitch.

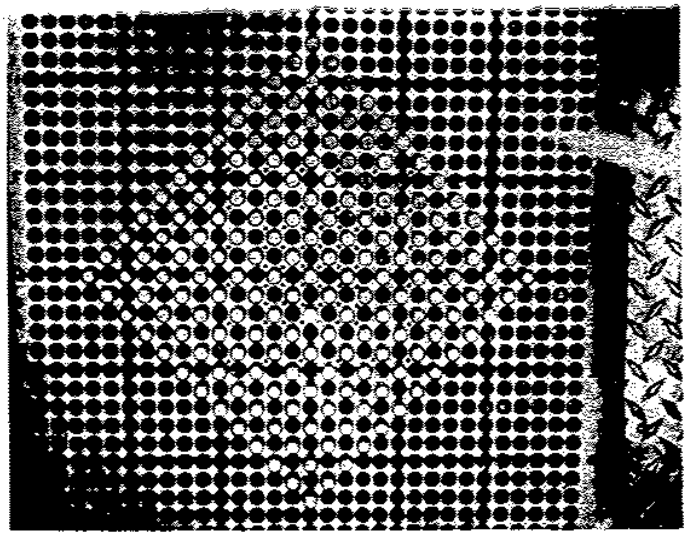

Fig. 3. Core configuration with a $\sqrt{2}$ lattice pitch.

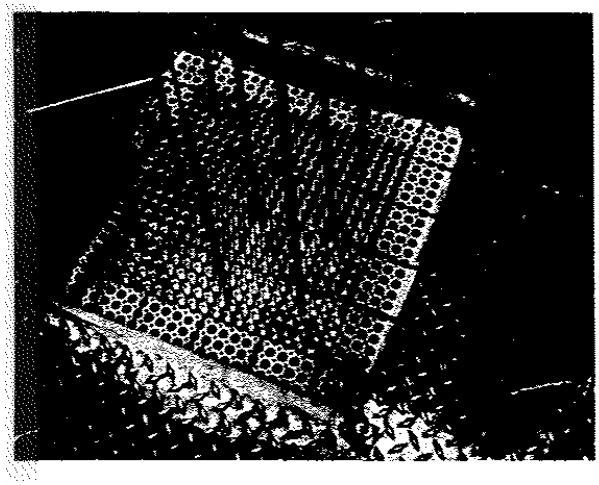

Fig. 4. Single-region core configuration with a uniformly distributed nine-rod local void pattern.

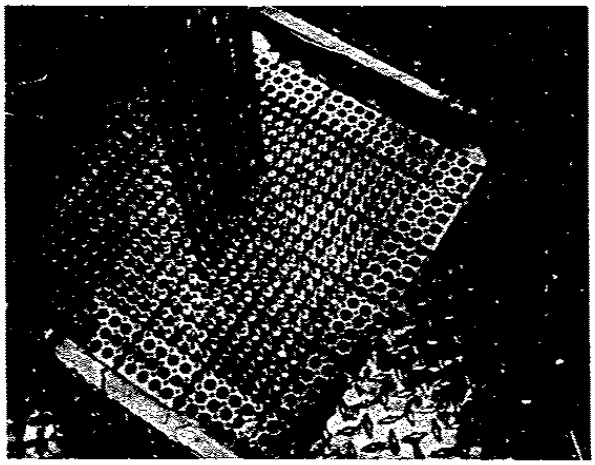

Fig. 5. Single-region configuration with a nine-rod slot pattern.

Table 1. Reported data for single-region experiments with 8% ^{240}Pu

Case No.	Core diagram (Fig. No.)	Measurement type	Lattice pitch (cm)	Number of fuel rods	Boron concentration (ppm)	CWH (cm)	Test configuration
1	6	Buckling	1.7526	514	0	97.93	–
2	7	Buckling	1.7526	552	0	85.87	–
3	8	Buckling	1.9050	321	0	95.86	–
4	9	Buckling	2.4785	160	0	93.52	–
5	10	Buckling	2.4785	169	0	85.62	–
6	11	Buckling	2.6942	152	0	94.51	–
7	12	Buckling	3.5052	249	0	94.40	–
8	13	Buckling	1.7526	631	261	95.86	–
9	14	Buckling	2.4785	243	261	93.48	–
10	15	Buckling	1.7526	749	526	94.75	–
11	16	Buckling	2.4785	379	526	92.28	–
12	–	Reactivity	1.7526	575	0	77.31	Reference clean core
13	17	Reactivity	1.7526	574	0	75.61	Center water hole
14	17	Reactivity	1.7526	574	0	86.88	Center Ag-In-Cd rod
15	17	Reactivity	1.7526	574	0	76.46	Center void (Zr tube)
16	17	Reactivity	1.7526	574	0	82.36	Center cobalt rod
17	18	Reactivity	1.7526	570	0	70.95	Center five-hole water slot
18	–	Reactivity	1.7526	729	0	53.19	Reference clean core
19	19	Reactivity	1.7526	720	0	68.17	Nine uniformly distributed Ag-In-Cd rods
20	20	Reactivity	1.7526	720	0	96.34	Nine loose cluster Ag-In-Cd rods
21	21	Reactivity	1.7526	720	0	92.82	Nine tight cluster Ag-In-Cd rod
22	22	Reactivity	1.7526	720	0	86.41	Nine center slot Ag-In-Cd rods
23	–	Reactivity	1.7526	729	116	60.91	Reference borated core
24	19	Reactivity	1.7526	720	116	83.15	Nine uniformly distributed Ag-In-Cd rods
25	19	Reactivity	1.7526	720	116	58.06	Nine uniformly distributed water holes
26	–	Reactivity	1.7526	729	261	73.47	Reference borated core
27	–	Reactivity	1.7526	729	315	78.82	Reference borated core
28	23	Reactivity	1.7526	728	315	77.76	Center water hole
29	23	Reactivity	1.7526	728	315	88.37	Center Ag-In-Cd rod
30	23	Reactivity	1.7526	728	315	79.37	Center void (Zr tube)
31	23	Reactivity	1.7526	728	315	83.97	Center cobalt rod
32	24	Reactivity	1.7526	724	315	75.10	Center five-hole water slot
33	–	Reactivity	1.9050	441	0	52.72	Reference core
34	25	Reactivity	1.9050	432	0	50.90	Nine uniformly distributed water holes
35	25	Reactivity	1.9050	432	0	77.26	Nine uniformly distributed Ag-In-Cd rods
36	26	Reactivity	1.9050	440	0	52.26	Center water hole
37	26	Reactivity	1.9050	440	0	56.72	Center Ag-In-Cd rod
38	26	Reactivity	1.9050	440	0	52.60	Center void (Zr tube)
39	27	Reactivity	1.9050	441	0	53.67	4 × 4 voids (Al tubes)
40	28	Reactivity	1.9050	441	0	59.03	10 × 10 voids (Al tubes)
41	17	Power distribution	1.7526	574	0	75.68	Center water hole
42	18	Power distribution	1.7526	570	0	70.95	Five-rod water slot
43	23	Power distribution	1.7526	728	315	77.77	Center water hole
44	24	Power distribution	1.7526	724	315	75.11	Five-rod water slot
45	25	Power distribution	1.9050	440	0	52.23	Center water hole

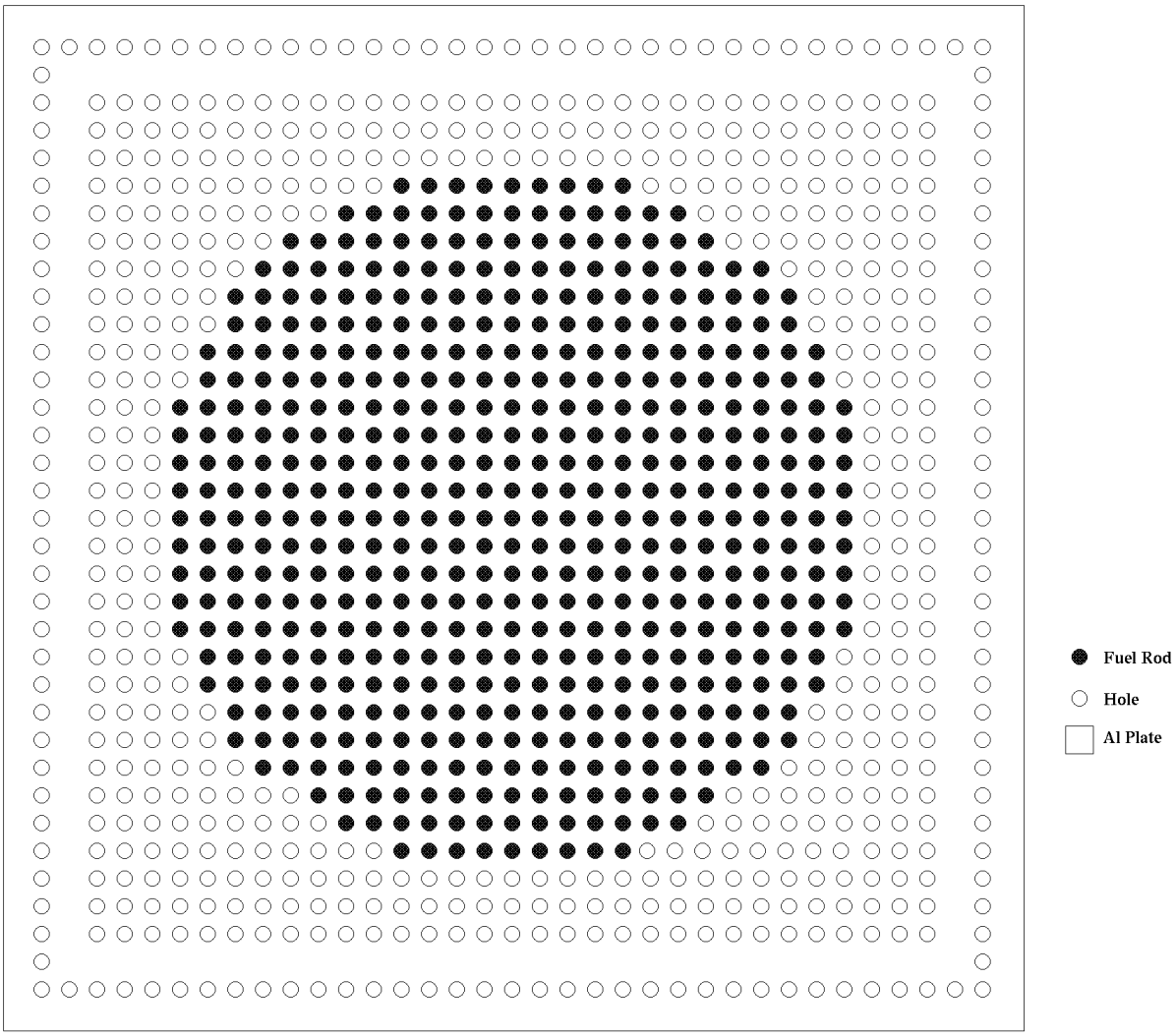

Fig. 6. Cylindrical core configuration with 8% ^{240}Pu in a 1.7526-cm lattice.

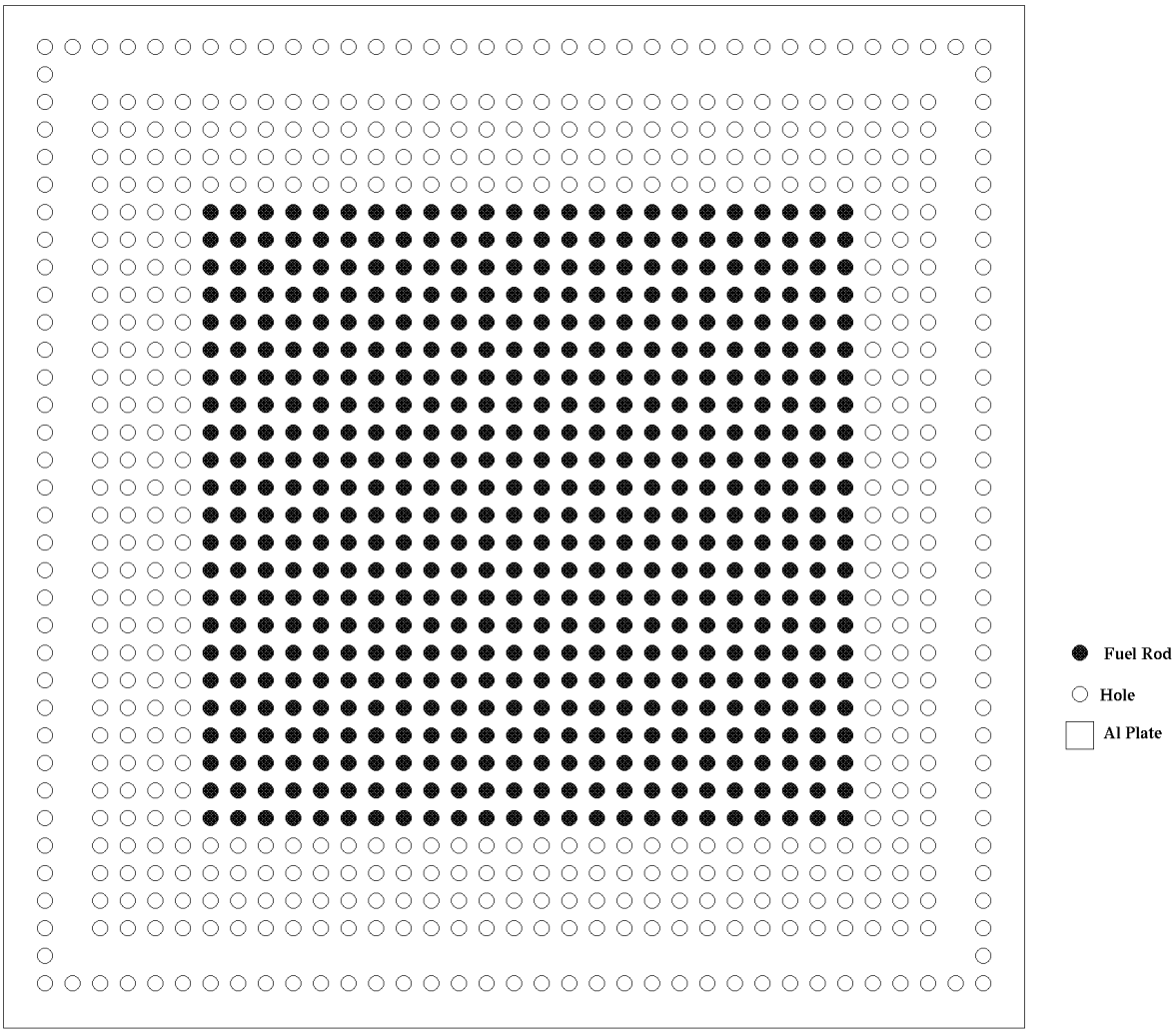

Fig. 7. A 24x23 rectangular core configuration with 8% ^{240}Pu in a 1.7526-cm lattice.

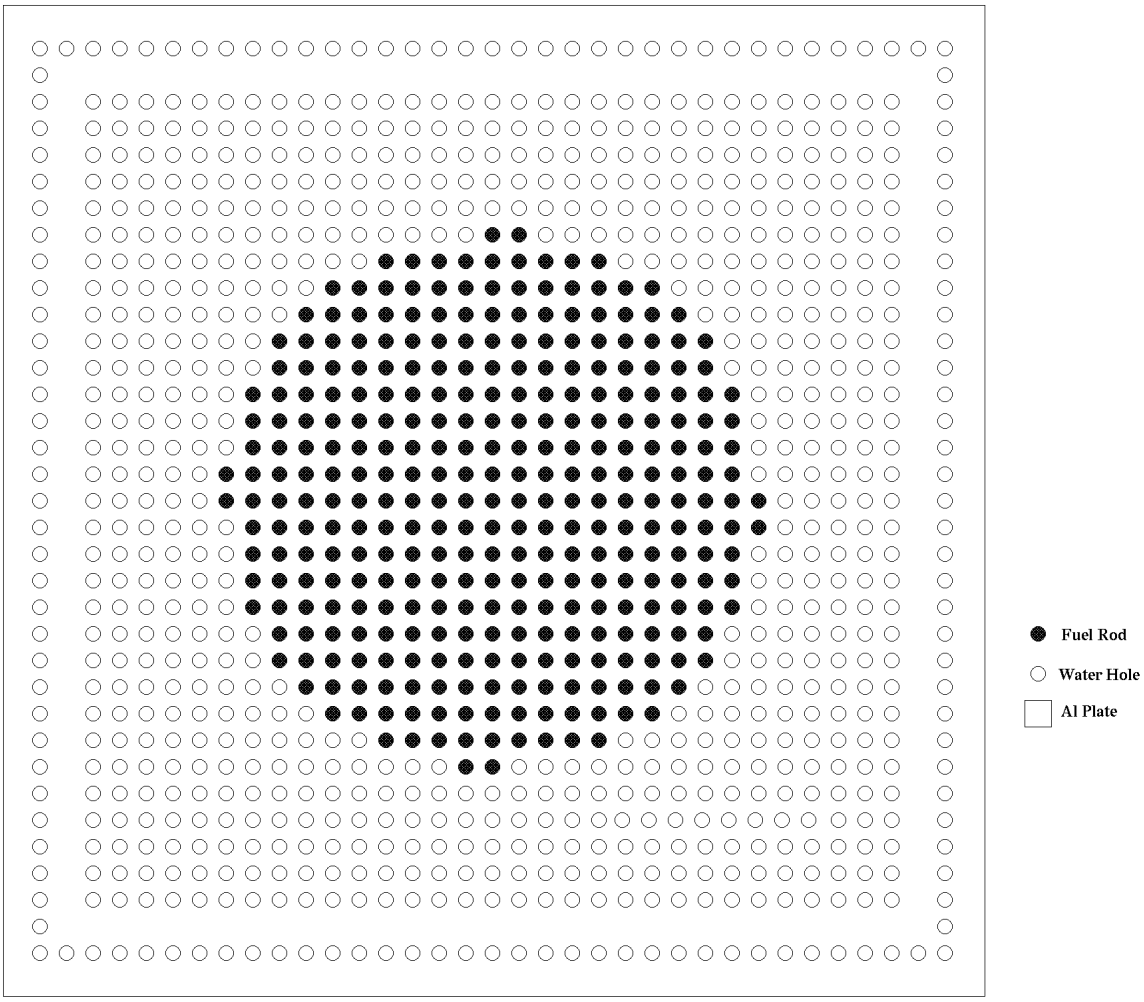

Fig. 8. Cylindrical core configuration with 8% ^{240}Pu in a 1.9050-cm lattice.

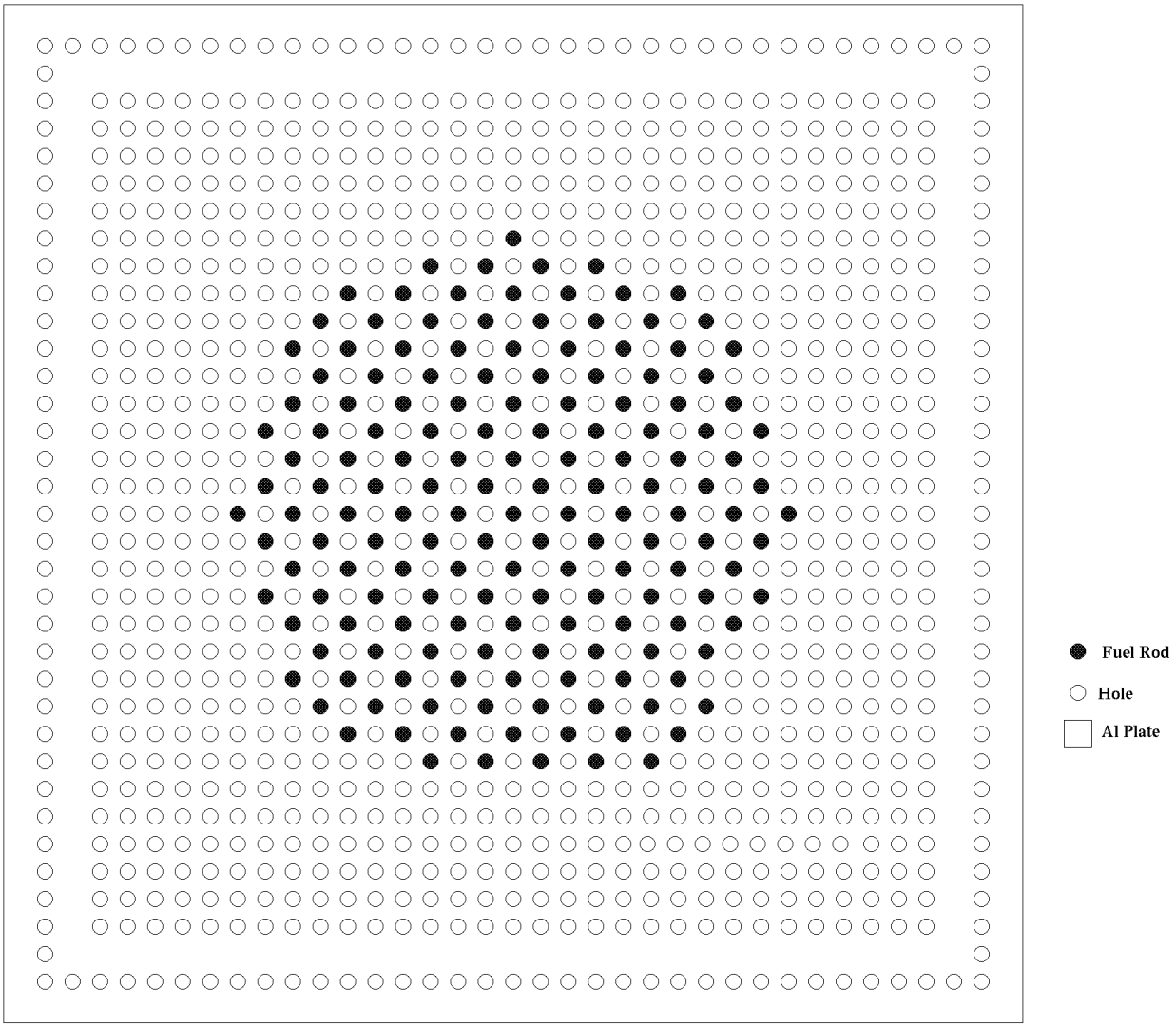

Fig. 9. Cylindrical core configuration with 8% ^{240}Pu in a 2.4785-cm lattice.

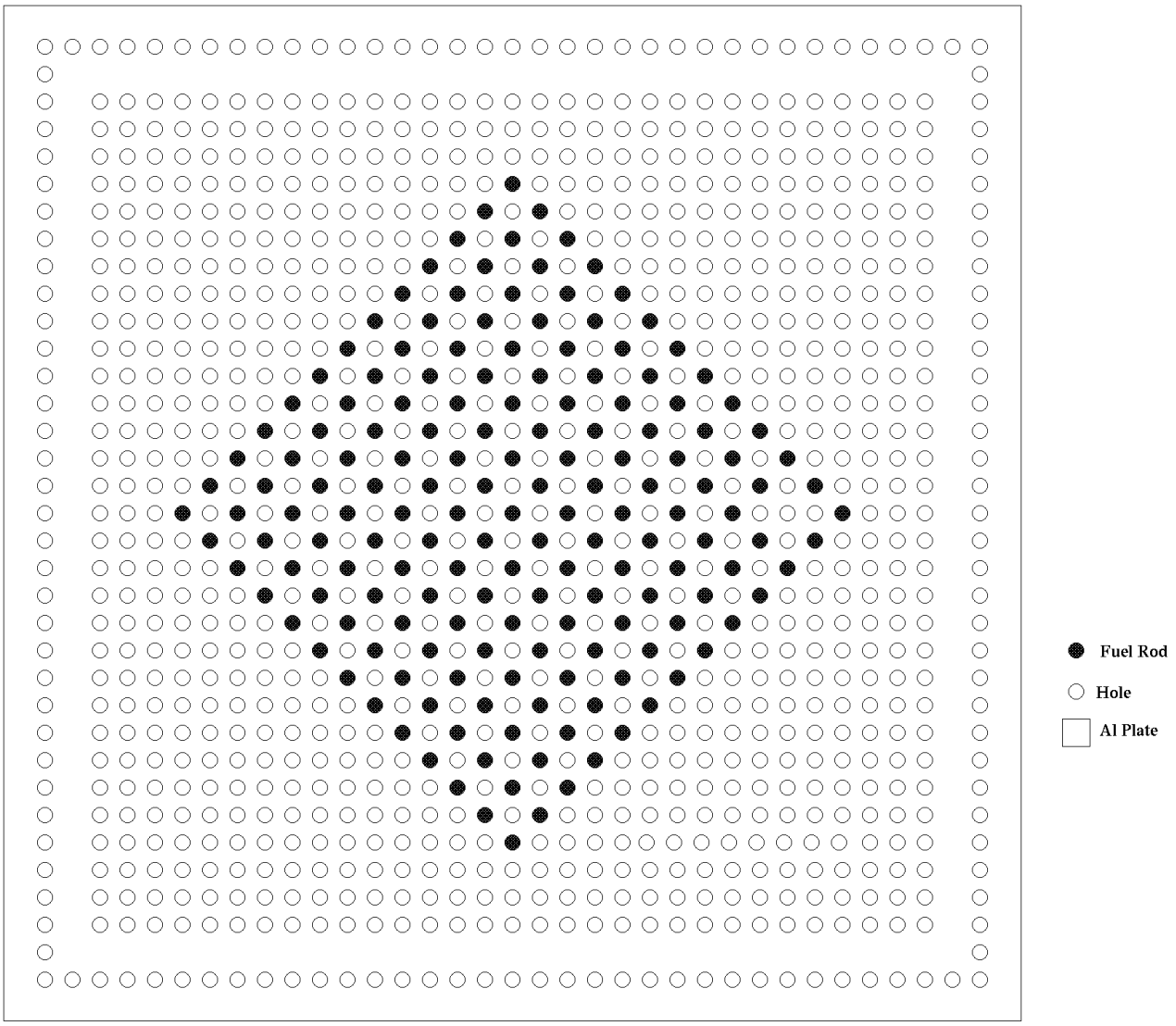

Fig. 10. A 13x13 square core configuration with 8% ^{240}Pu in a 2.4785-cm lattice.

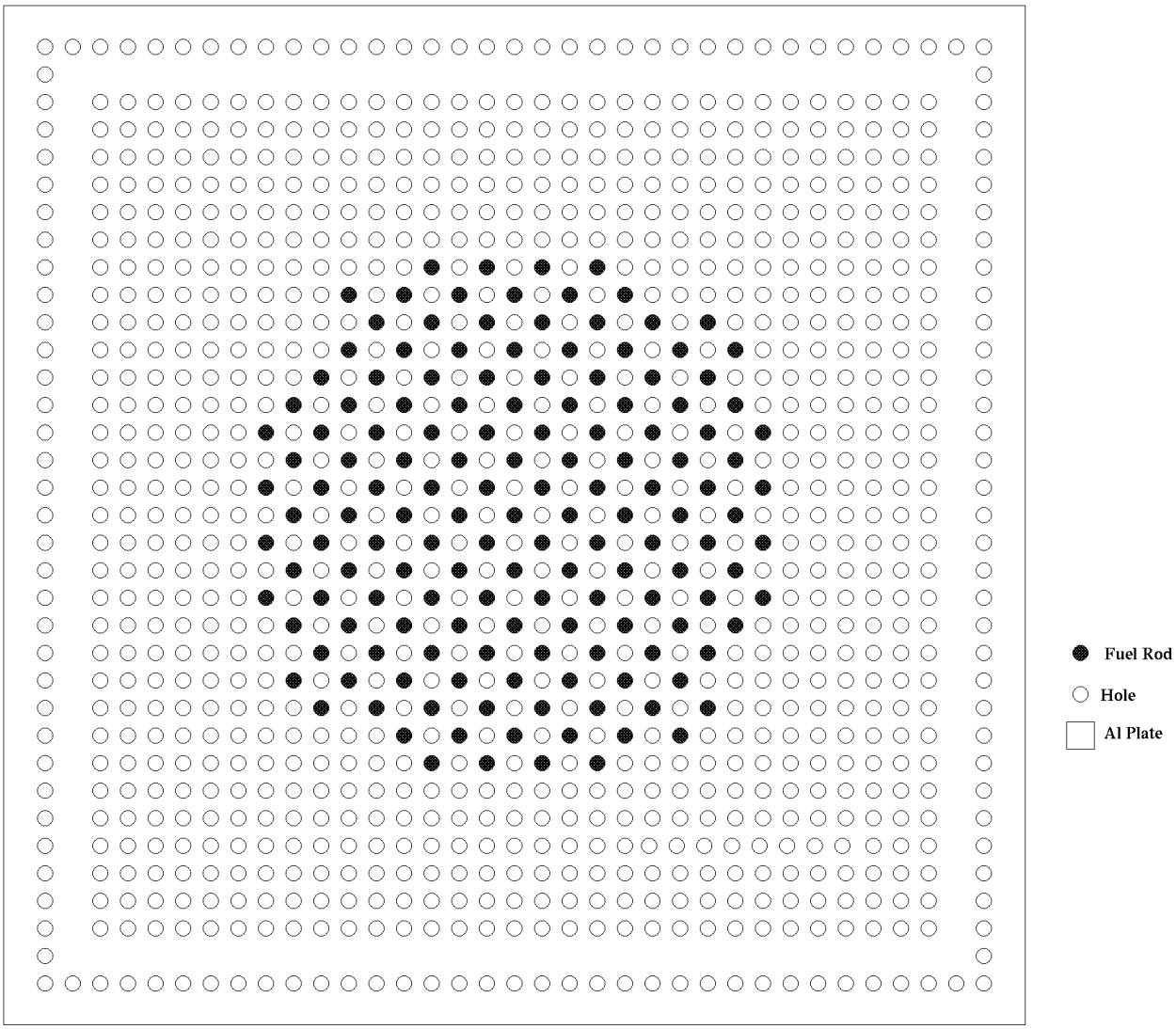

Fig. 11. Cylindrical core configuration with 8% ^{240}Pu in a 2.6942-cm lattice.

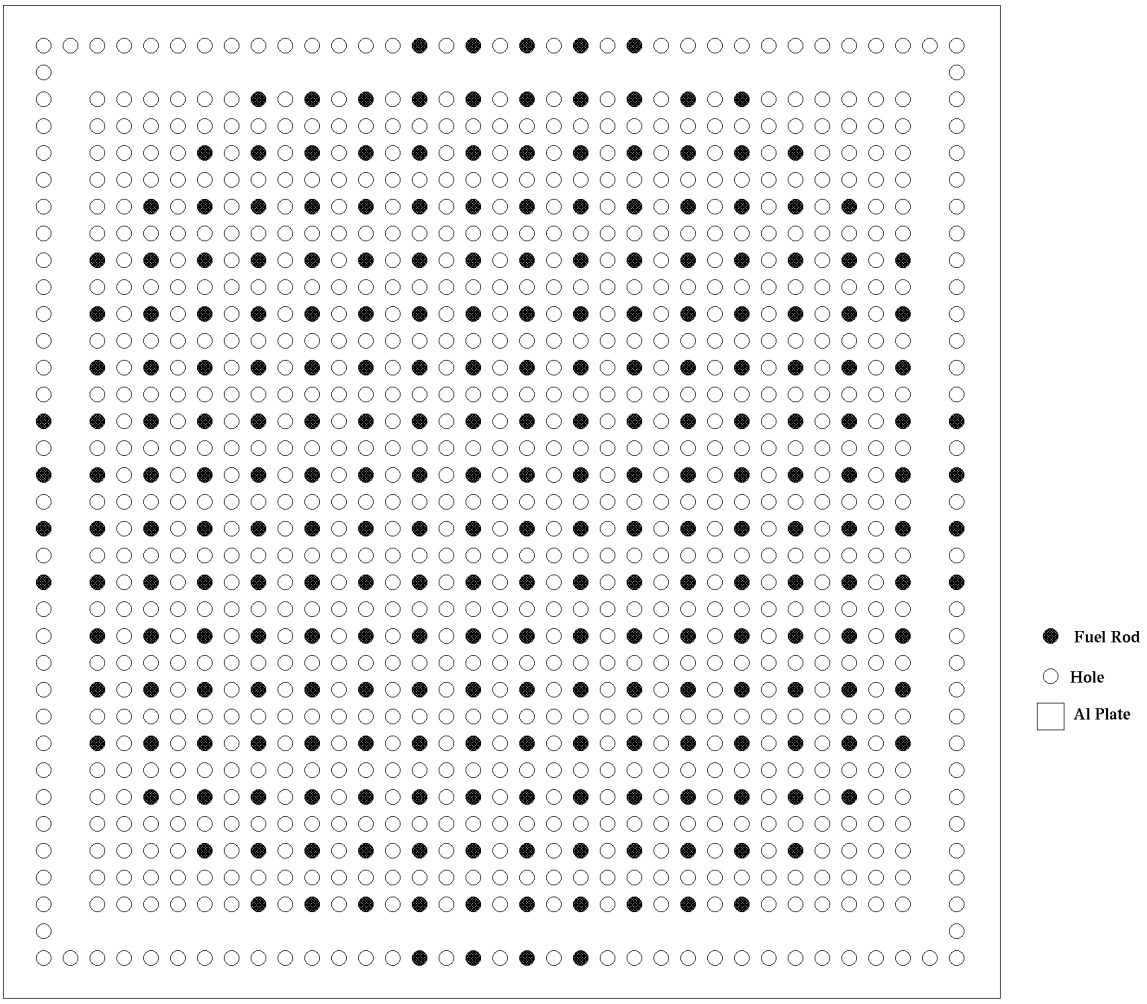

Fig. 12. Cylindrical core configuration with 8% ^{240}Pu in a 3.5052-cm lattice.

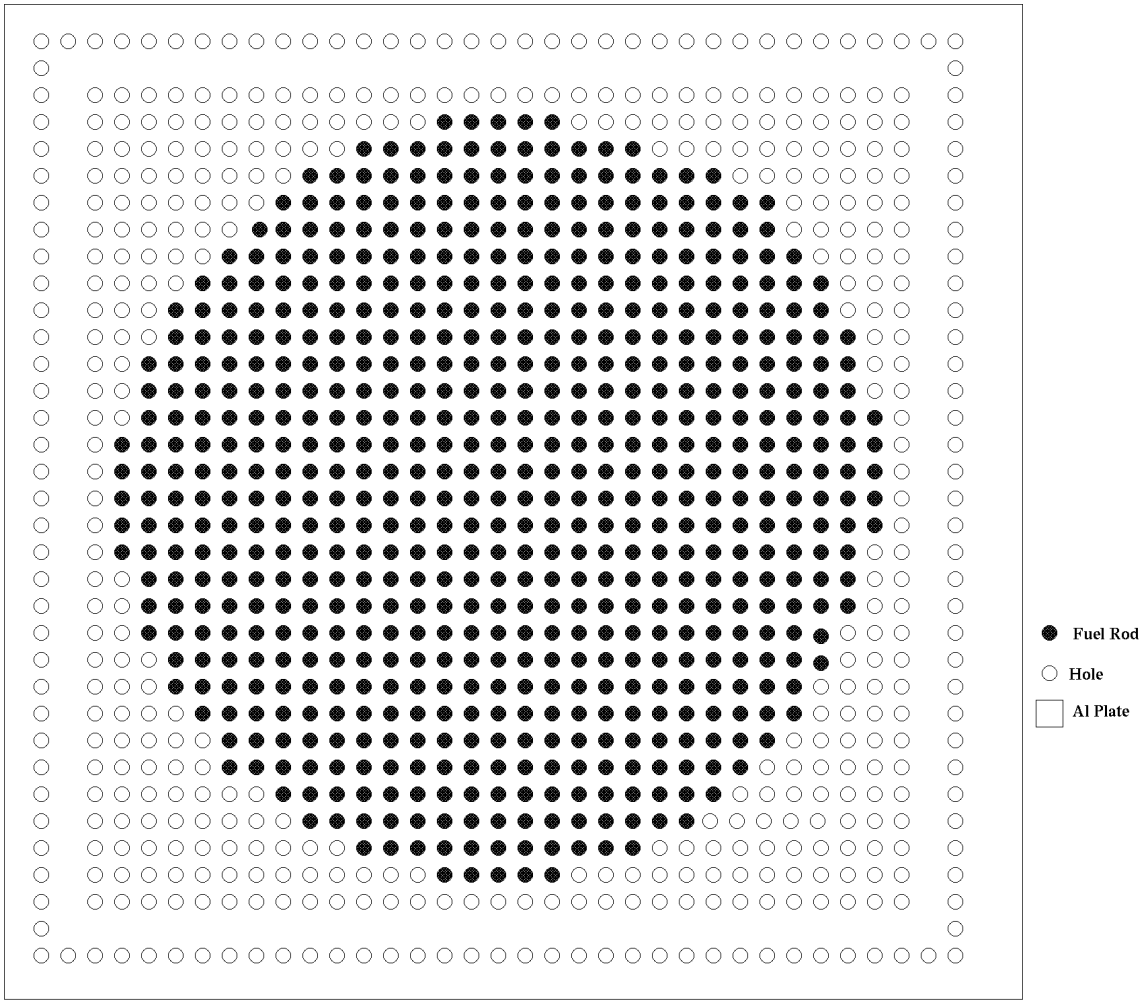

Fig. 13. Cylindrical borated core configuration with 8% ^{240}Pu in a 1.7526-cm lattice.

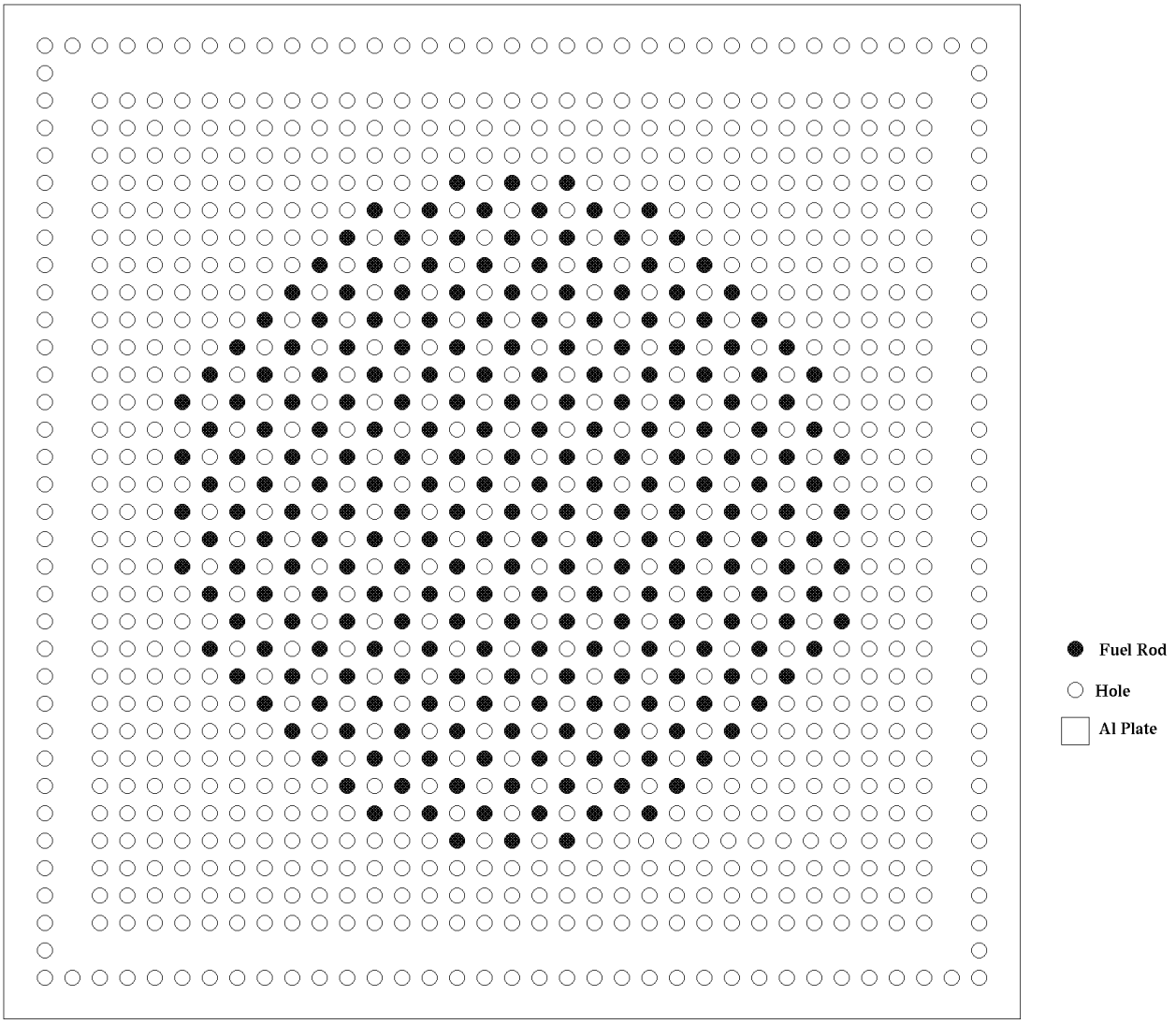

Fig. 14. Cylindrical borated core configuration with 8% ^{240}Pu in a 2.4785-cm lattice.

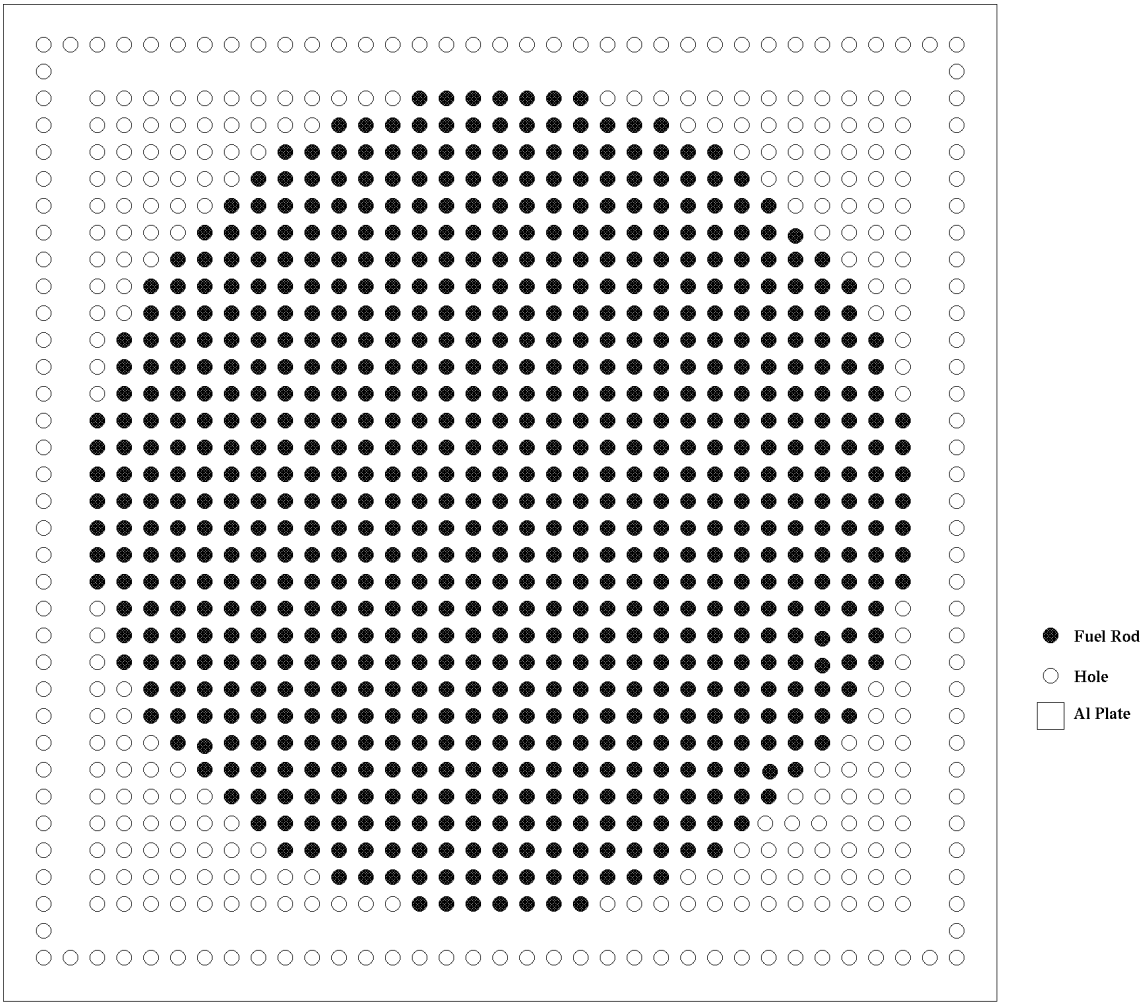

Fig. 15. Cylindrical borated core configuration with 8% ^{240}Pu in a 1.7526-cm lattice.

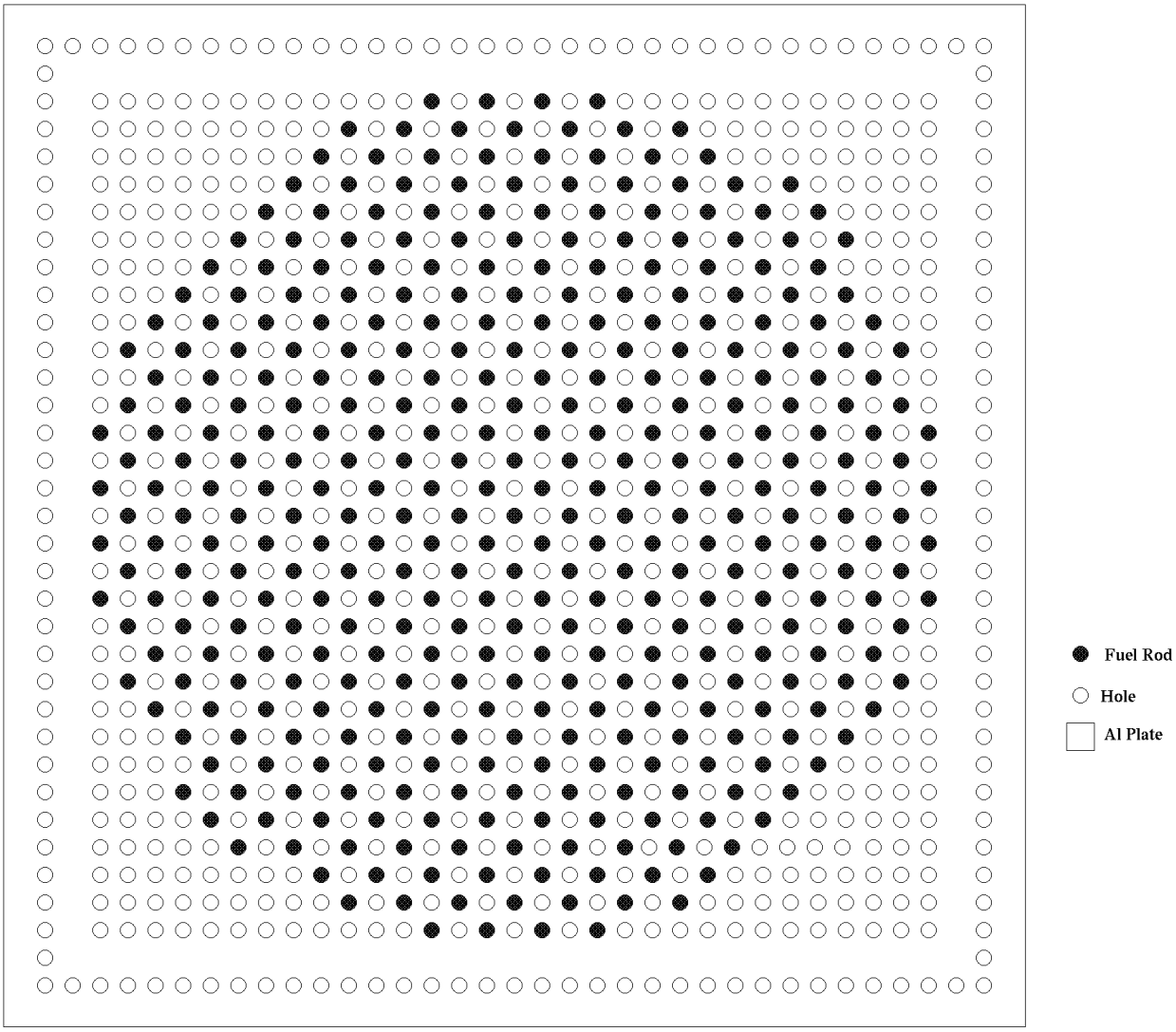

Fig. 16. Cylindrical borated core configuration with 8% ^{240}Pu in a 2.4785-cm lattice.

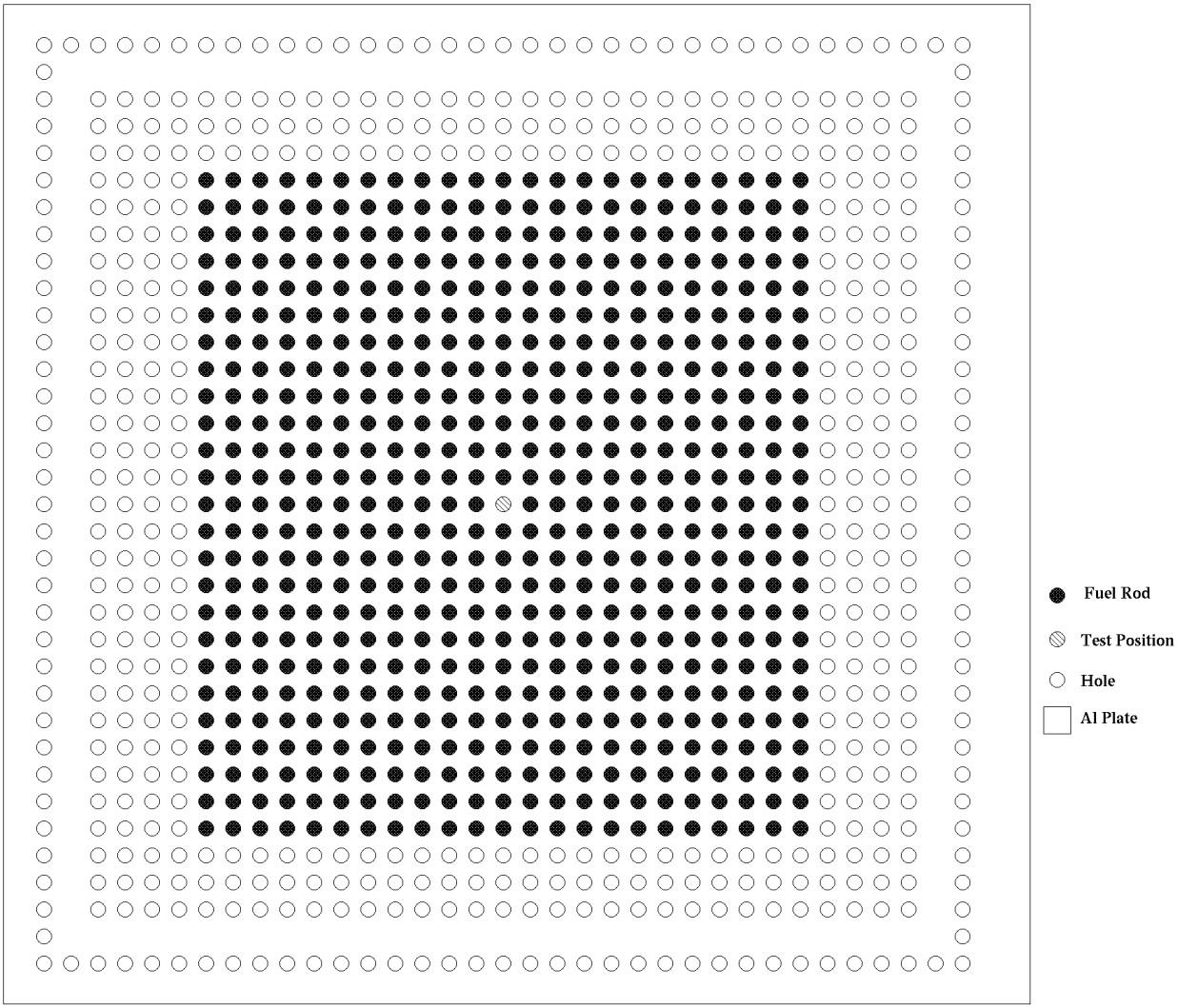

Fig. 17. A 23x25 rectangular core configuration with a center test position in a 1.7526-cm lattice.

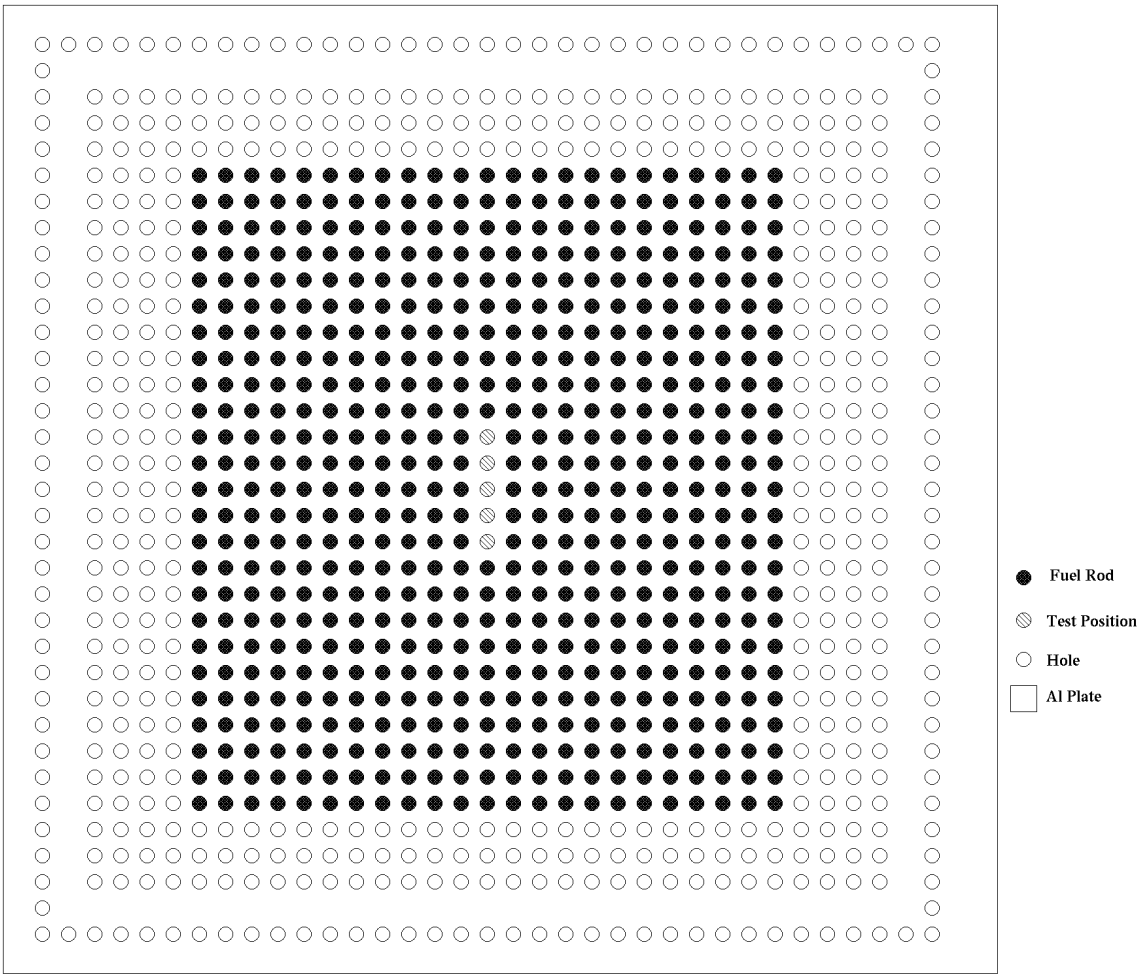

Fig. 18. A 23x25 rectangular core configuration with a five-rod slot pattern in a 1.7526-cm lattice.

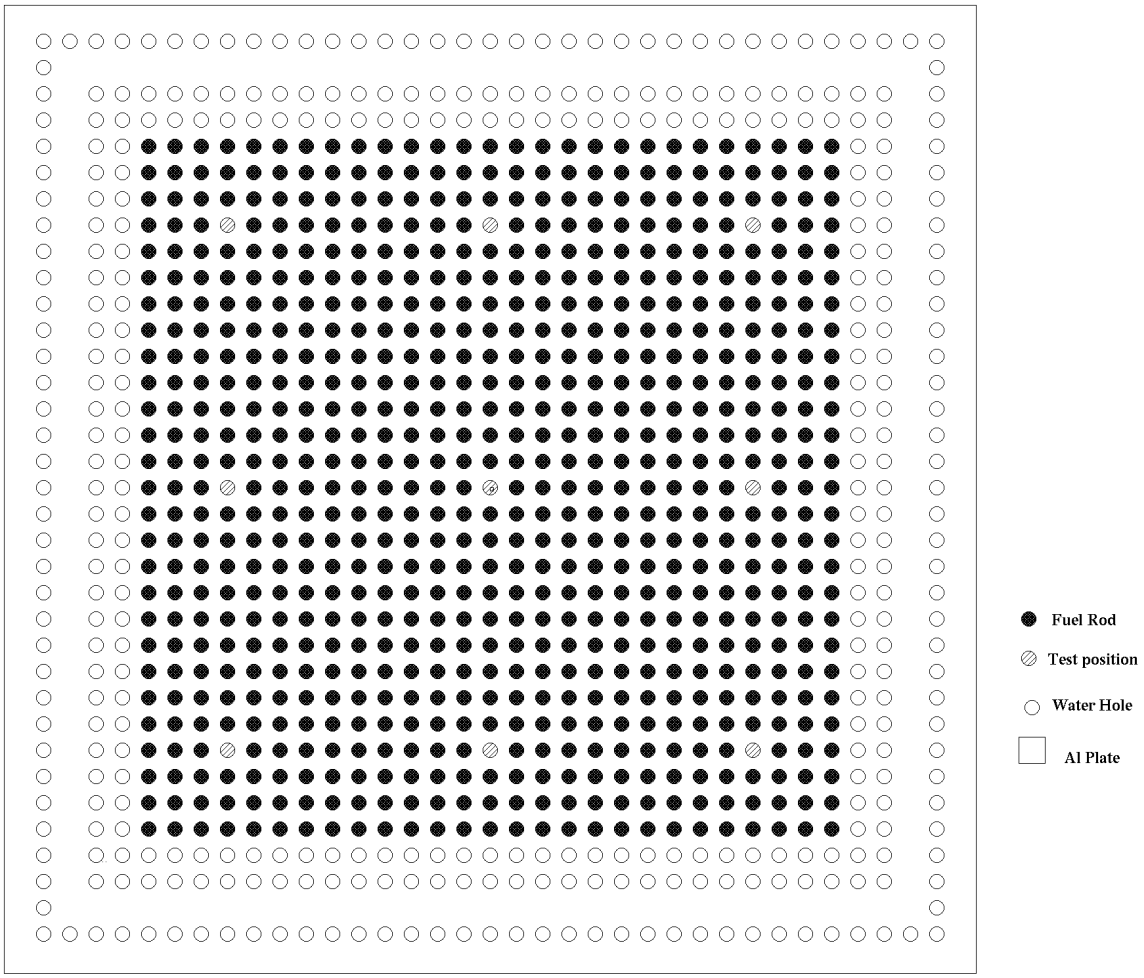

Fig. 19. A 27x27 rectangular core configuration with a nine uniformly distributed rod pattern in a 1.7526-cm lattice.

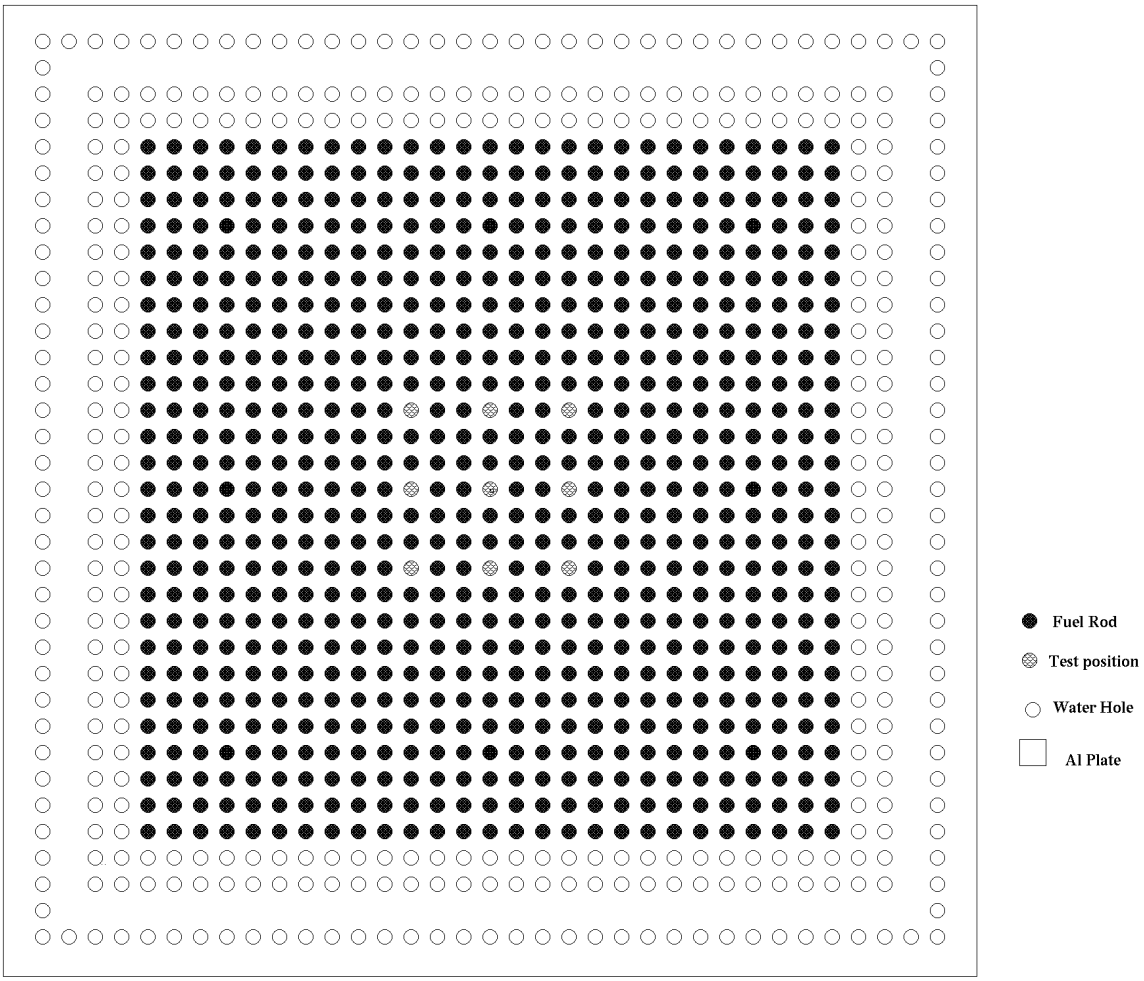

Fig. 20. A 27x27 rectangular core configuration with a nine loose cluster rod pattern in a 1.7526-cm lattice.

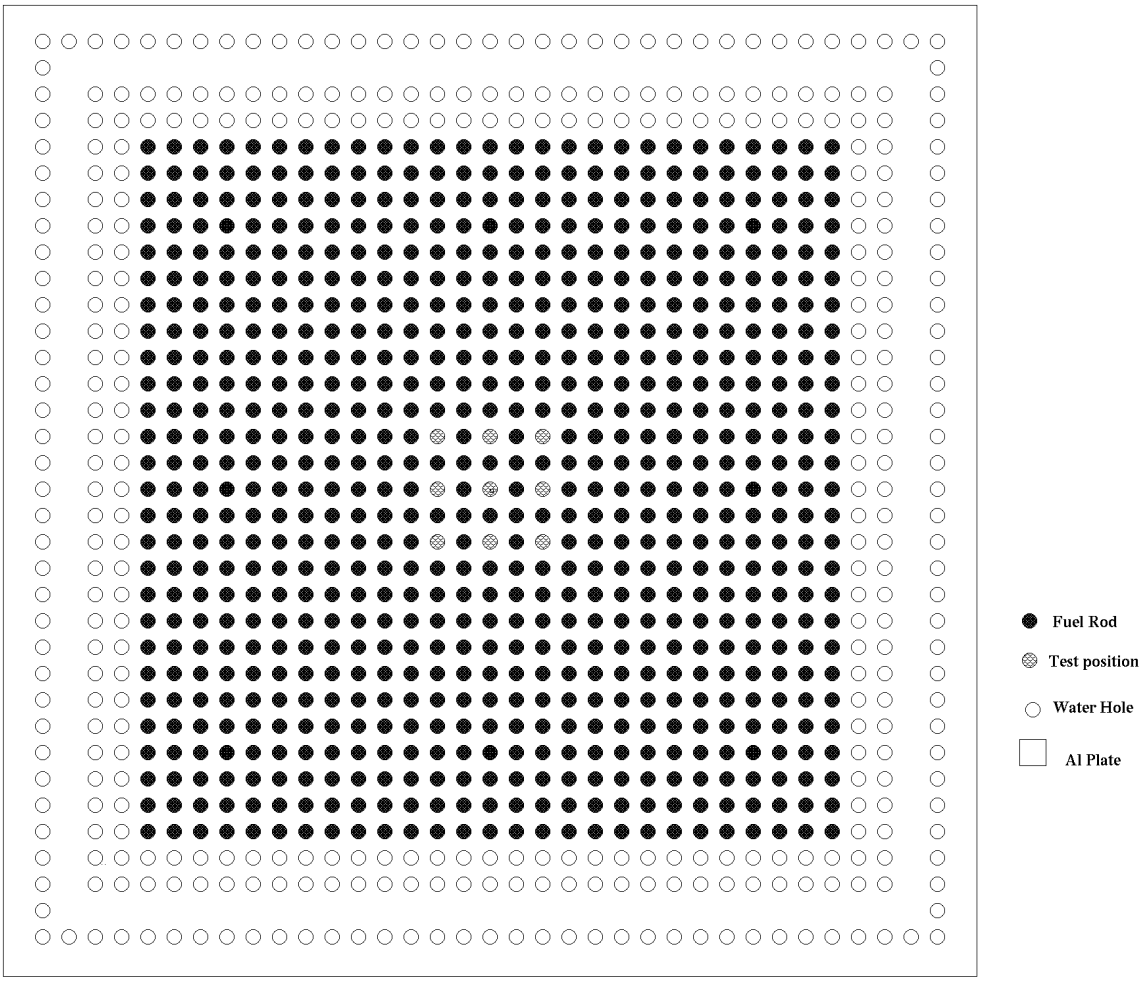

Fig. 21. A 27x27 rectangular core configuration with a nine tight cluster rod pattern in a 1.7526-cm lattice.

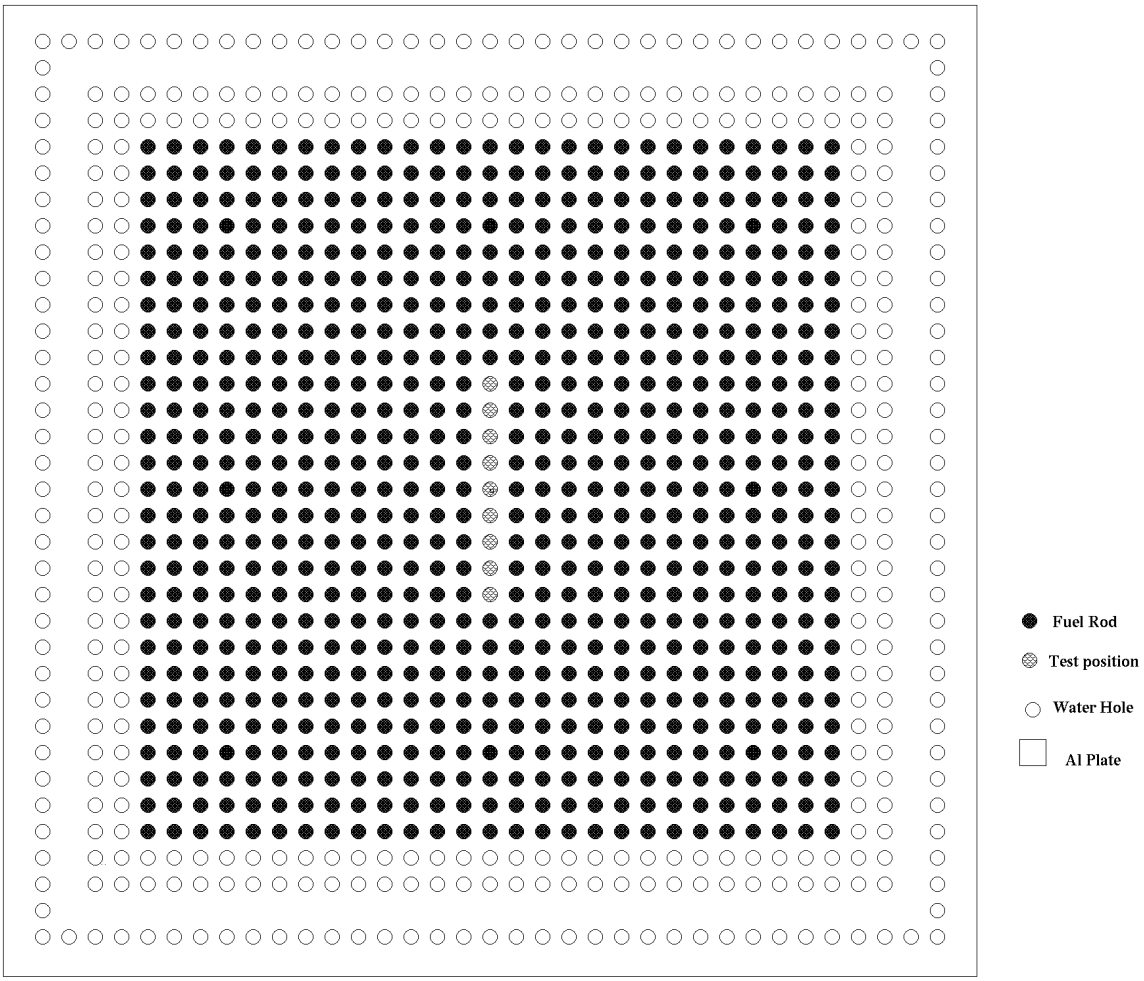

Fig. 22. A 27x27 rectangular core configuration with a nine-rod slot pattern in a 1.7526-cm lattice.

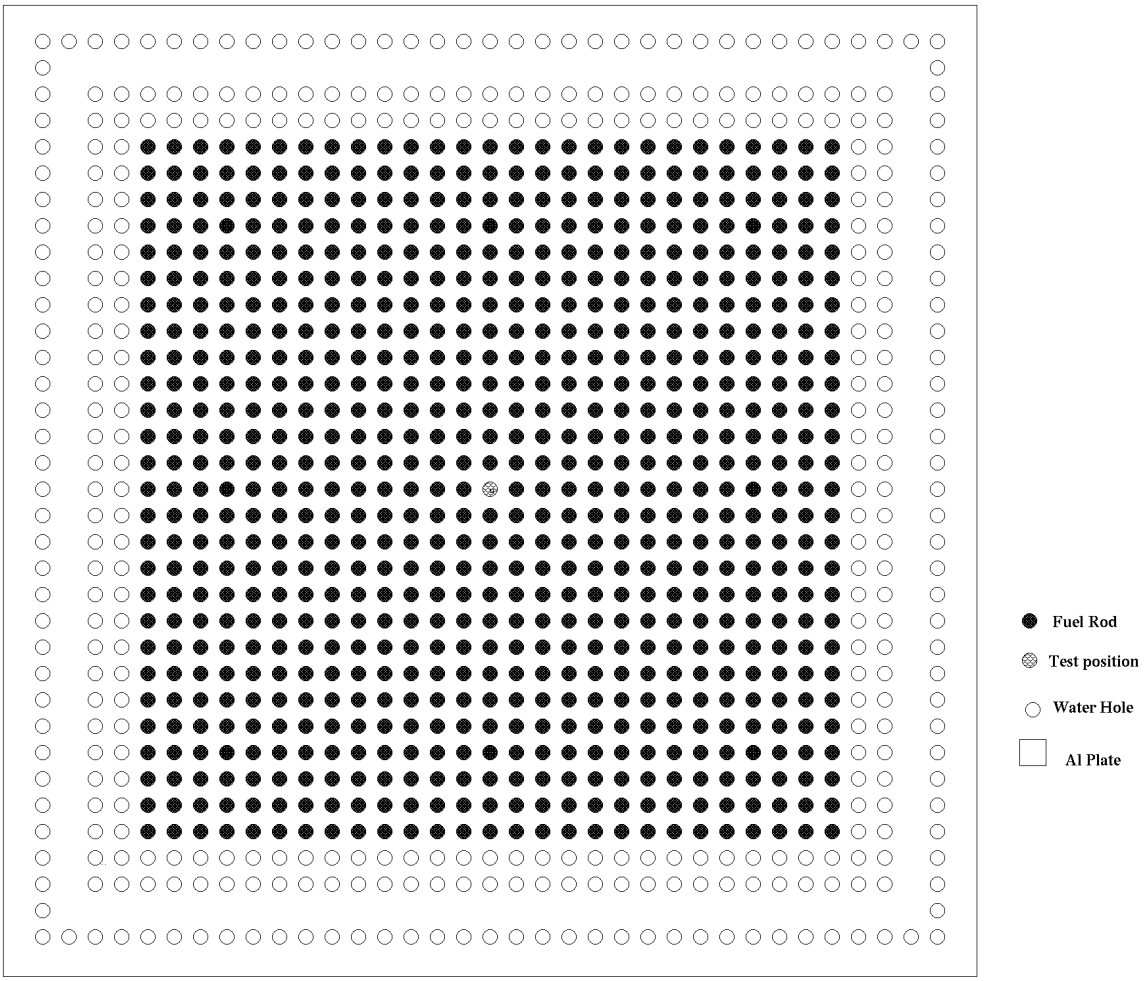

Fig. 23. A 27x27 rectangular core configuration with a center test position in a 1.7526-cm lattice.

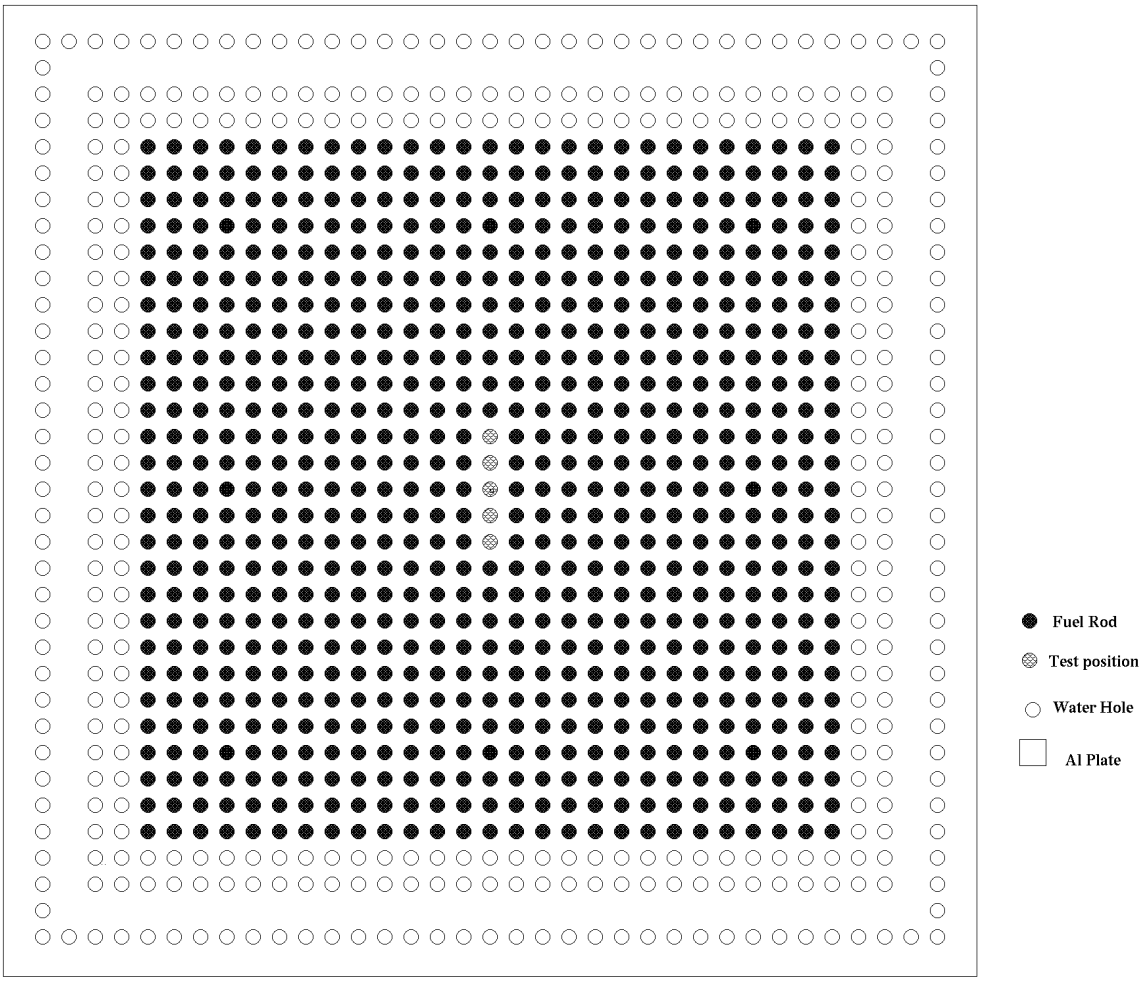

Fig. 24. A 27x27 rectangular core configuration with a five-rod slot pattern in a 1.7526-cm lattice.

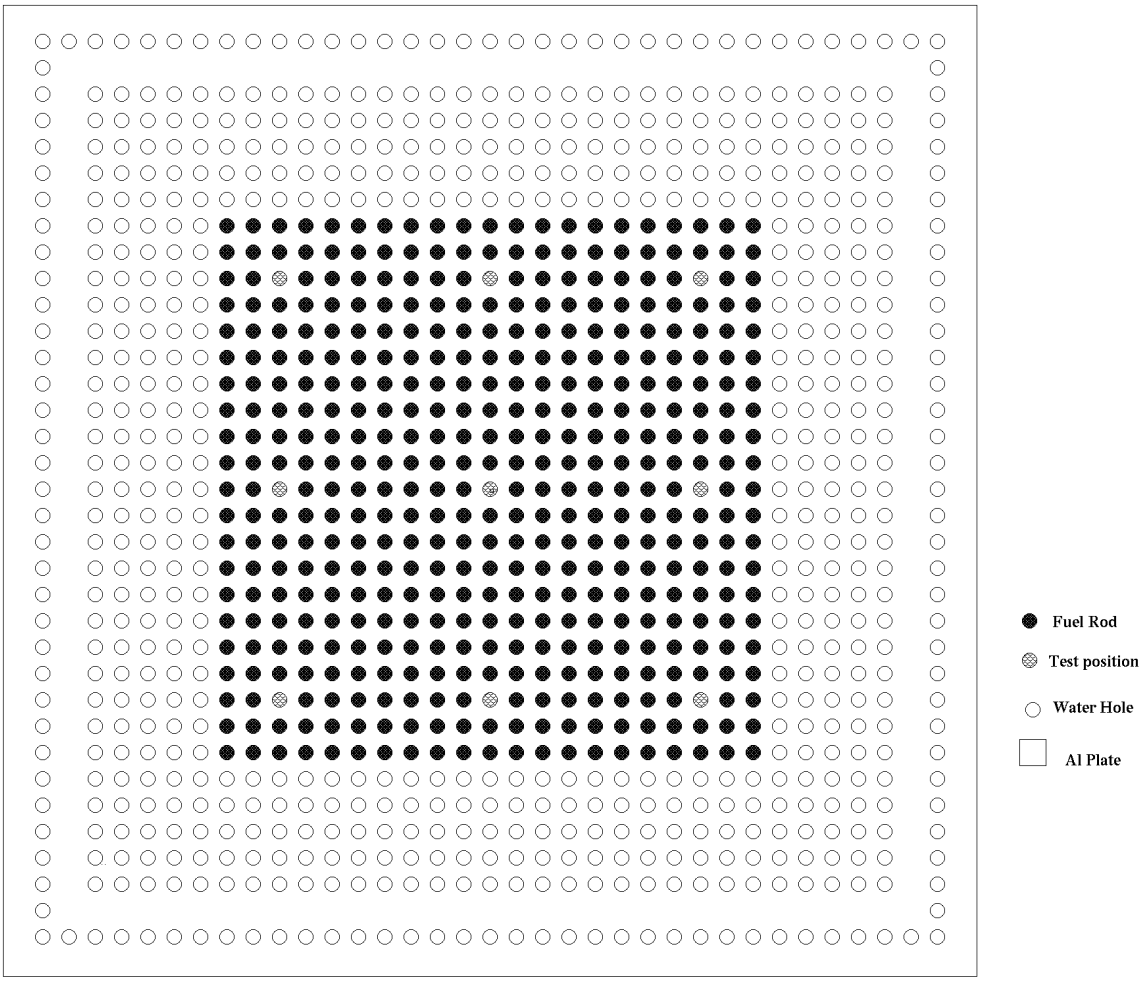

Fig. 25. A 21x21 rectangular core configuration with a nine uniformly distributed rod pattern in a 1.9050-cm lattice.

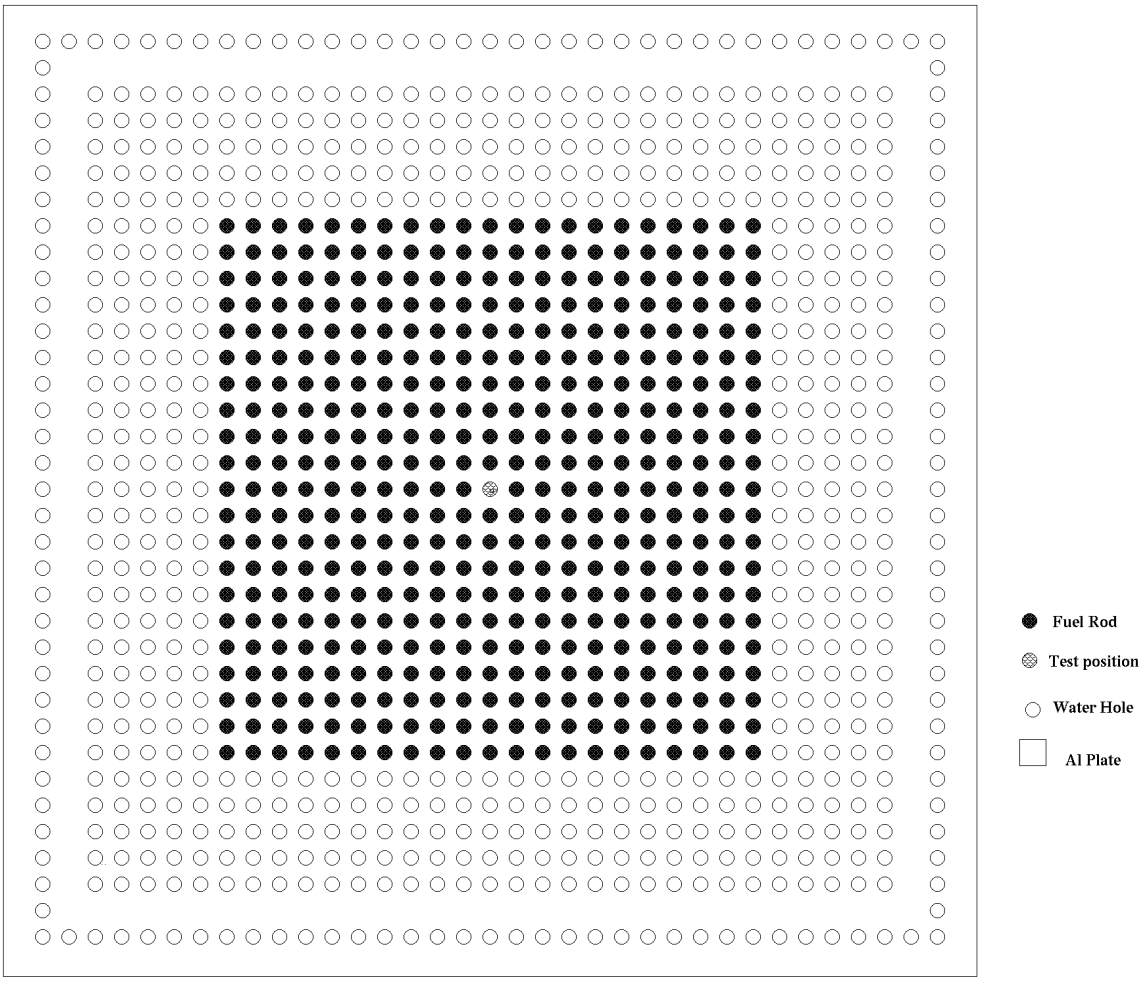

Fig. 26. A 21x21 rectangular core configuration with a center test position in a 1.9050-cm lattice.

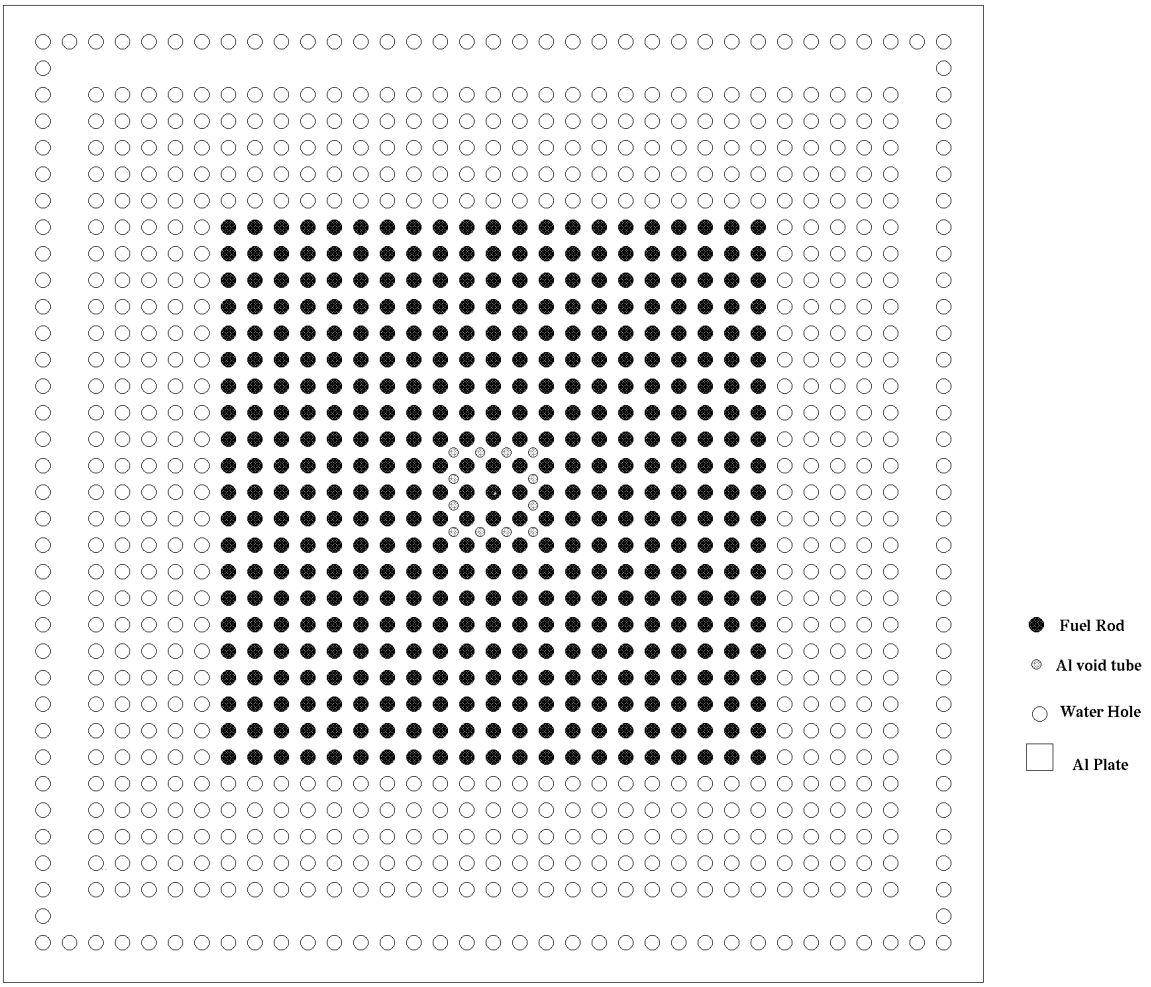

Fig. 27. A 21x21 rectangular core configuration with a 4×4 central void pattern in a 1.9050-cm lattice.

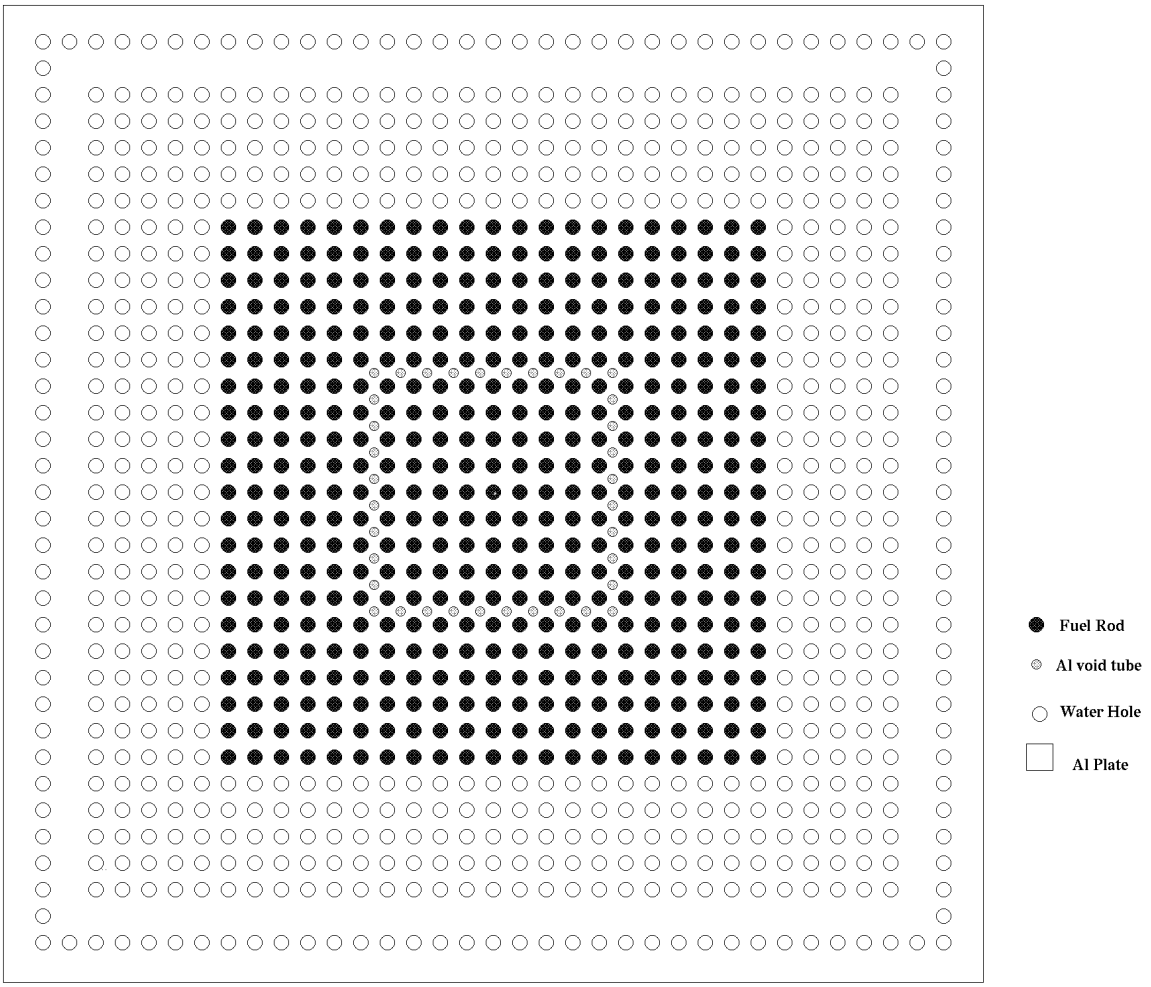

Fig. 28. A 21x21 rectangular core configuration with a 10×10 central void pattern in a 1.9050-cm lattice.

1.4 Single-Region Critical Experiments with 24 wt% ^{240}Pu MOX Fuel

This type of MOX fuel was identical in dimensions to 8% ^{240}Pu fuel. The only difference between these fuels was the vector of plutonium isotopes. The compositions of plutonium isotopes for both 8% and 24% ^{240}Pu fuel are given in Sect. 1.8.

Buckling and reactivity worth measurements were performed for this type of MOX fuel in single-region core configurations. Buckling measurements were made for 2.4785- and 2.6942-cm lattice pitches with cylindrical core configurations. Reactivity worth measurements were carried out for a 2.6942-cm lattice pitch. Reactivity worth of a center water hole and a silver-indium-cadmium control rod was measured. A power distribution measurement was performed for the 2.6942-cm lattice pitch. This configuration was identical to the configuration used for reactivity worth measurement. The CWH was the same for both measurements for this case. All experiments were performed for clean cores.

The installation of the MOX fuel is given in Fig. 1. Reported data for 24% ^{240}Pu including measurement type and core diagram number are presented in Table 2. Core configurations are shown in Figs. 29–31. For the schematic representation of the core configurations, the core mid-plane aluminum plate is taken as the reference plane. In these figures, the legend label "hole" refers to the fuel rod holes in the aluminum plate. In the absence of fuel or other rods (control rods), these holes were filled with water. Information on core diagram numbers and measurement types is also included in Table 2.

Table 2. Reported data for single-region experiments with 24% ^{240}Pu

Case No.	Core diagram (Fig. No.)	Measurement type	Lattice pitch (cm)	Number of fuel rods	Boron concentration (ppm)	CWH (cm)	Test configuration
46	29	Buckling	2.4785	247	0	94.32	–
47	30	Buckling	2.6942	243	0	92.87	–
48	–	Reactivity	2.6942	301	0	61.22	Reference core
49	31	Reactivity	2.6942	300	0	62.62	Center water hole
50	31	Reactivity	2.6942	300	0	69.18	Center Ag-In-Cd rod
51	31	Power distribution	2.6942	300	0	62.62	Center water hole

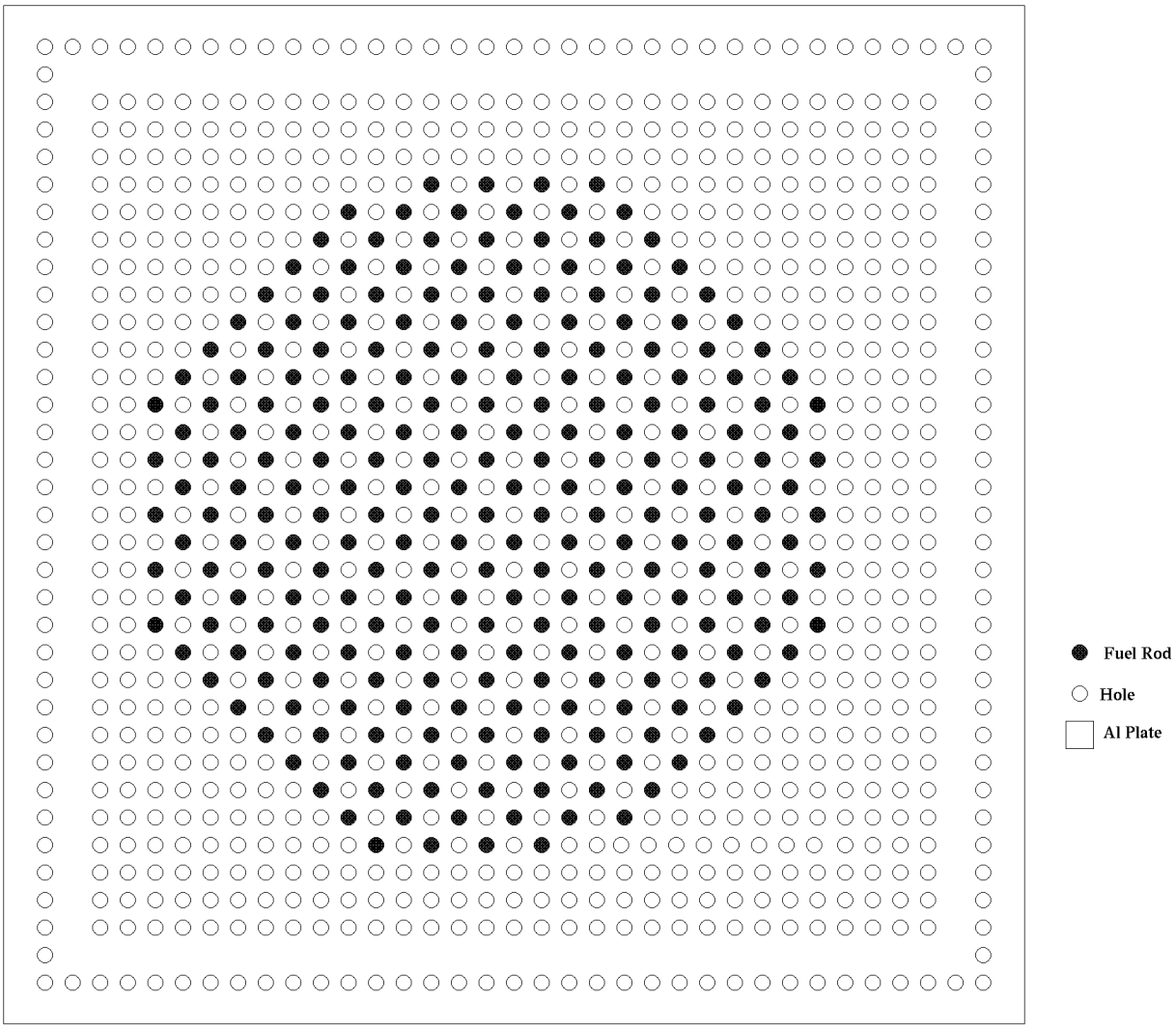

Fig. 29. Cylindrical core configuration with 24% ^{240}Pu in a 2.4785-cm lattice.

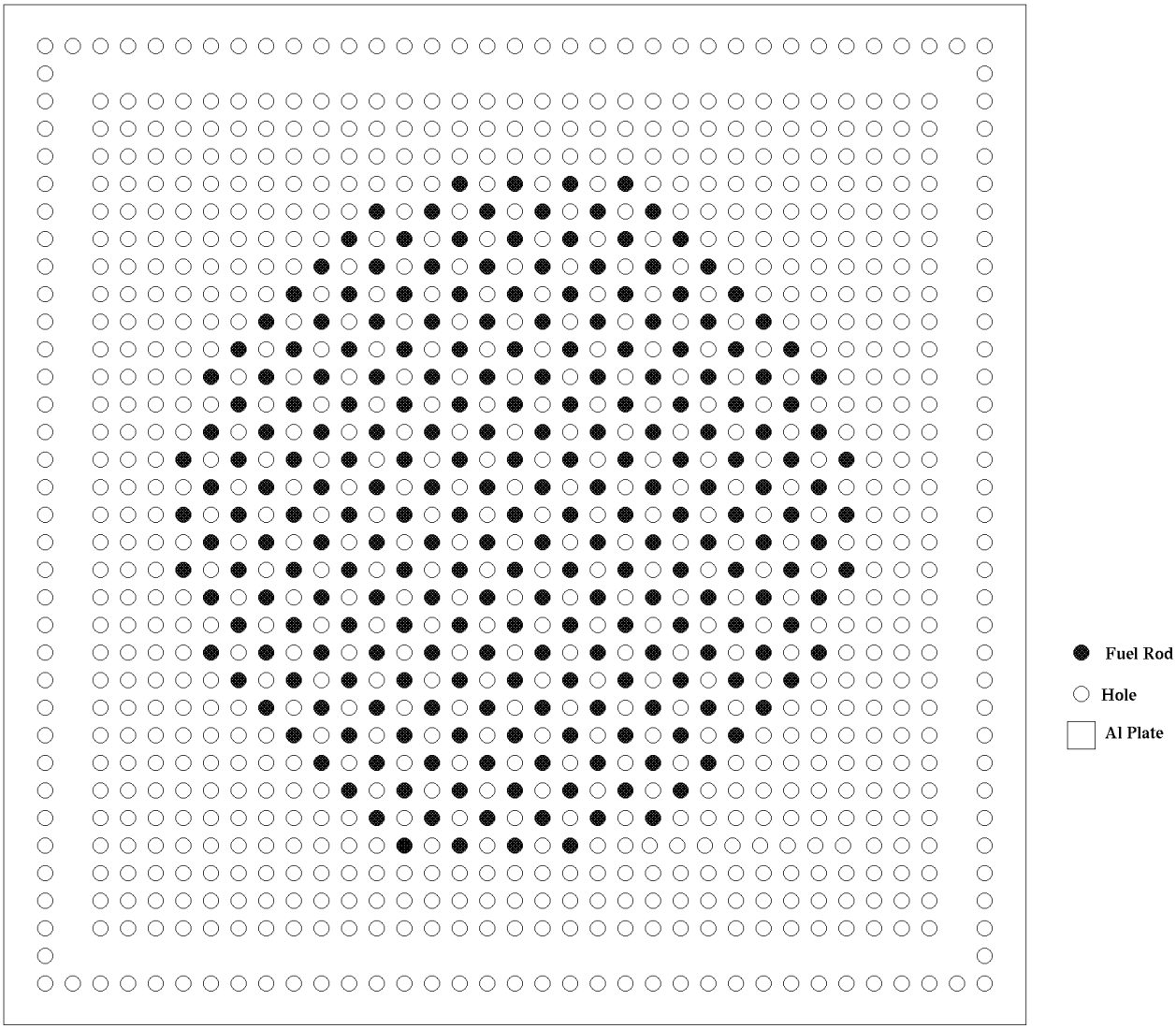

Fig. 30. Cylindrical core configuration with 24% ^{240}Pu in a 2.6942-cm lattice.

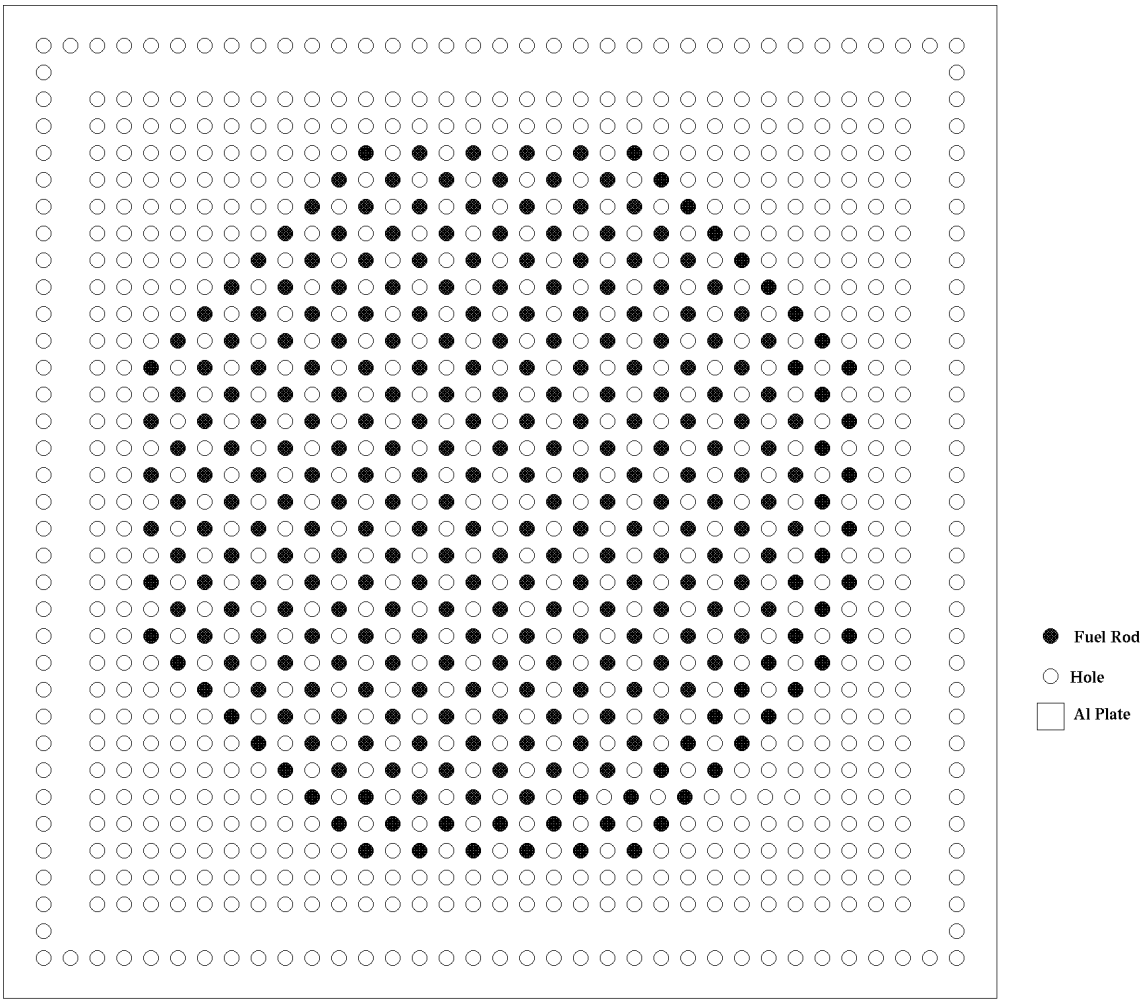

Fig. 31. Cylindrical core configuration with 24% ^{240}Pu in a 2.6942-cm lattice with a center test position.

1.5 Single-Region Critical Experiments with UO_2 Fuel

In addition to MOX fuels, a low-enriched (2.72 wt%) UO_2 fuel was used during the experimental program. Single-region experiments with UO_2 fuel were performed to compare with the plutonium data and later to use in multiregion experiments. Only two single-region experiments were performed with UO_2 fuel. Buckling measurement experiments were performed with lattice pitches of 1.7526 cm and 2.4785 cm. Both experiments were performed in clean cores. A cylindrical core configuration was constructed.

Installation of UO_2 fuel in a uniform lattice is shown in Fig. 32. Fuel rods were supported by three layers of aluminum plates. The thickness of the bottom and top plate was 1.27 cm, and the thickness of the central plate was 0.635 cm. Fuel rods rested on a 1.27-cm aluminum plate, and 0.635 cm above the plate, a second aluminum plate with a thickness of 3.175 cm was installed. Reported data for single-region experiments with UO_2 fuel are given in Table 3. Core configurations for these experiments are shown in Figs. 33 and 34. For the schematic representation of the core configurations, the midcore aluminum plate was taken as the reference plane. In these figures, the legend label "hole" represents the fuel rod holes in the aluminum plate. In the absence of fuel or other rods (control rods), these holes were filled with water. Information on core diagram numbers and measurement types are also included in Table 3.

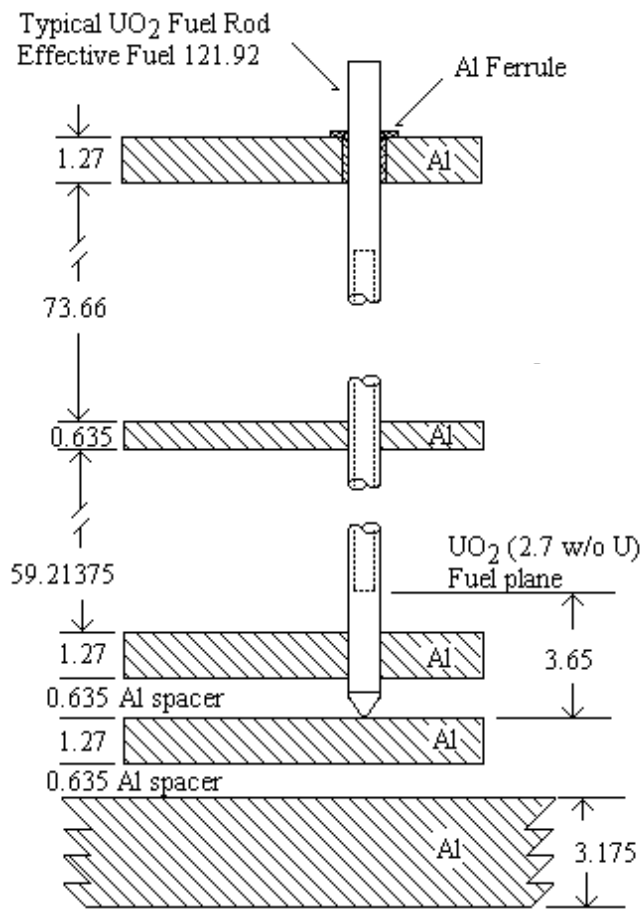

Fig. 32. Installation of UO_2 fuel in a uniform lattice.

(Not drawn to scale; units in centimeters except where specified otherwise.)

Table 3. Reported data for single-region experiments with 2.72 wt% UO_2

Case No.	Core diagram (Fig. No.)	Measurement type	Lattice pitch (cm)	Number of fuel rods	CWH (cm)
52	33	Buckling	1.7526	317	121.67
53	34	Buckling	2.4785	293	117.58

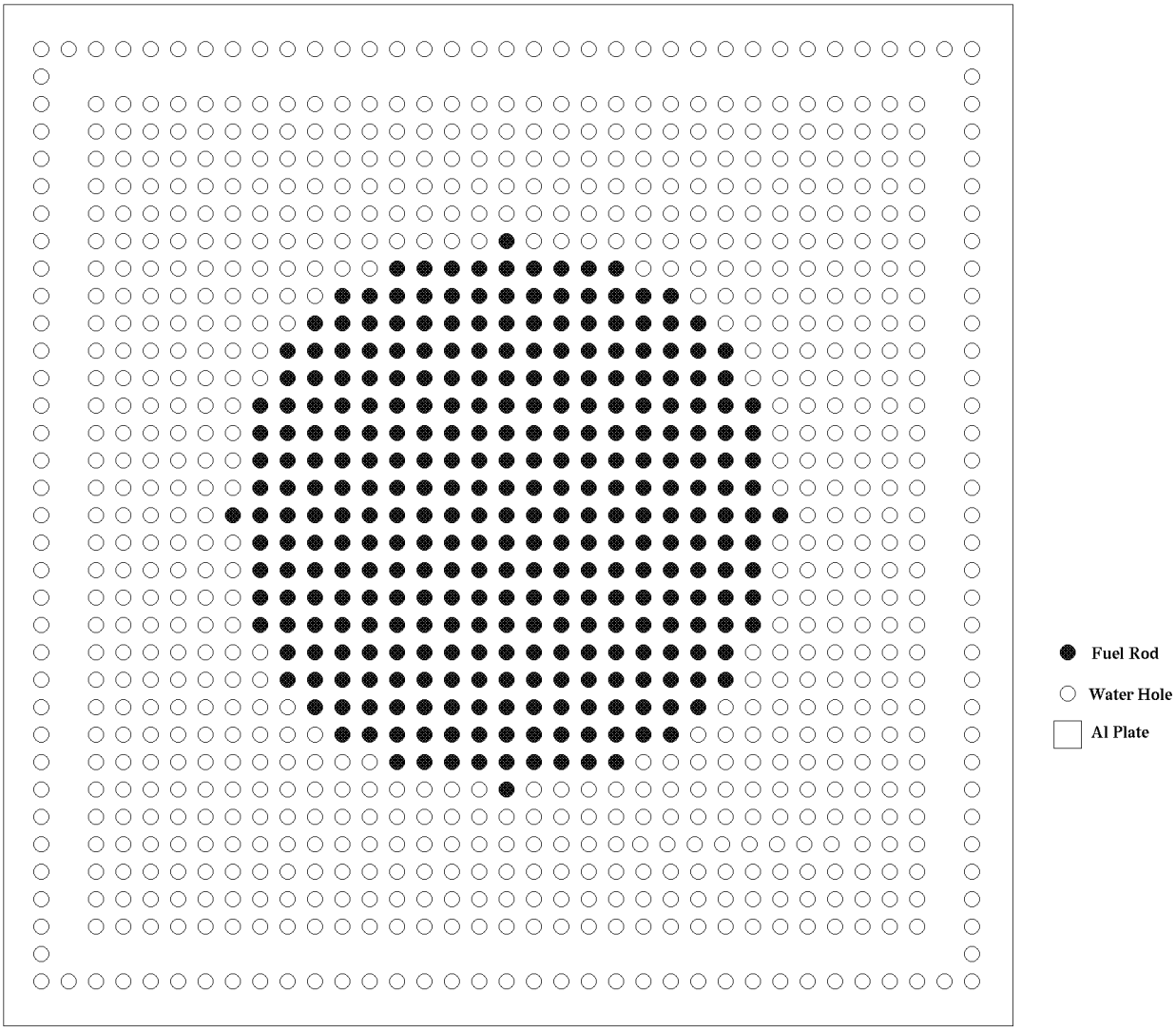

Fig. 33. Cylindrical core diagram for UO_2 fuel in a 1.7526-cm lattice.

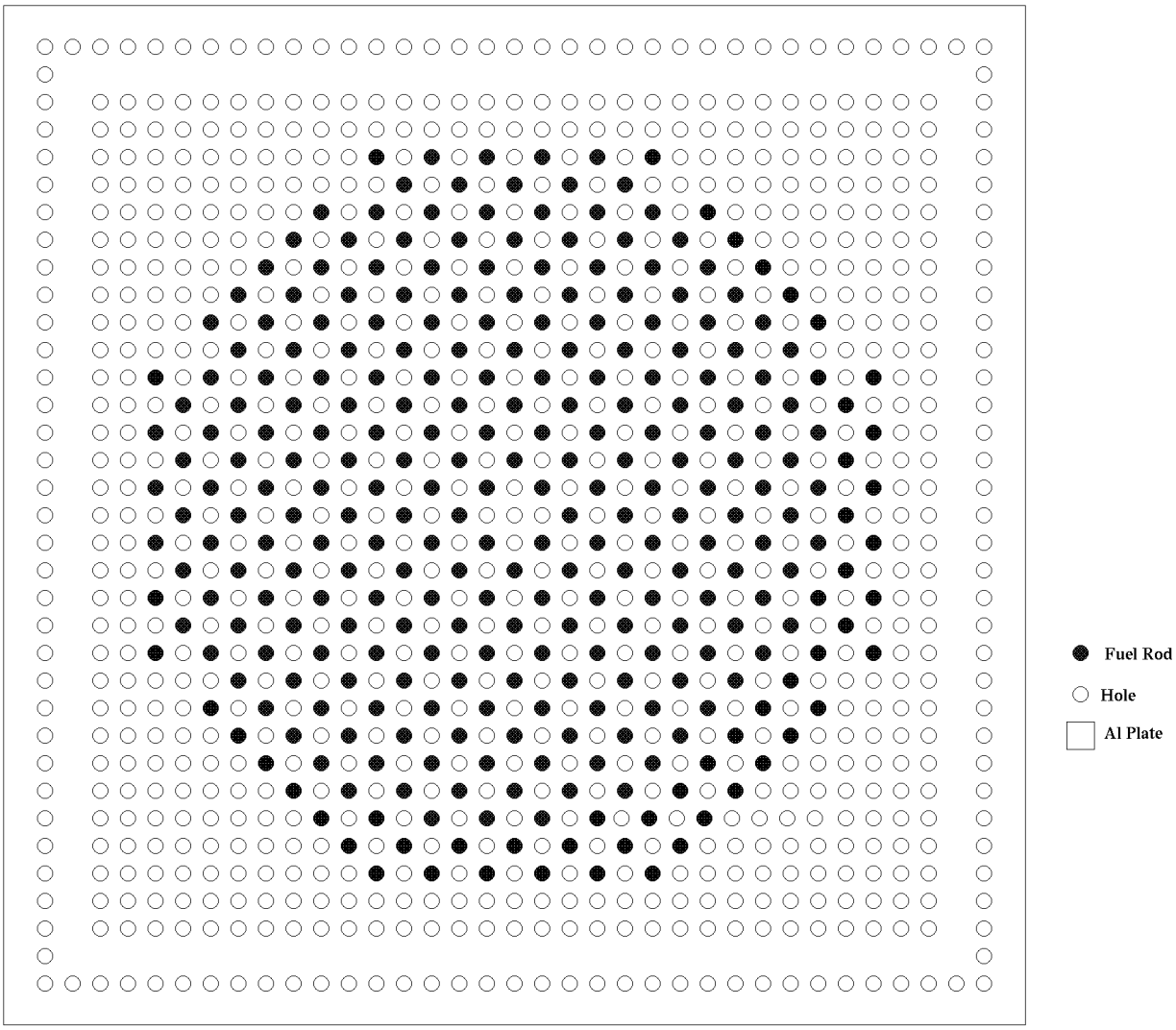

Fig. 34. Cylindrical core configuration for enriched UO_2 fuel in a 2.4785-cm lattice.

1.6 Description of Fuel Rods

The experiments were performed using the MOX fuel rods obtained from Battelle-Pacific Northwest Laboratories (PNNL).[1] The MOX fuels used in the ESADA program were also used in two different sets of experiments at PNNL.[4,5] One series of experiments at PNNL was conducted in 1965 using both types of MOX fuels,[6,7] and later 8% ^{240}Pu fuels were used in 1975-1976.[5]

The MOX fuel rod length was 92.96 cm with 91.44-cm active fuel length.[*] The outer diameter of the fuel rod including an 0.08-cm-thick Zircaloy-2 cladding was 1.443 cm. Two plugs were welded on each end of the fuel rods. The total mass of the loaded fuel rod was 1340 g/rod with 1128 g PuO_2-UO_2 per rod. The top end had 5 g of UO_2 powder. Dimensions of both types of MOX fuels were identical. A schematic representation of MOX fuel is given in Fig. 35.

The 2.72% (2.719%) enriched UO_2 fuel was the third type of fuel used in these experiments. The UO_2 fuel was obtained from the U.S. Atomic Energy Commission-sponsored Large Reactor Development Program to compare with the plutonium data and also to use later in multiregion experiments.[1]

The total mass of UO_2 fuel was 1028.02 g/rod with 905.93 g/rod uranium. The mass of the ^{235}U was 24.63 g/rod. The UO_2 fuel rod length was 140.18 cm with 121.92-cm active fuel length. The fuel pellet diameter was 1.016 cm. The outer diameter of the fuel rod was 1.196 cm. Fuel pellets were 1.52 cm in length. A schematic representation of the UO_2 fuel rod is given in Fig. 36. MOX and UO_2 fuel rod specifications are summarized in Table 4.

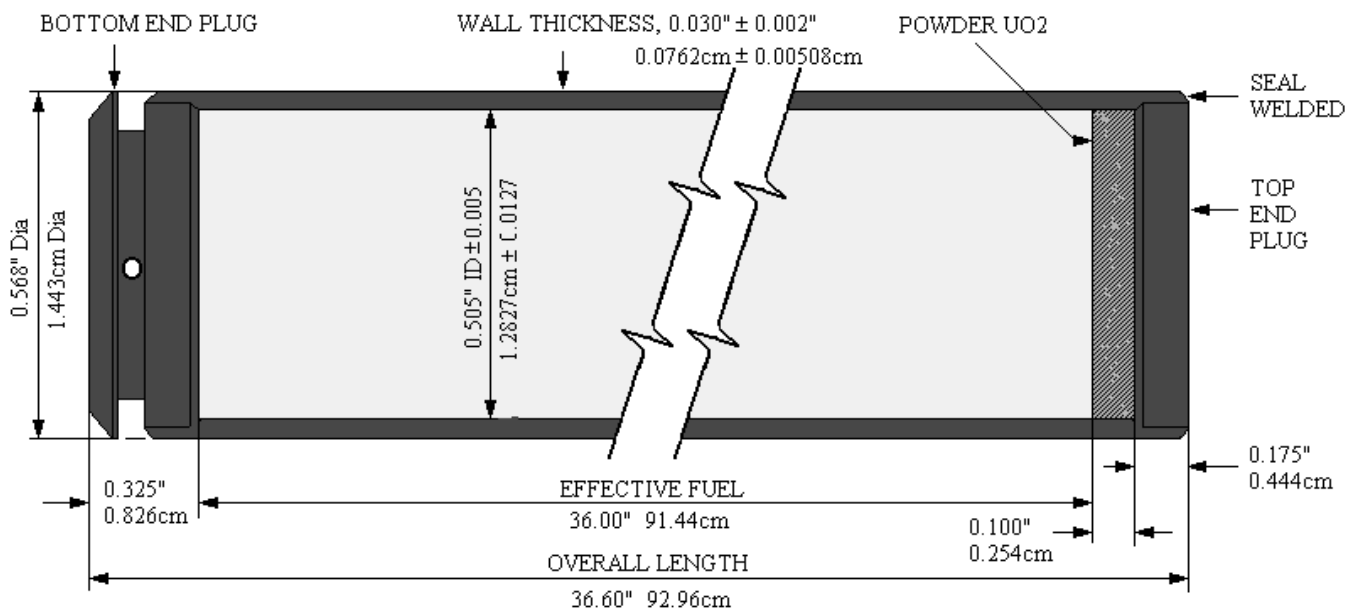

Fig. 35. MOX fuel rod.

[*] Although the fuel rods used in ESADA and PNNL experiments were the same, the dimensions were reported slightly differently in different sources. During this study, the dimensions reported in the ESADA document[1] are used. The dimensional differences in different sources and their effects are discussed in Sect. 2.1.1.

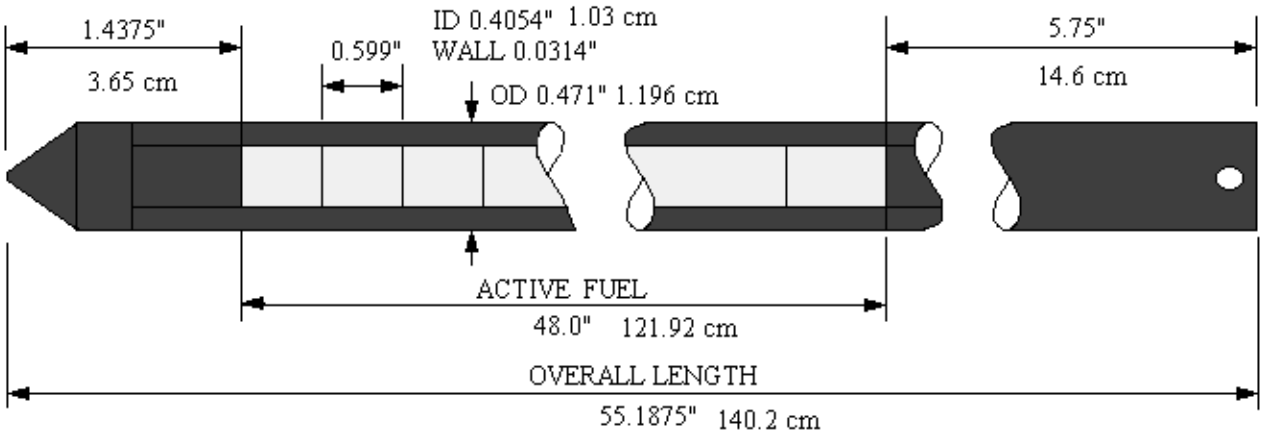

Fig. 36. Uranium fuel rod.

Table 4. MOX and UO_2 fuel rod specifications

Parameter	MOX	UO_2
Pellet diameter [cm (in.)]	1.2827 (0.505)	1.0160 (0.400)
Clad inner diameter [cm (in.)]	No gap[a]	1.0297 (0.4054)
Clad outer diameter [cm (in.)]	1.4427[a] (0.568)	1.1963 (0.471)[b]
Fuel length [cm (in.)]	92.9540 (36.6)	140.1762 (55.1875)
Active fuel length (cm) [cm (in.)]	91.4400 (36.0)	121.9200 (48.0)
Weight (g/rod)	1128 PuO_2-UO_2	1028.02 UO_2
	22.56 PuO_2	905.93 U
	19.85 Pu	24.63 ^{235}U
Clad material	Zircaloy-2	Zircaloy-4

[a]See Sect. 2.1.1 for the discussion of the clad outer diameter and the gap for MOX fuel.
[b]See Sect. 2.2.1 for the discussion of the inconsistency of the clad outer diameter for UO_2 fuel.

1.7 Description of Test Configurations

Many test positions were formed by removing fuel rods at several locations. These holes were filled either with control rods or left as empty water holes. A central test position was formed by removing a fuel rod in the center of the core. In the central test position, the reactivity worth of a water hole, a control rod composed of silver-indium-cadmium alloy, a void tube (sealed Zircaloy tube), and a cobalt rod were determined in both the clean and borated core configurations. A five-rod slot pattern was formed by removing five rods in a row at the center of the core. A nine-rod slot pattern was formed by removing nine rods in a row in the center of the core. A tight and a loose cluster of nine rods were arranged in a rectangular pattern in the center of the core. Also, a uniformly distributed nine-rod pattern was arranged as a test configuration. The reactivity worth of local voids was measured with voided aluminum tubes.

The isotopic composition of the control rod was 80% Ag, 15% In, and 5% Cd. The outer diameter of the Ag-In-Cd control rods was 1.0236 cm. These rods were placed in a 0.0254-cm-thick stainless steel tube. The outer diameter of the stainless steel tube was 1.087 cm. For the reactivity worth measurement experiments with the salt and pepper core configuration, bare Ag-In-Cd control rods with an outer diameter of 1.0236 cm were used.

As another test configuration material, a Zircaloy-4 tube was sealed to produce a void. The inner diameter of this tube was 1.0297 cm with an outer diameter of 1.189 cm. Also, a cobalt rod with an outer diameter of 0.998 cm was used for reactivity worth measurements. In addition, aluminum tubes were sealed to produce voids. The outer diameter of these aluminum tubes was 0.476 cm with 0.0559-cm thickness.

1.8 Description of Materials

Three different types of fuel rods were used during the experimental program. Two different types of MOX fuels and a low-enriched UO_2 fuel were used. MOX fuels were distinguished by the composition (vector) of plutonium isotopes. The composition of plutonium isotopes used in MOX fuel for the nominally 8% and 24% ^{240}Pu fuels is given in Table 5.

Both types of MOX fuels contained 2.0 wt% PuO_2 in natural (0.72 wt% ^{235}U) UO_2. The total weight of a MOX fuel rod was 1128 g with 22.56 g/rod PuO_2. Fuel density was reported as 9.54 g/cm^3 (Ref. 1). The weight percentages of the elements in the MOX fuel rods are given in Table 6.

Table 5. Isotopic composition of the metal plutonium in the MOX fuel rods

Isotope	Composition, 8% ^{240}Pu (wt%)	Composition, 24% ^{240}Pu (wt%)
^{239}Pu	91.615	71.762
^{240}Pu	7.654	23.503
^{241}Pu	0.701	4.080
^{242}Pu	0.030	0.656

Table 6. Percentages of the elements in the MOX fuel rods

Element	Composition (wt%)
PuO_2	2.0
UO_2	98.0
Plutonium metal	1.77
Uranium metal	86.39
O	11.84

Zircaloy-2 was used as the cladding material for MOX fuel, but its composition is not reported in Ref. 1. During this work, the average values of weight fractions given in Ref. 8 are taken for the composition of Zircaloy-2. Density of Zircaloy-2 is taken as 6.56 g/cm^3. Isotopic composition of Zircaloy-2 clad is given in Table 7.

Table 7. Zircaloy-2 composition used for MOX fuel

Element	Composition (wt%)
Zr	98.27
Sn	1.45
Fe	0.13
Cr	0.10
Ni	0.05

The 2.72% (2.719%) enriched UO_2 fuel was used as a third type of fuel. The total mass of the UO_2 was 1028.02 g/rod with 905.93 g/rod uranium, and the mass of the ^{235}U was 24.63 g/rod. Fuel density was 95% of the theoretical density. A detailed chemical analysis* of UO_2 fuel is given in Table 8. The clad material for the UO_2 fuel rod was Zircaloy-4. Chemical analysis† of Zircaloy-4 is given in Table 9.

Table 8. Chemical analysis of UO_2 fuel[1]

Isotope	2.72% U^{235}
U (wt%)	88.15
C (ppm)	<10
F (ppm)	<10
Al (ppm)	40
B (ppm)	<0.5
Bi (ppm)	<1
Cd (ppm)	<0.3
Co (ppm)	<4
Ca (ppm)	9.5
Cr (ppm)	34
Cu (ppm)	2.0
Fe (ppm)	266
In (ppm)	<3
Mg (ppm)	4.4
Mn (ppm)	2.4
Mo (ppm)	6.2
Ni (ppm)	24.3
Pb (ppm)	<8
Si (ppm)	21
Sn (ppm)	<2
Ti (ppm)	3.9
V (ppm)	<1
W (ppm)	<50
N (ppm)	<18
Zn (ppm)	<8
O	Remainder

*See Table 31 in Sect. 3.3 for the UO_2 fuel contents used in this evaluation.
†See Table 32 in Sect. 3.3 for the Zircaloy-4 composition used in this evaluation.

Table 9. Chemical analysis of Zircaloy-4 clad used for UO_2 fuel[1]

Composition	Zircaloy-4
Zr (wt%)	98.2
Sn (wt%)	1.4
Fe (wt%)	0.21
Cr (wt%)	0.10
Ni (wt%)	<0.004
C (ppm)	95
Hf (ppm)	<100
Al (ppm)	<20
B (ppm)	0.2
Cd (ppm)	0.2
Co (ppm)	10
Cu (ppm)	33
Mg (ppm)	<10
Mn (ppm)	<20
Mo (ppm)	<20
Pb (ppm)	<20
Si (ppm)	58
Ti (ppm)	<20
V (ppm)	<20
W (ppm)	<50
N (ppm)	45

No information was given on the type of aluminum used in these experiments.[1] During this study Al-6061 was assumed for the grid structure material. The density of aluminum is taken to be 2.7 g/cm^3. The characteristics of this type of aluminum are given in Table 10.[8]

Table 10. Isotopic distribution of Al-6061

Element	Composition (wt%)
Al	96.95
Mg	1.00
Fe	0.70
Si	0.60
Cu	0.25
Cr	0.20
Ti	0.15
Mn	0.15

Control rods composed of Ag-In-Cd rods were used for reactivity worth measurements. The isotopic composition of the control rod was provided in the report,[1] but the density was not provided. The isotopic composition of these rods is given in Table 11.[1] The density of the control rod is taken as 9.75 g/cm^3.

Table 11. Isotopic composition of Ag-In-Cd control rod

Element	Composition (wt%)
Ag	80
In	15
Cd	5

These control rods were clad by stainless steel. The isotopic composition of stainless steel was not provided in the Westinghouse report.[1] Table 12 lists the isotopic composition of stainless steel used in this study.[8] The density of stainless steel is taken as 7.92 g/cm^3.

Table 12. Isotopic composition of stainless steel

Element	Composition (wt%)
Fe	69.5
Cr	19.0
Ni	9.5
Mn	2.0

1.9 Supplemental Experimental Measurements

Two standard lattice plates were used during the experimental program. By changing the loading pattern, standard lattice pitches were increased by a factor of $\sqrt{2}$ or 2. In this way, buckling measurement experiments were performed for five different lattice pitches. The number of reactivity worth measurements was increased by varying the test array materials and their positions.

The number of power distribution measurements in multiregion cores was increased by utilizing a number of additional core configurations. Measurements in concentric region cores using different fuels and cores with interspersed fuels in a salt and pepper distribution were examined as different methods for extending the scope of the experimental program.

In addition to buckling, reactivity, and power distribution, heat rate measurements were performed during the program. In the heat rate experiments, thermally insulated and instrumented fuel rods were irradiated, and the temperature response was measured. After shutdown, these same rods were counted in the fuel rod gamma counter. The resulting ratio of heating rate to gamma activity provides a time-dependent "calorimetric" correction factor.

Using both uranium and plutonium fuels, heat rate experiments were conducted to correlate earlier power-to-gamma activity measurements made in the Saxton program.[9] Since fuel rods in this experiment were of different physical dimensions, new data were taken to reevaluate the time-dependent correction factors. Improved (over that used in Saxton) digital temperature measurements were taken by instrumenting the fuel rods during and after irradiation and, specifically, the speed of the temperature measurements was greatly increased. The measurements of relative power distribution ratios of UO_2 vs 24 wt% ^{240}Pu, UO_2 vs 8 wt% ^{240}Pu, and 8 wt% ^{240}Pu vs 24 wt% ^{240}Pu are reported to be about ±1% accuracy. However, the effects caused by differences in thermal capacitance of the different fuel rod types have to be taken into account.

2 EVALUATION OF THE EXPERIMENTAL DATA

The effects of some of the uncertainties in the measured data on the k_{eff} value were calculated using the ONEDANT code[10] with ENDF/B-IV 27 group cross sections with the homogenized lattice-cell fuel region. The homogenized lattice-cell cross section sets for ONEDANT were prepared using the CSASIX[11] control module of the SCALE code.

The ONEDANT calculations were performed using S_8 quadrature and P_3 scattering order. The buckling values were adjusted to make the k_{eff} value equal to 1.0000. The convergence criterion on the k_{eff} value was chosen to be 10^{-6}. The mesh spacing was chosen approximately as 0.5 cm.

2.1 Sensitivity Calculations for Core Configurations with MOX Fuel

The sensitivity calculations for MOX fuels were performed for five cases with different lattice pitches for 8% ^{240}Pu and for two cases with different lattice pitches for 24% ^{240}Pu MOX fuels. The sensitivity calculations for the 8% ^{240}Pu fuel were performed for Cases 1, 3, 4, 6, and 7 of Table 1. The calculations for 24% ^{240}Pu fuel were performed for Cases 46 and 47 of Table 2.

The one-dimensional (1-D) model for the MOX fuel core configurations was composed of six regions: the lower reflector below the aluminum plate that has a thickness of 30 cm, an aluminum plate with a thickness of 5.24 cm, water with the bottom portion of the clad, homogenized fuel with water and aluminum supporting plates, water with the top portion of the clad, and the top reflector. The total effects of the uncertainties in the parameters discussed below on the k_{eff} values for the specified cases are reported in Sect. 2.15 for the core configurations with 8% ^{240}Pu and 24% ^{240}Pu MOX fuels, respectively.

2.1.1 Fuel Rod Characterization

Fuel Rod Density: The density of the MOX fuel was reported as 9.54 g/cm^3 in Ref. 1. The mass of the UO_2-PuO_2 mixture was reported as 1128 g/rod with 1.2827-cm fuel diameter and 91.44-cm active fuel length. By considering these data, fuel density is calculated as 9.546 g/cm^3 and the difference is taken as the uncertainty in fuel density. As can be seen from Tables 13 and 14, the maximum effect of uncertainty in fuel density on the k_{eff} value is 0.012% for 8% ^{240}Pu, 0.013% for 24% ^{240}Pu MOX fuel.

The density of UO_2 powder was not reported in Ref. 1. The weight of this powder is given as 5 g/rod, and the thickness is reported as 0.254 cm (0.100 in.). However, these data yield an unrealistic density of 15.23 g/cm^3. In Ref. 1, the fuel density was reported as 9.54 g/cm^3; however, it was not clearly stated whether this density is only for the MOX region or for MOX plus the UO_2 powder region. If the powder density is also assumed as 9.54 g/cm^3, the weight of UO_2 is decreased to 3.13 g/rod. Sensitivity calculations were performed assuming the powder density as 9.54 g/cm^3 and the powder weight as 3.13 g/rod. As shown in Tables 13 and 14, the sensitivity of k_{eff} to the UO_2 powder density is negligible.

Table 13. Sensitivity of k_{eff} to uncertainties in fuel rod characterization for core configurations with 8% ^{240}Pu MOX fuel

Parameter	Uncertainty considered (1σ)	Δk_{eff}(%)				
		Case 1	Case 5	Case 6	Case 9	Case 10
MOX fuel density[a]	0.006 g/cm^3	0.001	0.004	0.007	0.010	0.016
UO_2 powder density[b]	5.69 g/cm^3	0.009	0.006	0.003	0.003	0.002
Plutonium weight[c]	0.15 g/rod	0.041	0.055	0.098	0.117	0.163
Fuel diameter[d]	±0.0127 cm	0.091	0.018	0.212	0.287	0.472
Gap between fuel and clad[e]	0.004 cm	0.046	0.0367	0.020	0.011	0.012
Clad thickness[f]	±0.00508 cm	0.661	0.476	0.148	0.086	0.036
Dimensional differences[g]		0.019	0.023	0.039	0.038	0.060
Zircaloy-2 composition[h]		0.011	0.013	0.011	0.014	0.016
Uncertainty in k_{eff}*		0.671	0.481	0.280	0.325	0.505

[a]The MOX fuel density is reported[1] as 9.54 g/cm^3 and calculated as 9.546 g/cm^3 using the reported dimensions and mass. This difference is taken as the uncertainty in MOX fuel density.

[b]In the report[1] it was not clearly stated whether the reported fuel density (9.54 g/cm^3) is valid only for the MOX region or for both the MOX and the UO_2 powder region. The calculated UO_2 powder density with the given dimensions and weight yield an unrealistic value of 15.23 g/cm^3.

[c]In Ref. 1, the average and nominal plutonium weights are reported as 19.85 g/rod and 20 g/rod, respectively. This difference is taken as the uncertainty (σ) in plutonium weight.

[d]The reported uncertainty in the fuel diameter.[1] Sensitivity calculations performed for both an increase and a decrease in fuel diameter and the change yielding the maximum Δk_{eff} value are listed. The maximum uncertainty is obtained with the increase in fuel diameter.

[e]When the reported dimensions of the fuel outer diameter, clad thickness, and the clad outer diameter are considered, initially it was assumed that a 0.004-cm-thick gap is present between fuel and clad. However, later it was found that in Ref. 1 clad outer diameter was different from all other sources, and there is no gap between fuel and clad.

[f]The reported uncertainty in the clad thickness.[1] Sensitivity calculations performed for both an increase and a decrease in clad thickness and the change yielding the maximum Δk_{eff} value are listed. The maximum uncertainty is obtained with the increase in clad thickness.

[g]The dimensions of the MOX fuel rod were reported as slightly different in different sources. In this case, the dimensions given in Refs. 5 and 6 are used. The dimensions shown in Fig. 35 are modified so that the MOX fuel, UO_2 powder, and top plug lengths are taken as 90.94, 0.5, and 0.6985 cm, respectively.

[h]The uncertainties in k_{eff} value due to the maximum zirconium content and minimum zirconium content are calculated, and the composition yielding the maximum Δk_{eff} value is listed. The maximum uncertainty is obtained using the maximum zirconium content.

*Square root of sum of squares of individual Δk_{eff}s.

Table 14. Sensitivity of k_{eff} to uncertainties in fuel rod characterization for core configurations with 24% ^{240}Pu MOX fuel

Parameter	Uncertainty considered (1σ)	Δk_{eff}(%)	
		Case 1	Case 2
MOX fuel density[a]	0.006 g/cm^3	0.005	0.011
UO_2 powder density[b]	5.69 g/cm^3	0.001	0.003
Plutonium weight[c]	0.15 g/rod	0.094	0.112
Fuel diameter[d]	±0.0127 cm	0.203	0.276
Gap between fuel and clad[e]	0.004 cm	0.011	0.001
Clad thickness[f]	±0.00508 cm	0.116	0.059
Dimensional differences[g]		0.042	0.039
Zircaloy-2 composition[h]		0.011	0.010
Uncertainty in k_{eff}*		0.256	0.307

[a]The MOX fuel density is reported[1] as 9.54 g/cm^3 and calculated as 9.546 g/cm^3 using the reported dimensions and weight. This difference is taken as the uncertainty in MOX fuel density.

[b]In the report[1] it was not clearly stated whether the reported fuel density (9.54 g/cm^3) is valid only for the MOX region or for both the MOX and the UO_2 powder region. The calculated UO_2 powder density with the given dimensions and weight yield an unrealistic value of 15.23 g/cm^3.

[c]In Ref. 1, the average and nominal plutonium weights are reported as 19.85 g/rod and 20 g/rod, respectively. This difference is taken as the uncertainty in plutonium weight.

[d]The reported uncertainty in the fuel diameter.[1] Sensitivity calculations performed for both an increase and a decrease in fuel diameter and the change yielding the maximum Δk_{eff} value are listed. The maximum uncertainty is obtained with the increase in fuel diameter.

[e]When the reported dimensions of the fuel outer diameter, clad thickness, and the clad outer diameter are considered, initially it was assumed that a 0.004-cm-thick gap is present between fuel and clad. However, later it was found that in Ref. 1 clad outer diameter was different from all other sources, and there is no gap between fuel and clad.

[f]The reported uncertainty in the clad thickness.[1] Sensitivity calculations performed for both an increase and a decrease in clad thickness and the change yielding the maximum Δk_{eff} value are listed. The maximum uncertainty is obtained with the increase in clad thickness.

[g]The dimensions of the MOX fuel rod were reported as slightly different in different sources. In this case, the dimensions given in Refs. 5 and 6 are used. The dimensions shown in Fig. 35 are modified so that the MOX fuel, UO_2 powder, and top plug lengths are taken as 90.94, 0.5, and 0.6985 cm, respectively.

[h]The uncertainties in k_{eff} value due to the maximum zirconium content and minimum zirconium content are calculated, and the composition yielding the maximum Δk_{eff} value is listed. The maximum uncertainty is obtained using the maximum zirconium content.

*Square root of sum of squares of individual Δk_{eff}s.

Plutonium Content: The average plutonium weight was reported as 19.85 g/rod in Ref. 1, and the nominal plutonium weight was given as 20 g/rod. The difference in these weights (0.15 g/rod) is considered as the uncertainty in plutonium weight for all plutonium isotopes. The sensitivity calculations show that the uncertainty on the k_{eff} value due to the uncertainty in the plutonium weight is increasing with increasing lattice pitch. The maximum uncertainty in the k_{eff} value due to uncertainty in the plutonium weight is 0.158% for the largest lattice pitch (3.5052 cm).

Dimensions: The uncertainties in the MOX fuel diameter and the clad thickness were reported as ±0.0127 cm (±0.005 in.) and ±0.00508 cm (±0.002 in.), respectively, in Fig. D-1, p. 124, Ref. 1. The uncertainty in the fuel length was not provided. The magnitude of uncertainty in the fuel length is taken as one-half the value of the least significant digit: ±0.0127 cm (±0.005 in.). The effect on the k_{eff} value due to uncertainty in the fuel length was calculated as <0.001%. Therefore, this uncertainty is considered to be negligible and is not listed in Tables 13 and 14.

As mentioned in Sect. 1.6, the fuel rods used in ESADA and PNNL experiments were the same, but the dimensions were reported as slightly different in different sources. One of the reasons for this difference is due to the length of the UO_2 powder region. References 1 and 7 give the fuel length as 36.0 in. excluding the powder; however, Refs. 5 and 6 give the fuel length as 36.0 in. including powder region. Due to this difference in UO_2 powder length, the top plug was also reported differently in different sources. The top plug was reported as 0.444 cm (0.175 in.) in Refs. 1 and 7, whereas it was reported as 0.6985 cm (0.275 in.) in Refs. 5 and 6.

As another case related to the uncertainty in fuel length, the inconsistency in the reported data in different sources is considered. Sensitivity calculations are performed to observe the sensitivity of the k_{eff} value to these differences in reported dimensions, and the dimensions given in Refs. 5 and 6 are used. For this purpose, the dimensions shown in Fig. 35 are modified so that the MOX fuel, UO_2 powder, and top end plug lengths are assumed as 90.94 cm, 0.5 cm, and 0.6985 cm, respectively. As shown in Tables 13 and 14, the maximum uncertainty in the k_{eff} value due to these inconsistent dimensions is 0.060% for 8% ^{240}Pu fuel and 0.042% for 24% ^{240}Pu fuel.

Another difference in dimensions was due to the clad outer diameter. The clad outer diameter was reported as 1.443 cm (0.568 in.) in Ref. 1, but it was reported as 1.435 cm (0.565 in.) in all the other sources.[5,6,7] This difference in clad outer diameter is within the reported uncertainty for wall thickness. When the reported dimensions of the fuel outer diameter, clad outer diameter, and clad thickness given in Ref. 1 (which was also given in Fig. 35 of this document) are considered, it was assumed that there was a gap between fuel and clad. However, these fuels were vibratory compacted, and there was no gap between fuel and clad.[1,5,6,7] The MCNP calculations for core configurations with MOX fuel were performed assuming that there was a gap with a thickness of 0.004 cm between fuel and clad. The effect on the k_{eff} value due to the postulated gap was calculated and presented in Tables 13 and 14 for 8% ^{240}Pu and 24% ^{240}Pu MOX fuels, respectively.

Based on the sensitivity calculations for the uncertainties in dimensions, it has been observed that the maximum uncertainty on the k_{eff} value was due to uncertainties in clad thickness for small lattice pitches, whereas it was due to fuel diameter for larger lattice pitches. The total uncertainties on the k_{eff} value due to uncertainties in dimensions are 0.669%, 0.478%, 0.262%, 0.302%, and 0.477% for Cases 1, 3, 4, 6, and 7 for 8% ^{240}Pu MOX fuel; and 0.238% and 0.285% for Cases 46 and 47 for 24% ^{240}Pu MOX fuel.

Clad Material: The clad material for MOX fuel was reported as Zircaloy-2; however, the isotopic composition and the density were not reported in Ref. 1. The effect of uncertainty in the Zircaloy-2 composition on the k_{eff} value was calculated by considering two extreme cases: (1) maximum zirconium content with an isotopic composition of 98.65 wt% Zr, 1.20 wt% Sn, 0.07 wt% Fe, 0.05 wt% Cr, 0.03 wt% Ni; and (2) minimum zirconium content with an isotopic composition of 97.89 wt% Zr, 1.70 wt% Sn, 0.20 wt% Fe, 0.15 wt% Cr, 0.06 wt% Ni. The composition yielding the maximum Δk_{eff} value for each case is considered and the maximum Δk_{eff} values are listed in Table 13 for 8% ^{240}Pu and in Table 14 for 24% ^{240}Pu MOX fuel. The maximum uncertainty in the k_{eff} value due to uncertainty in the Zircaloy-2 composition is 0.016%.

2.1.2 Structural Material

Aluminum Type: Aluminum was used as the resting plate and supporting grid material. The composition and the density of aluminum were not provided in Ref. 1. During this study Al-6061 with the isotopic distribution given in Table 10 is used. Sensitivity calculations are performed using 100% aluminum.

Water Holes in Fuel Support Plates: Although there is no information reported in Ref. 1, holes must have been present in the supporting aluminum grid plates through which fuel rods could pass. The

volume fraction of the holes was assumed to be 20% of the aluminum plate volume and, in the computer model, these holes contained water.[5]

The effects on k_{eff} due to aluminum type and the holes were calculated. The results are presented in Tables 15 and 16, and the maximum variation in the k_{eff} value due to the uncertainty in aluminum type is calculated as 0.062%; for the presence of holes in the base plate, it is determined to be 0.044%.

Table 15. Sensitivity of k_{eff} to uncertainties in aluminum type and holes in the aluminum supporting plate for core configurations with 8% ^{240}Pu MOX fuel

Parameter	Δk_{eff}(%)				
	Case 1	Case 5	Case 6	Case 9	Case 10
Aluminum type[a]	0.006	0.012	0.026	0.036	0.062
Water holes in aluminum plate[b]	0.041	0.044	0.013	0.014	0.003
Uncertainty in k_{eff}*	0.041	0.046	0.029	0.039	0.062

[a]Aluminum type is changed from Al-6061 to 100% aluminum.
[b]There was no information for the holes in aluminum plate in Ref. 1. Water holes with 20% of the volume fraction are assumed to be available in the aluminum plate.
*Square root of sum of squares of individual Δk_{eff}s.

Table 16. Sensitivity of k_{eff} to uncertainties in aluminum type and holes in aluminum supporting plate for core configurations with 24% ^{240}Pu MOX fuel

Parameter	Δk_{eff}(%)	
	Case 1	Case 2
Aluminum type[a]	0.027	0.038
Water holes in aluminum plate[b]	0.008	0.013
Uncertainty in k_{eff}*	0.028	0.040

[a]Aluminum type is changed from Al-6061 to 100% aluminum.
[b]There was no information for the holes in aluminum plate in Ref. 1. Water holes with 20% of the volume fraction are assumed to be available in the aluminum plate.
*Square root of sum of squares of individual Δk_{eff}s.

2.1.3 Moderator

Reference Plane for CWH Measurements: The reference plane for the CWH measurements was not reported in Ref. 1. However, the absolute accuracy of the CWH was reported to be ±0.01 cm. During this study, the active fuel bottom plane was taken as the reference plane. The sensitivity calculations were performed assuming the clad bottom plane as the reference plane for the CWH measurements. In this way, the moderator level was assumed to be decreased by 0.826 cm. The sensitivity calculation results are presented in Tables 17 and 18. The maximum uncertainty in the k_{eff} value due to the uncertainty in reference plane is calculated to be 0.035%.

Uncertainties in CWH Measurements: In addition to the reference plane for CWH, the uncertainties in the CWH measurements are also considered. Ref. 1 reports that "the (water level measurement) system achieves a relative accuracy of ±0.01 cm." This uncertainty is considered to be negligible, and the results of these sensitivity calculations are not presented in Tables 17 and 18.

Table 17. Sensitivity of k_{eff} to uncertainty in the reference plane for CWH measurements for core configurations with 8% ^{240}Pu MOX fuel

	Δk_{eff}(%)				
	Case 1	Case 5	Case 6	Case 9	Case 10
Reference plane for CWH[a]	0.023	0.034	0.038	0.030	0.029

[a]The reference plane for CWH measurements was not reported in Ref. 1. The reference plane for measurements might be active fuel bottom plane or clad bottom plane. The difference between two planes is 0.826 cm.

Table 18. Sensitivity of k_{eff} to uncertainty in the reference plane for CWH measurements for core configurations with 24% ^{240}Pu MOX fuel

	Δk_{eff}(%)	
	Case 1	Case 2
Reference plane for CWH[a]	0.034	0.034

[a]The reference plane for CWH measurements was not reported in Ref. 1. The reference plane for measurements might be active fuel bottom plane or clad bottom plane. The difference between two planes is 0.826 cm.

Bottom Reflector: The installations of MOX and UO_2 fuels for the construction of core configurations were provided in Ref. 1 and are also provided in Figs. 1 and 32 of this report. However, Ref. 1 does not provide any detailed information related to the thickness of the bottom reflector.

During this study, the thickness of the bottom reflector was assumed as 30 cm, and the MCNP calculations were performed accordingly. However, according to the information given in Ref. 9 (which was given for SAXTON experiments but should be relevant because ESADA and SAXTON experiments were performed at the same facility, WREC) the actual thickness of the bottom reflector is larger than 30 cm. The sensitivity calculations were performed, considering a larger bottom reflector thickness, by varying the bottom reflector thickness from 30 cm to 100 cm. The sensitivity calculations showed that there is no effect on the k_{eff} value with increasing bottom reflector thickness. Therefore, the results of the sensitivity calculations are not presented in Tables 17 and 18.

2.1.4 Others

The Effect of ^{241}Am: The MCNP calculations were performed by taking the plutonium isotopic compositions reported in Ref. 1, which are also presented in Table 1. However, in the given compositions the ^{241}Am content was not reported in the same reference. Because ^{241}Pu decays with a half life of ~14.5 years, fissile plutonium will deplete with the corresponding buildup of ^{241}Am.

The measurement and separation dates of fuel were not reported in Ref. 1. It has been reported in Ref. 6 that the isotopic compositions for 8% ^{240}Pu fuel given in Table 5 were measured in January 1965, and the effective average time of separation was in April 1962. For 24% ^{240}Pu fuel, the measurement date and estimated separation dates were reported in Ref. 6 as May 1965 and December 1961, respectively. The exact date for each ESADA experiment was not reported in Ref. 1. However, it was reported in Ref. 12 that "the fuel could be lent (from PNNL) for six months only, and the final experiment was completed in January 1967." Based on this information, the experiments were assumed to be performed between August 1966 and January 1967. The average effective time of measurement is considered as October 1966. The time between isotopic composition measurement date and time of the experiment was taken as 22 months for 8% ^{240}Pu and 17 months for 24% ^{240}Pu measurements. By using these time differences for each fuel, ^{241}Am and ^{241}Pu compositions were calculated for each fuel.

The effects of ^{241}Am concentration on the k_{eff} value were determined with the sensitivity calculations, and the results are presented in Tables 19 and 20. The uncertainty of ^{241}Am content on the k_{eff}

Table 19. Sensitivity of k_{eff} to ^{241}Am content and PuO_2 particle effect for core configurations with 8% ^{240}Pu MOX fuel

Parameter	Δk_{eff}(%)				
	Case 1	Case 5	Case 6	Case 9	Case 10
^{241}Am effect[a]	0.054	0.050	0.048	0.040	0.047
PuO_2 particle effect bias[b]	0.024	0.048	0.126	0.151	0.217
Uncertainty in k_{eff}*	0.059	0.069	0.135	0.156	0.222

[a]The concentration of ^{241}Am in MOX fuels is not provided in Ref. 1 The ^{241}Am buildup is calculated as 0.0588 wt% (in 22 months) for 8% ^{240}Pu and 0.267 wt% (in 17 months) for 24% ^{240}Pu MOX fuel. During the sensitivity calculations ^{241}Pu contents for both MOX fuels, given in Table 5, are also reduced.
[b]The particle effect bias is assumed 50% of the values given in Table B.1.
*Square root of sum of squares of individual Δk_{eff}s.

Table 20. Sensitivity of k_{eff} to ^{241}Am content and PuO_2 particle effect for core configurations with 24% ^{240}Pu MOX fuel

Parameter	Δk_{eff}(%)	
	Case 1	Case 2
^{241}Am effect[a]	0.248	0.244
PuO_2 particle effect bias[b]	0.094	0.118
Uncertainty in k_{eff}*	0.265	0.271

[a]The concentration of ^{241}Am in MOX fuels is not provided in Ref. 1 The ^{241}Am buildup is calculated as 0.0588 wt% (in 22 months) for 8% ^{240}Pu and 0.267 wt% (in 17 months) for 24% ^{240}Pu MOX fuel. During the sensitivity calculations ^{241}Pu contents for both MOX fuels, given in Table 5, are also reduced.
[b]The particle effect bias is assumed 50% of the values given in Table B.1.
*Square root of sum of squares of individual Δk_{eff}s.

value for 8% ^{240}Pu fuel is 0.054% at maximum. The effect is low since the ^{241}Pu content in this fuel was quite small. However, due to higher ^{241}Pu content, this uncertainty increases to 0.248% for 24% ^{240}Pu fuel.

The Effects of PuO_2 Particles: The finite-size particle effect is discussed in Appendix B. The increase in the k_{eff} value due to the PuO_2 particles is given in Table B.1. The estimated uncertainty of the particle effect bias is assumed as 50% of the values provided in Table B.1.[5] The uncertainties are presented in Tables 19 and 20.

2.1.5 Total Uncertainties

The last row of Tables 21 and 22 gives the total uncertainties in the k_{eff} value due to perturbations in the parameters discussed above for 8% ^{240}Pu and 24% ^{240}Pu MOX fuels, respectively. The maximum uncertainty in k_{eff} value is 0.675% for 8% ^{240}Pu fuel for the smallest lattice pitch and 0.412% for 24% ^{240}Pu fuel for the 2.6942-cm lattice pitch. The sensitivity calculations show that the maximum uncertainty in k_{eff} value was due to the uncertainties in fuel dimensions for both MOX fuels. Also it has been observed that k_{eff} is very sensitive to the ^{241}Am content for 24% ^{240}Pu fuel.

2.2 Sensitivity Calculations for Core Configurations with UO_2 Fuel

Sensitivity calculations were performed for both cases of the core configurations with UO_2 fuel. The moderator level for both cases was lower than the active fuel top plane. The 1-D model for UO_2 fuel core configurations was composed of eight regions: the lower reflector below the aluminum plate with thickness of 30 cm, the aluminum plate with a thickness of 3.175 cm, the water between the two aluminum plates, the second aluminum plate with a thickness of 1.27 cm, the bottom end cap with water and the bottom aluminum supporting plate, homogenized fuel with water and middle aluminum supporting plate, top fuel with air, and top clad with top aluminum supporting plate and air. The total effects of the uncertainties in the parameters discussed below on the k_{eff} values for the core configurations with UO_2 fuels for two cases are given at the end of this section.

Table 21. Total uncertainty in k_{eff} due to uncertainties in experimental data for core configurations with 8% ^{240}Pu MOX fuel

Parameter	Δk_{eff}(%)				
	Case 1	Case 5	Case 6	Case 9	
Fuel rod characterization	0.671	0.481	0.280	0.325	0.505
Structural material and holes	0.041	0.046	0.029	0.039	0.062
Moderator	0.023	0.034	0.038	0.030	0.029
^{241}Am and PuO_2 particle effects	0.059	0.069	0.135	0.156	0.222
Total uncertainty in k_{eff}*	0.675	0.490	0.314	0.363	0.556

*Square root of sum of squares of individual Δk_{eff}s.

Table 22. Total uncertainty in k_{eff} due to uncertainties in experimental data for core configurations with 24% ^{240}Pu MOX fuel

Parameter	Δk_{eff}(%)	
	Case 1	Case 2
Fuel rod characterization	0.256	0.307
Structural material and holes	0.028	0.040
Moderator	0.034	0.034
^{241}Am and PuO_2 particle effects	0.265	0.271
Total uncertainty in k_{eff}*	0.371	0.413

*Square root of sum of squares of individual Δk_{eff}s.

2.2.1 Fuel Rod Characterization

Fuel Density: The fuel density was calculated as 10.40 g/cm^3 by using a 1.016-cm (0.400-in.) fuel rod diameter and 121.92-cm (48.00-in.) fuel rod length with 1028.02 g of UO_2 per rod. The fuel density was reported as the 95% of theoretical density.[1] The uncertainty in fuel density is assumed as 0.01 g/cm^3. The maximum uncertainty in k_{eff} value due to fuel density is calculated as 0.026%.

Enrichment: The uncertainty in the fuel enrichment was not reported in Ref. 1. The magnitude of uncertainty in the fuel enrichment is taken as one-half of the value of the least significant digit: ±0.005 wt%. The effect on the k_{eff} value due to the uncertainty in the fuel enrichment is calculated and presented in Table 23. As it can be seen from Table 23, the maximum uncertainty is 0.08%.

Dimensions: The uncertainty in the fuel diameter was not provided in Ref. 1. The magnitude of the uncertainty is taken as one-half of the value of the least significant digit: ±0.00127 cm (±0.0005 in.). The uncertainty in the clad thickness was not provided in Ref. 1. However, the clad outer diameter was reported as 1.196 cm (0.471 in.) and 1.1895 cm (0.4683 in.) of Ref. 1 (p. 125 and p. 123, respectively). The difference in these reported clad outer diameters is taken as the uncertainty in the clad thickness.

The uncertainties in the fuel length were not provided in Ref. 1. The magnitude of uncertainty in the fuel length is taken as one-half of the value of the least significant digit: ±0.0127 cm (±0.005 in.). The effect on the k_{eff} value due to uncertainty in fuel length was calculated as less than 0.001%. Hence, this uncertainty is considered to be negligible and is not listed in Table 23.

The total uncertainties on the k_{eff} value due to the uncertainties in dimensions are determined as 0.231% for Case 1 and 0.066% for Case 2.

Table 23. Sensitivity of k_{eff} to uncertainties in fuel rod characterization for core configurations with UO_2 fuel

Parameter	Uncertainty considered (1σ)	Δk_{eff}(%)	
		Case 1	Case 2
Fuel density[a]	0.01 g/cm^3	0.009	0.026
Enrichment[b]	±0.005 wt%	0.052	0.080
Fuel diameter[c]	±0.00127 cm	0.027	0.065
Clad thickness[d]	±0.00325 cm	0.229	0.011
Uncertainty in k_{eff}*		0.237	0.107

[a]The difference between reported[1] and calculated density.
[b]The uncertainty in enrichment was not reported in Ref. 1; the uncertainty is taken as one-half of the value of the least significant digit of reported enrichment.
[c]The uncertainty in the fuel diameter was not reported in Ref 1. The uncertainty is taken as one-half of the value of the least significant digit of reported fuel diameter. Sensitivity calculations performed for both increase and decrease in fuel diameter and the change yielding the maximum Δk_{eff} value are listed. The maximum uncertainty is obtained for the case of increase in fuel diameter.
[d]The clad outer diameter was reported differently in different pages of Ref. 1, and this difference is taken as the uncertainty in clad thickness.
*Square root of sum of squares of individual Δk_{eff}s.

2.2.2 Structural Material

Aluminum Type: As discussed in Sect. 2.1.2, the type and composition of aluminum were not reported. During this study, Al-6061, with the isotopic composition given in Table 10, is used. The sensitivity calculations were performed assuming 100% aluminum. The maximum uncertainty in the k_{eff} value due to the uncertainty in the aluminum type is calculated as 0.018% (see Table 24).

Table 24. Sensitivity of k_{eff} to aluminum type for core configurations with UO_2 fuel

Parameter	Δk_{eff}(%)	
	Case 1	Case 2
Aluminum type[a]	0.008	0.018

[a]Aluminum type is changed from Al-6061 to 100% aluminum.

2.2.3 Moderator

CWH Measurement: As discussed in Sect. 2.1.3, the reference plane for the CWH measurements was not reported. The uncertainty due to this factor was calculated by assuming the clad bottom plane as the reference plane. This assumption reduces the moderator level by 3.65 cm. The uncertainties in the k_{eff} value due to uncertainty in the reference plane are given in Table 25, and the maximum uncertainty is 0.071%.

The uncertainty due to the CWH measurements (±0.01 cm) was calculated, and the uncertainty in the k_{eff} value was determined as less than 0.001%. Therefore, the uncertainty in CWH measurement is considered to be negligible and is not listed in Table 25.

Bottom Reflector: As discussed in Sect. 2.1.3, during this study the thickness of bottom reflector was assumed as 30 cm while the actual thickness of the bottom reflector is larger than 30 cm. The sensitivity calculations were performed considering larger bottom reflector thickness by varying the bottom reflector thickness from 30 cm to 100 cm for the core configurations with UO_2 fuels as well. The sensitivity calculations showed that there is no effect on the k_{eff} value with increasing bottom reflector thickness. Therefore, the results of the sensitivity calculations are not presented in Table 25.

Table 25. Sensitivity of k_{eff} to uncertainty in the reference plane for CWH measurements for core configurations with UO_2 fuel

Parameter	Δk_{eff}(%)	
	Case 1	Case 2
Reference plane for CWH[a]	0.068	0.071

[a]The reference plane for CWH measurements is not reported in Ref. 1. The reference plane could be active fuel bottom plane or clad bottom plane. The difference between two planes is 3.65 cm.

2.2.4 Others

The Effect of ^{234}U: Ref. 1 provides the weights of the ^{235}U and total uranium as 24.63 g/rod and 905.93 g/rod, respectively. It does not provide any information about the concentration of ^{234}U in the fuel. However, it is known that the ^{234}U concentration increases during the enrichment process. For low enriched fuel, the concentration of ^{234}U (in wt%) is 0.008 times the enrichment.[13] Accordingly, the concentration of ^{234}U is taken as 0.02175 wt%, and the remaining 97.2595 wt% is taken as ^{238}U. The uncertainty on the k_{eff} value due to the ^{234}U content is given in Table 26.

Table 26. Sensitivity of k_{eff} to uncertainties in fuel rod characterization for core configurations with UO_2 fuel

Parameter	Uncertainty considered (1σ)	Δk_{eff}(%)	
		Case 1	Case 2
^{234}U concentration[a]	0.02175 wt%	0.136	0.097

[a]The ^{234}U concentration in UO_2 fuel is not provided in Ref. 1, but is calculated here as 0.008 times the enrichment.

2.2.5 Total Uncertainties

The last row of Table 27 gives the total uncertainties in the k_{eff} value for UO_2 fuel due to the parameters discussed above. The total uncertainty in the k_{eff} value is calculated as 0.281% for Case 1 and 0.162% for Case 2.

Table 27. Total uncertainty in k_{eff} due to uncertainties in experimental data for core configurations with UO_2 fuel

Parameter	Δk_{eff}(%)	
	Case 1	Case 2
Fuel rod characteristic	0.237	0.107
Structural material	0.008	0.018
Moderator	0.068	0.071
^{234}U concentration	0.136	0.097
Total uncertainty in k_{eff}*	0.281	0.162

*Square root of sum of squares of individual Δk_{eff}s.

3 BENCHMARK SPECIFICATIONS

3.1 Description of Model

Three different types of fuel rods were used during the experimental program. Two types of MOX fuel with different plutonium contents and a low-enriched UO_2 fuel were used. Fuel rods were inserted in a square lattice pitch. Two standard lattice pitches were available. Additional lattice pitches were achieved by changing the fuel loading pattern. Buckling measurements, calculations of reactivity worth of different materials, and power distribution measurements were performed for single-region core configurations with all types of available fuels. Installations of MOX and UO_2 fuel for single-region configurations are given in Figs.1 and 32, respectively. Fuel rods rested on a bottom aluminum plate and were further supported by middle and top aluminum grid plates.

3.2 Dimensions

Schematic diagrams of MOX and UO_2 fuel rods are shown in Figs. 35 and 36, respectively. Also, the specifications of the MOX and UO_2 fuel rods are given in Table 4.

3.3 Material Data

The details of the atomic number density calculations are given in Appendix A. Atomic densities for 8% and 24% ^{240}Pu MOX fuels are calculated using the weight fractions given in Tables 5 and 6. The total weight of the PuO_2-UO_2 was reported as 1128 g/rod, and fuel density was reported as 9.54 g/cm^3. The calculated atomic number densities are given in Table 28.

Table 28. Atomic densities for the 8% and 24% ^{240}Pu MOX fuels

Element	Atom density for 8% ^{240}Pu (atom/b-cm)	Atom density for 24% ^{240}Pu (atom/b-cm)
^{235}U	1.50490E-4	1.50490E-4
^{238}U	2.07511E-2	2.07511E-2
^{239}Pu	3.87455E-4	3.03494E-4
^{240}Pu	3.22350E-5	9.89834E-5
^{241}Pu	2.93999E-6	1.71115E-5
^{242}Pu	1.29476E-7	2.73988E-6
O	4.18019E-2	4.18019E-2

The top UO_2 powder density was not reported in the original report.[1] The fuel density was reported as 9.54 g/cm^3, but it was not clear whether this density was for MOX only or for MOX plus UO_2 powder. It was reported that this layer is 5 g UO_2 with a thickness of 0.254 cm. The UO_2 powder density is calculated as 15.23 g/cm^3 by using the reported weight and thickness, an unrealistic value. Table 29 lists the atomic densities for the UO_2 powder using a density of 9.54 g/cm^3.

Table 29. Atomic densities for the UO_2 powder at the top of the MOX fuels

Element	Atom density (atom/b-cm)
^{235}U	1.55089E-4
^{238}U	2.11145E-2
O	4.25392E-4

Cladding material for MOX fuel was reported as Zircaloy-2, but the composition of Zircaloy-2 was not provided. Atomic densities for Zircaloy-2 are calculated by taking the weight fractions given in Table 7 with the density taken as 6.56 g/cm^3. Calculated atomic number densities are given in Table 30.

Table 30. Atomic densities for the Zircaloy-2 clad used for MOX fuel

Element	Atom density (atom/b-cm)
Zr	4.25563E-2
Sn	4.82539E-4
Fe	9.19592E-5
Cr	7.59770E-5
Ni	3.36556E-5

The chemical composition of UO_2 fuel is given in Table 8. The fuel density was calculated as 10.40 g/cm^3 by using the 1.016-cm (0.400-in.) fuel rod diameter and the 121.92-cm (48.00-in.) fuel rod length with 1028.02 g/rod UO_2. The atomic densities are calculated using the weights given in Ref. 1 rather than the given detailed chemical analysis. Although the uranium weight fraction is given as 88.15 wt% in Ref. 1 (p. 123), which was also given here in Table 8, different weight fractions are calculated in Ref. 1. The uranium weight fraction was reported differently in two different places of Ref. 1. On p. 123, the uranium weight fraction was given as 88.124% (U in UO_2), while it was reported as 88.15% in the chemical analysis on the same page. Therefore, during this study, the weights reported in Ref. 1 are taken as basis instead of the given weight fractions. The weights and weight fractions along with the calculated atomic densities using 10.40-g/cm^3 fuel density for the UO_2 fuel are given in Table 31.

Table 31. Atomic densities for the UO_2 fuel

Element	Weight (g)	Weight fraction (wt%)	Atom density (atom/b-cm)
^{235}U	24.63	2.39587	6.38404E-4
^{238}U	881.30	85.7279	2.25545E-2
O	122.09	11.8762	4.64896E-2

Zircaloy-4 was used as the clad material for UO_2 fuel. The chemical analysis of Zircaloy-4 is given in Table 9. Atom densities for the impurities listed in Table 9 are not calculated. The density is taken as 6.56 g/cm^3, and the calculated atomic number densities are presented in Table 32.

Table 32. Atomic densities for the Zircaloy-4 clad

Element	Weight fraction (wt%)	Atom density (atom/b-cm)
Zr	98.286	4.25632E-2
Sn	1.400	4.65900E-4
Fe	0.210	1.48550E-4
Cr	0.100	7.59770E-5
Ni	0.004	2.69245E-6

The type of aluminum used in the benchmark calculations is Al-6061. The density of aluminum is taken to be 2.7 g/cm^3. The isotopic composition of Al-6061 is given in Table 10 and the calculated atomic densities for Al-6061 are given in Table 33.

Table 33. Atomic densities for the Al-6061

Element	Atom density (atom/b-cm)
Al	5.84243E-2
Mg	6.68985E-4
Fe	2.03803E-4
Si	3.47361E-4
Cu	6.39681E-5
Cr	6.25420E-5
Ti	5.09388E-5
Mn	4.43946E-5

The density of water at 23° C is taken as 0.997518 g/cm^3. Atomic densities for water are given in Table 34.

Table 34. Atomic densities for water

Element	Atom density (atom/b-cm)
H	6.66898E-02
O	3.33449E-02

The ESADA measurements were performed using four, non-zero different boron concentrations: 116, 261, 315, and 526 ppm. The details of the atomic density calculations for borated water are given in Appendix A. The calculated atomic densities for the corresponding boron concentrations are presented in Table 35.

Table 35. Atomic densities for borated water for the specified boron concentrations

Boron concentration (ppm)	Density[a] (g/cm^3)	Element	Atom density (atom/b-cm)
		H	6.66862E-02
116	0.997836	O	3.33528E-02
		^{10}B	1.27651E-06
		^{11}B	5.28655E-06
		H	6.66816E-02
261	0.998234	O	3.33626E-02
		^{10}B	2.87329E-06
		^{11}B	1.18995E-05
		H	6.66799E-02
315	0.998382	O	3.33662E-02
		^{10}B	3.46828E-06
		^{11}B	1.43636E-05
		H	6.66733E-02
526	0.998962	O	3.33805E-02
		^{10}B	5.79484E-06
		^{11}B	2.39988E-05

[a]Borated water density (see Appendix A).

The density of air is taken as 1.20E-4 g/cm^3. The nitrogen and oxygen weight fractions are taken as 0.78 wt% and 0.22 wt%, respectively. The calculated atomic densities for air are given in Table 36.

Table 36. Atomic densities for air

Element	Atom density (atom/b-cm)
N	4.02428E-6
O	9.93684E-7

Table 37 gives the atomic densities for the Ag-In-Cd control rod using the weight fractions given in Table 11 and a density of 9.75 g/cm^3. The density of stainless steel is taken as 7.92 g/cm^3, and the weight fractions are given in Table 12. Table 38 lists the calculated atomic densities of stainless steel.

Table 37. Atomic densities for the control rod

Element	Atom density (atom/b-cm)
Ag	4.35461E-2
In	7.67055E-3
Cd	2.61167E-3

Table 38. Atomic densities for the stainless steel

Element	Atom density (atoms/b-cm)
Fe	5.93551E-2
Cr	1.74284E-2
Ni	7.72027E-3
Mn	1.73632E-3

As another test material, the cobalt rod with an outer diameter of 0.998 cm (0.393 in.) was used. However, there was no information in Ref. 1 for the density and composition of these rods. During this study, 100% cobalt with a density of 8.9 g/cm^3 is used. The atomic density of 100% cobalt is given in Table 39.

Table 39. Atomic densities for the cobalt rod

Element	Atom density (atoms/b-cm)
Co	9.09448E-02

3.4 Temperature Data

No temperature data were specified in the original report.[1] But another report[14] indicated that these experiments were performed at 23°C.

4 RESULTS OF CALCULATIONS

All experimental configurations were modeled in detail using the MCNP-4A[15] Monte-Carlo code using both ENDF/B-V and ENDF/B-VI nuclear data libraries. The S(α,β) thermal neutron scattering treatment was used for hydrogen in water at 300° K. Calculations were performed on an IBM-RISC/6000 workstation. The average CPU time for each run was ~8 h.

Calculations were performed in two steps. First, an initial run with a smaller number of histories was made and source distributions were accumulated. For the first step, calculations were run with 200 generations of 1000 neutrons each. The converged source from the last generation of the initial run was used as the starting source for the final production run. During the second step, all cases were run with 350 generations of 4000 neutrons each, and the first 50 generations were skipped. Therefore, the computed results are based on 1.2 million active histories with one standard deviation ranging from 0.0006 to 0.0007.

A detailed geometry model was prepared for the calculations. Fuel rods were modeled in a square lattice pitch. In the models of the MOX and UO_2 fuel rods, the reductions in dimensions for the bottom end Zircaloy plugs were neglected. In the calculational model, 30 cm of water was placed under the aluminum plate.

The MCNP criticality calculation results, with ENDF/B-V and ENDF/B-VI nuclear data libraries, for single-region core configurations for 8% ^{240}Pu MOX fuel are presented in Table 40.

Table 40. MCNP benchmark calculation results for 8% ^{240}Pu MOX fuel

Case No.	Lattice pitch (cm)	ENDF/B-VI $k_{eff} \pm \sigma$	ENDF/B-V $k_{eff} \pm \sigma$
1	1.7526	0.98535 ± 0.0007	0.99191 ± 0.0007
2	1.7526	0.98408 ± 0.0007	0.99082 ± 0.0007
3	1.9050	0.98660 ± 0.0007	0.99566 ± 0.0007
4	2.4785	0.99550 ± 0.0007	1.00302 ± 0.0007
5	2.4785	0.99501 ± 0.0006	1.00256 ± 0.0007
6	2.6942	0.99641 ± 0.0007	1.00465 ± 0.0007
7	3.5052	0.99985 ± 0.0007	1.00694 ± 0.0007
8	1.7526	0.98506 ± 0.0007	0.99192 ± 0.0007
9	2.4785	0.99712 ± 0.0007	1.00304 ± 0.0007
10	1.7526	0.98508 ± 0.0007	0.99177 ± 0.0007
11	2.4785	0.99818 ± 0.0007	1.00433 ± 0.0007
12	1.7526	0.98329 ± 0.0007	0.98867 ± 0.0007
13	1.7526	0.98363 ± 0.0007	0.98923 ± 0.0007
14	1.7526	0.98393 ± 0.0007	0.98907 ± 0.0007
15	1.7526	0.98327 ± 0.0006	0.98891 ± 0.0007
16	1.7526	0.98366 ± 0.0007	0.98820 ± 0.0006
17	1.7526	0.98392 ± 0.0006	0.98905 ± 0.0007
18	1.7526	0.98361 ± 0.0007	0.98827 ± 0.0006
19	1.7526	0.98431 ± 0.0007	0.98925 ± 0.0006
20	1.7526	0.98618 ± 0.0007	0.98893 ± 0.0006
21	1.7526	0.98607 ± 0.0007	0.99174 ± 0.0007
22	1.7526	0.98517 ± 0.0007	0.98931 ± 0.0006
23	1.7526	0.98380 ± 0.0007	0.98938 ± 0.0006
24	1.7526	0.98465 ± 0.0006	0.99022 ± 0.0006
25	1.7526	0.98419 ± 0.0006	0.98956 ± 0.0006
26	1.7526	0.98442 ± 0.0006	0.99044 ± 0.0007
27	1.7526	0.98353 ± 0.0006	0.98978 ± 0.0007
28	1.7526	0.98464 ± 0.0007	0.98618 ± 0.0007
29	1.7526	0.98556 ± 0.0006	0.99217 ± 0.0007
30	1.7526	0.98404 ± 0.0006	0.99186 ± 0.0007
31	1.7526	0.98489 ± 0.0007	0.99132 ± 0.0007
32	1.7526	0.98405 ± 0.0006	0.99159 ± 0.0007
33	1.9050	0.99010 ± 0.0007	0.99384 ± 0.0007
34	1.9050	0.98834 ± 0.0007	0.99482 ± 0.0007
35	1.9050	0.98506 ± 0.0007	0.99275 ± 0.0007
36	1.9050	0.98805 ± 0.0007	0.99329 ± 0.0007
37	1.9050	0.98852 ± 0.0007	0.99494 ± 0.0007
38	1.9050	0.98783 ± 0.0007	0.99380 ± 0.0007
41	1.7526	0.98363 ± 0.0007	0.98923 ± 0.0007
42	1.7526	0.98392 ± 0.0006	0.98905 ± 0.0007
43	1.7526	0.98464 ± 0.0007	0.98875 ± 0.0006
44	1.7526	0.98405 ± 0.0006	0.99159 ± 0.0007
45	1.9050	0.98805 ± 0.0007	0.99329 ± 0.0007

The MCNP criticality calculation results, with ENDF/B-V and ENDF/B-VI nuclear data libraries, for single-region core configurations for 24% ^{240}Pu MOX fuel are presented in Table 41.

Table 41. MCNP benchmark calculation results for 24% ^{240}Pu

Case No.	Lattice pitch (cm)	ENDF/B-VI $k_{eff} \pm \sigma$	ENDF/B-V $k_{eff} \pm \sigma$
46	2.4785	0.99915 ± 0.0007	1.00637 ± 0.0006
47	2.6942	1.00269 ± 0.0007	1.00752 ± 0.0006
48	2.6942	1.00371 ± 0.0006	1.00826 ± 0.0006
49	2.6942	1.00200 ± 0.0006	1.00896 ± 0.0006
50	2.6942	1.00306 ± 0.0006	1.00755 ± 0.0006
51	2.6942	1.00200 ± 0.0006	1.00896 ± 0.0006

The MCNP criticality calculation results, with ENDF/B-V and ENDF/B-VI nuclear data libraries, for single-region core configurations with UO_2 fuel are presented in Table 42.

Table 42. MCNP benchmark calculation results for 2.72 % UO_2 fuel

Case No.	Lattice pitch (cm)	ENDF/B-VI $k_{eff} \pm \sigma$	ENDF/B-V $k_{eff} \pm \sigma$
52	1.7526	0.98944 ± 0.0006	0.99395 ± 0.0006
53	2.4785	0.99237 ± 0.0006	0.99670 ± 0.0006

REFERENCES

1. R. D. Leamer et al., *PuO_2-UO_2 Fueled Critical Experiments*, Westinghouse Electric Corporation, WCAP-3726-1, July 1967. Note: text found at http//208.200.37.251/pdfs/i00130.pdf.
2. W. L. Orr, "Westinghouse Pu Recycle Experience and Design," *Proceedings of the Topical Meeting on the Plutonium Fuel Cycle*, May 1977.
3. R. C. Liikala, V. O. Uotinenen, and U. P. Jenguin, *Uncertainties in the Analysis of Plutonium Fueled Light Water Moderated Assemblies*, BNWL-1656, May 1973.
4. V. O. Uotinen, B. R. Leonard, Jr., and R. C. Liikala, "The Neutronics of Plutonium Recycling," *Nucl. Technol.*, **18**, 115 (1973).
5. H.-K. Joo, *Rectangular Arrays of Water-Moderated UO_2-2 wt.% PuO_2 (8% ^{240}Pu) Fuel Rods*, NEA/NSC/DOC/95(03)/VI, Revision 0, OECD Nuclear Energy Agency, 1997.
6. V. O. Uotinen, J. H. Lauby, L. C. Schmid, and W. P. Stinson, "Lattices of Plutonium-Enriched Rods in Light Water—Part I: Experimental Results," *Nucl. Technol.*, **15**, 257 (1972).
7. D. F. Newman, "Measurement of k_∞ and Relative Reaction Rates in an H_2O Moderated UO_2-PuO_2 Particulate Fueled Lattice," *Nucl. Technol.*, **15**, 192 (1972).
8. H. Etherington, *Nuclear Engineering Handbook*, 1st ed., McGraw-Hill Book Company, New York, 1958.
9. E. G. Taylor et al., *Saxton Plutonium Program- Critical Experiments for the Saxton Partial Plutonium Core*, Westinghouse Electric Corporation, EURAEC-1493, WCAP-3385-54, December 1965.
10. R. E. Alcouffe, R. S. Baker, F. W. Brinkley, D. R. Marr, R. D. O'Dell, and W. F. Walters, *DANTSYS: A Diffusion Accelerated Neutral Particle Transport Code System*, LA-12965-M, Los Alamos National Laboratory, 1995.
11. N. F. Landers and L. M. Petrie, *CSAS: Control Module for Enhanced Criticality Safety Analysis Sequences*, NUREG/CR-0200, Vol. 1 Sect. C4, ORNL/NUREG/CSD/-2/V2/R6, Lockheed Martin Energy Research Corp., Oak Ridge National Laboratory, 1998.
12. R. J. Allio and R. S. Miller, "Plutonium Recycle in Pressurized Water Reactors," *Proc. Symp. of Plutonium as a Reactor Fuel*, International Atomic Energy Agency, Brussels, 1967.
13. R. D. Mosteller, *Critical Lattices of UO_2 Fuel Rods and Perturbing Rods in Borated Water*, NEA/NSC/DOC/95(03)/IV, Revision 0, OECD Nuclear Energy Agency (1996).

14. L. C. Schmid et al., *Reactor Physics Data for The Utilization of Plutonium in Thermal Power Reactors*, BNWL-801, May 1968.
15. J. F. Briesmeister, *MCNP-A General Monte Carlo N-Particle Transport Code*, LA-12625-M, Los Alamos National Laboratory, 1994.
16. H. Windsor and R. Goldstein, "Analysis of Lattices Containing Mixed-Oxide Fuel in Particulate Form," *Trans. Am. Nucl. Soc.*, **15**, 107 (1972).
17. R. Cobb, "Analysis of Grain Reactivity Effects using the Method of Walti," *Trans. Am. Nucl. Soc.*, **15**, 108 (1972).

Appendix A. ATOMIC NUMBER DENSITY CALCULATIONS

Atomic densities of the fuels are calculated using Avogadro's number and atomic weights from[*] using the following formula;

$$N_i = \frac{\rho\, w_e w_i N_A}{A_i} \quad ,$$

where

N_i	=	atom density of ith isotope
ρ	=	density of mixture
w_e	=	weight fraction of the element in the mixture
w_i	=	weight fraction of the ith isotope in the element
N_A	=	Avogadro's number
A_i	=	atomic weight of the ith isotope

The density of MOX fuel[1] is taken as 9.54 g/cm^3.

The H, O, ^{10}B, ^{11}B number densities are calculated by using the borated water density formula:[†]

$$\rho_{bwat} = \frac{0.997518 + C_B / 1000}{1 + C_B / 1920} \quad ,$$

where 0.997518 g/cm^3 is the density of water at 23°C temperature and ρ_{bwat} is the density (g/cm^3) of borated water by adding C_B grams of H_3BO_3 crystals to 1 L of water at 23°C temperature.

The H_3BO_3 density in the borated water is calculated using the formula:[†]

$$\rho_{H_3BO_3} = \frac{C_B}{1000 \leftrightarrow (1 + C_B / 1920)} \quad .$$

The H_2O density in borated water is calculated using the formula;[†]

$$\rho_{H_2O} = \frac{997.518}{1000 \leftrightarrow (1 + C_B / 1920)} \quad .$$

The ^{10}B and ^{11}B atomic fractions in boron are 19.8% and 80.2%, respectively. Then, the fraction of boron in H_3BO_3 is calculated as:

$$f_B = \frac{(0.198 \leftrightarrow 10.0129 + 0.802 \leftrightarrow 11.0093)}{3 \leftrightarrow 1.0079 + (0.198 \leftrightarrow 10.0129 + 0.802 \leftrightarrow 11.0093) + 3 \leftrightarrow 15.9994} = 0.17485571 \quad .$$

C_B can be determined using the reported boron concentration p (in ppm) and the formula:

$$C_B = \frac{997.518 \leftrightarrow p}{(f_B \leftrightarrow 10^6 - p)} \quad .$$

The H_3BO_3 and H_2O densities are determined by substituting the calculated C_B value into the equations given above. Then, the boron number density is calculated with H_3BO_3 density, ^{10}B and ^{11}B atomic

---

[*]F. W. Walker, J. R. Parrington, and F. Feiner, *Nuclides and Isotopes*, 14th Ed., General Electric Nuclear Energy Operations, 1989.

[†]H.-K. Joo, *Rectangular Arrays of Water-Moderated UO_2-2 wt% PuO_2 (8% ^{240}Pu) Fuel Rods*, NEA/NSC/DOC/95(03)/VI, Revision 0, OECD Nuclear Energy Agency, 1997.

fractions, and Avogadro's number. The H and O number densities are calculated by summing the atomic number densities from H_2O and H_3BO_3.

The boron concentrations were reported as 116, 261, 315, and 526 ppm. The calculated values of C_B, ρ_{bwat}, $\rho_{H_3BO_3}$, and ρ_{H_2O}, using the formulas given above, are summarized in Table A.1. The calculated number densities using these values were given in Sect. 3.3 (Table 41).

Table A.1. The calculated values of the C_B and the densities for the specified boron concentrations

Parameter (unit)	Concentration (ppm)			
	116	261	315	526
C_B (g)	6.62197E-1	1.49118	1.80026	3.00978
ρ_{bwat} (g/cm^3)	9.97836E-1	9.98234E-1	9.98382E-1	9.98962E-1
$\rho_{H_3BO_3}$ (g/cm^3)	6.61969E-4	1.49002E-3	1.79857E-3	3.00507E-3
ρ_{H_2O} (g/cm^3)	9.97174E-1	9.96744E-1	9.96584E-1	9.95957E-1

Appendix B. PuO_2 PARTICLE EFFECT

During the calculations, the fuel is assumed to be a solid solution in the UO_2-PuO_2 fuel. This is a known source of error for MOX fuel calculations. The fuels used in these experiments contain a finite PuO_2 particle size that causes a reactivity defect.[*,†,‡] The average particle size[§] for the fuel rods used in ESADA experiments was 25 μm. The reactivity change from having finite-size particles relative to homogeneous fuel is mainly caused by changes in ^{239}Pu fission and capture and ^{240}Pu absorption rates. Self-shielding of ^{239}Pu with increasing PuO_2 particle size reduces the ^{239}Pu fission reaction rate in the fuel, thus leading to a negative reactivity effect.[†] It has been noted that the net reactivity effect due to self-shielding within the PuO_2 particles can be negative or positive depending on the neutron energy spectrum, the isotopic composition of plutonium, and the size of the PuO_2 particle.[†] Moreover, the reactivity effect depends also on lattice pitch, plutonium content, and rod size.

The effect of particle size was calculated for fuel rods that were used in PNNL experiments. As discussed in Sect. 1.6, the same MOX fuel rods were used in both PNNL and ESADA experiments. Therefore, the average particle size for the fuel rods used in both experiments was 25 μm. The particle size effect calculations were performed by using the HRG and THERMOS codes with the BNWML cross-section library for PNNL experiments. The change in the k_{eff} value with increasing lattice pitch for PNNL experiments is shown in Fig. B.1.[*] The results of these calculations show that the effect is very small for

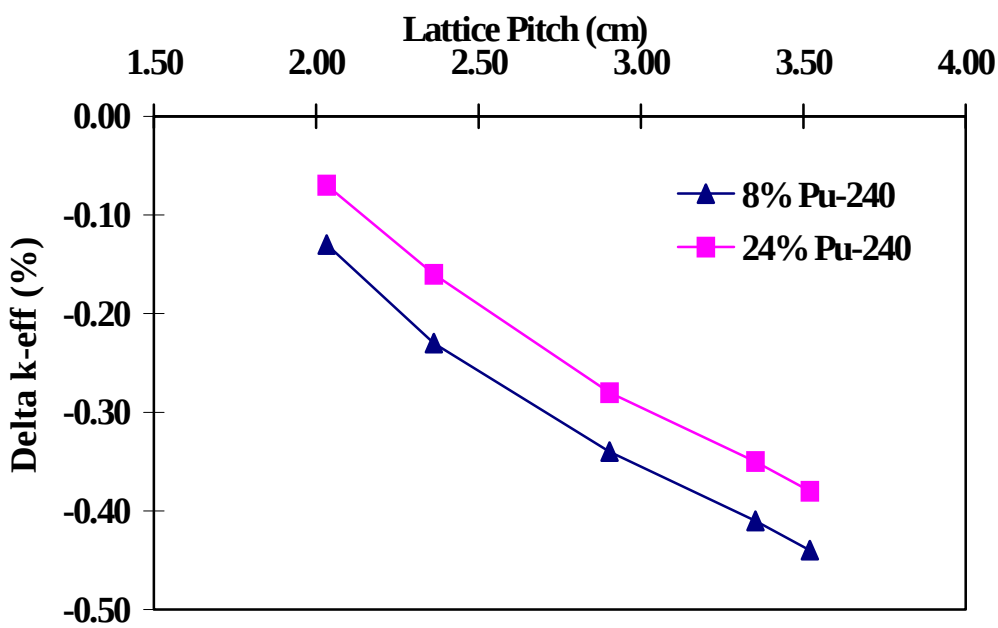

Fig. B.1. Change in the k_{eff} value for 25-μm particle effect with increasing lattice pitch for 8% and 24% ^{240}Pu fuel.*

the tight lattices and noticeable for the loose lattices. Furthermore, for MOX fuel containing a higher concentration of ^{240}Pu, the entire curve is shifted toward the positive direction.

---

[*]R. C. Liikala, V. O. Uotinenen, and U. P. Jenguin, *Uncertainties in the Analysis of Plutonium Fueled Light Water Moderated Assemblies*, BNWL-1656, May 1973.

[†]D. F. Newman, "Measurement of k_∞ and Relative Reaction Rates in an H_2O Moderated UO_2-PuO_2 Particulate Fueled Lattice," *Nucl. Technol.*, **15**, 192 (1972).

[‡]H. Windsor and R. Goldstein, "Analysis of Lattices Containing Mixed-Oxide Fuel in Particulate Form," *Trans. Am. Nucl. Soc.*, **15**, 107 (1972).

[§]R. Cobb, "Analysis of Grain Reactivity Effects using the Method of Walti," *Trans. Am. Nucl. Soc.*, **15**, 108 (1972).

The results of these calculations are used to provide an estimate of the self-shielding effect for the ESADA experiments. The PNNL experiments were performed using different lattice pitches compared to the ESADA experiments. The lattice pitches used in the PNNL experiments were 0.80, 0.93, 1.05, 1.143, 1.32, and 1.386 in. The calculation results for PNNL experiments, given in Fig. B.1, are extrapolated to estimate the self-shielding effect for the lattice pitches that were used in the ESADA experiments. These estimates are presented in Table B.1.

Also, there is another study in which the particle size effect calculation results for ESADA experiments were presented.[‡] However, the calculation results were provided for only two lattice pitches.[‡] The estimated self-shielding effects are compared to the results provided in this reference, and it has been observed that these estimates are in good agreement with the work carried for ESADA experiments.

The MCNP calculational results of k_{eff} for 8% ^{240}Pu fuel with five different lattice pitches can be corrected for the grain size effect using the data given in Table B.1. The corrected k_{eff} values along with the k_{eff} values without correction with increasing lattice pitch are presented in Fig. B.2. The increase in k_{eff} from the smallest lattice pitch to the largest one is decreased from 1.5% to 1.0% with the grain size correction, but the trend of increasing k_{eff} with increasing lattice pitch is still present.

Table B.1. Change in k_{eff} for 25-μm grain size for 8% and 24% ^{240}Pu fuel

Lattice pitch (cm)	Δk(%)	
	8% ^{240}Pu	24% ^{240}Pu
1.7526	-0.047	0.013
1.9050	-0.095	-0.033
2.4785	-0.252	-0.187
2.6942	-0.301	-0.236
3.5052	-0.434	-0.375

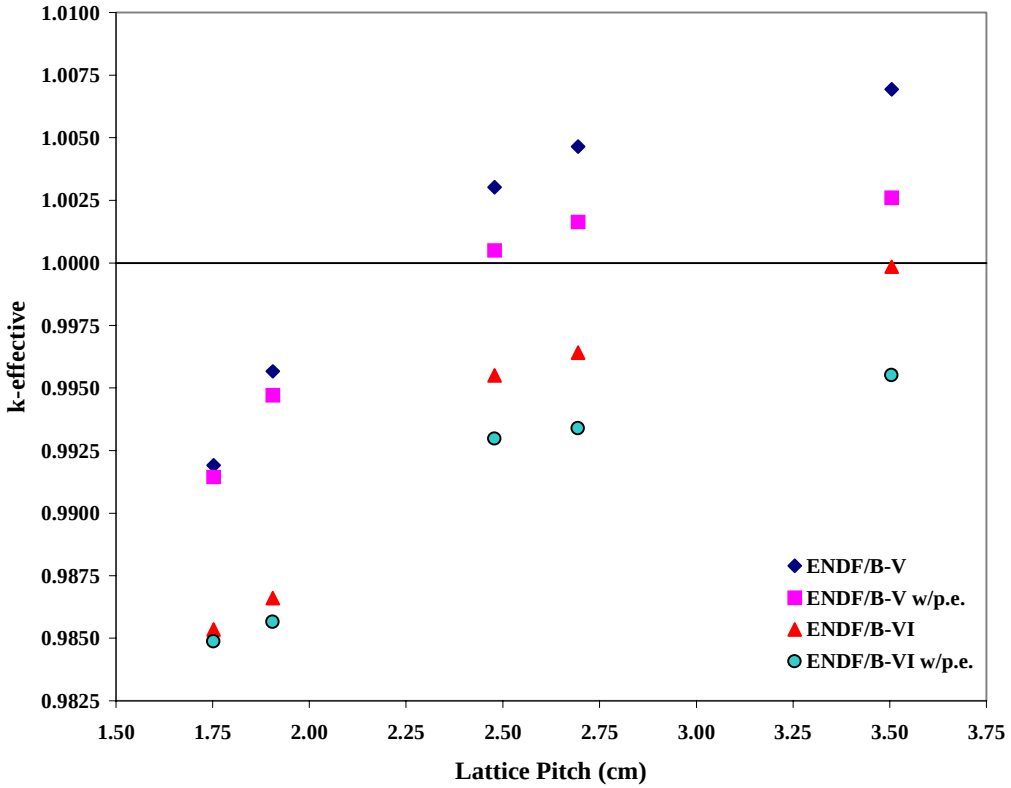

Fig. B.2. Change of corrected k_{eff} values along with the uncorrected values of k_{eff} for grain size effect with increasing lattice pitch for 8% ^{240}Pu fuel.

INTERNAL DISTRIBUTION

1–5. B. B. Bevard
6. J. J. Carbajo
7. E. D. Collins
8. B. S. Cowell
9. M. D. DeHart
10. F. C. Difilippo
11. R. J. Ellis
12–16. J. C. Gehin
17. S. R. Greene
18. T. W. Horning
19. D. T. Ingersoll
20. H. T. Kerr
21. M. A. Kuliasha
22. G. E. Michaels
23. B. D. Murphy
24. D. L. Moses
25. C. V. Parks
26–30. R. T. Primm III
31. C. C. Southmayd
32. Central Research Library
33–34. ORNL Laboratory Records (OSTI)
35. ORNL Laboratory Records–RC

EXTERNAL DISTRIBUTION

36. N. Abdurrahman, College of Engineering, Dept. of Mechanical Engineering, University of Texas, Austin, Texas 78712
37. M. L. Adams, Department of Nuclear Engineering, Texas A&M University, Zachry 129, College Station, TX 77843
38. H. Akkurt, College of Engineering, Dept. of Mechanical Engineering, University of Texas, Austin, Texas 78712
39. D. Alberstein, Los Alamos National Laboratory, MS-E502, P.O. Box 1663, Los Alamos, NM 87545
40. J. Baker, Office of Fissile Materials Disposition, U.S. Department of Energy, MD-3, 1000 Independence Avenue SW, Washington, DC 20585
41. J. B. Briggs, Idaho National Environmental and Engineering Laboratory, P.O. Box 1625-3855, Idaho Falls, ID 83415-3855
42. L. Holgate, Office of Fissile Materials Disposition, U.S. Department of Energy, MD-1/2, 1000 Independence Avenue SW, Washington, DC 20585
43. A. Caponiti, Office of Fissile Materials Disposition, U.S. Department of Energy, MD-3, 1000 Independence Avenue SW, Washington, DC 20585
44. K. Chidester, Los Alamos National Laboratory, MS-E502, P.O. Box 1663, Los Alamos, NM 87545
45. W. Danker, U.S. Department of Energy, MD-3, 1000 Independence Avenue SW, Washington, DC 20585
46. T. Gould, Lawrence Livermore National Laboratory, P.O. Box 808, MS-L186, Livermore, CA 94551
47. L. Jardine, Lawrence Livermore National Laboratory, P.O. Box 808, MS-L166, Livermore, CA 94551
48. Dr. A. Kalashnikov, Institute of Physics and Power Engineering, 1 Bondarenko Square, Obninsk, Kaluga Region, Russia 249020

49–53. D. E. Klein, Associate Vice Chancellor for Special Engineering Programs, The University of Texas System, 210 West Sixth Street, Austin, TX 78701

54. J. O. Nulton, Office of Fissile Materials Disposition, U.S. Department of Energy, MD-3, 1000 Independence Avenue SW, Washington, DC 20585
55. S. L. Passman, Sandia National Laboratories, Suite 110, 950 L'Enfant Plaza S.W., Washington, DC 20024-2123

56–60. Dr. A. Pavlovitchev, Russian Research Center "Kurchatov Institute," Institute of Nuclear Reactors VVER Division, VVER Physics Department, 123182, Kurchatov Square, 1, Moscow, Russia

61. K. L. Peddicord, Associate Vice Chancellor, Texas A&M University, 120 Zachry, College Station, TX 77843-3133

62. G. Radulescu, Framatom Cogema Fuels, 1261 Town Center Drive, MS-423, Las Vegas, Nevada 89143

63. W. D. Reece, Texas A&M University, Department of Nuclear Engineering, Zachry 129, College Station, TX 77843-3133

64. P. T. Rhoads, Office of Fissile Materials Disposition, U.S. Department of Energy, MD-4, 1000 Independence Avenue SW, Washington, DC 20585

65. J. Thompson, Office of Fissile Materials Disposition, U.S. Department of Energy, MD-4, 1000 Independence Avenue SW, Washington, DC 20585

66. F. Trumble, Westinghouse Savannah River Company, Building 730R, Room 3402, WSRC, Aiken, SC 29808